



**NTNU – Trondheim**  
Norwegian University of  
Science and Technology

# Design of a Composite Rotor Structure for a Tidal Turbine Generator

**Jon Ivar Koa**

Master of Science in Mechanical Engineering

Submission date: June 2014

Supervisor: Nils Petter Vedvik, IPM

Co-supervisor: Jørg Høyland, SmartMotor AS

Norwegian University of Science and Technology  
Department of Engineering Design and Materials



**MASTER THESIS SPRING 2014  
FOR  
STUD. TECHN. JON IVAR KOA**

**DESIGN OF LIGHTWEIGHT ROTOR STRUCTURE**

SmartMotor AS has engineered a unique tidal energy generator which is currently in the final testing stages before sea deployment at the European Marine Energy Centre (EMEC). The magnetic circuit of the rotor includes an relatively thick electric steel lamination package. The thickness of the steel lamination package is required to avoid losses caused by induced currents in the underlying steel carrying structure. An alternative non-magnetic carrying structure can potentially reduce the thickness of this member and consequently provide a rotor with lower weight and inertia.

The major objective of this study is to enable reduced weight and inertia through a redesign of the rotor structure utilizing non-magnetic composite materials and design for efficient manufacturing. Detailed tasks relevant for the engineering process are

- Development of a composite rotor structure including a bolted composite-steel connection
- Evaluate solutions for improving axial stiffness of the rotor structure
- Utilize FEA for optimization and study of the composite rotor structure performance and integrity
- Apply DNV-OS-C501 Composite components for basic design philosophy
- Detailed analyses of bolted joints and composite-metal interface

Optionally, experimental approaches may include prototyping and testing of detailed solutions for bolted joints and metal-composite interfaces.

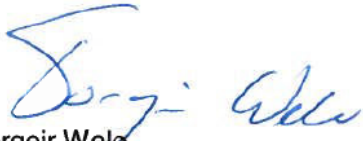
Three weeks after start of the thesis work, an A3 sheet illustrating the work is to be handed in. A template for this presentation is available on the IPM's web site under the menu "Masteroppgave" (<http://www.ntnu.no/ipm/masteroppgave>). This sheet should be updated one week before the Master's thesis is submitted.

Performing a risk assessment of the planned work is obligatory. Known main activities must be risk assessed before they start, and the form must be handed in within 3 weeks of receiving the problem text. The form must be signed by your supervisor. All projects are to be assessed, even theoretical and virtual. Risk assessment is a running activity, and must be carried out before starting any activity that might lead to injury to humans or damage to materials/equipment or the external environment. Copies of signed risk assessments should also be included as an appendix of the finished project report.

The thesis should include the signed problem text, and be written as a research report with summary both in English and Norwegian, conclusion, literature references, table of contents, etc. During preparation of the text, the candidate should make efforts to create a well arranged and well written report. To ease the evaluation of the thesis, it is important to cross-reference text, tables and figures. For evaluation of the work a thorough discussion of results is appreciated.

The thesis shall be submitted electronically via DAIM, NTNU's system for Digital Archiving and Submission of Master's thesis.

The contact person at SmartMotor AS is Jørg Høyland.



Torgeir Welø  
Head of Division



Nils Petter Vedvik  
Professor/Supervisor



# Abstract

Reduction targets for greenhouse gas emissions and the need of national energy security has led to a push in R&D of renewable energy sources such as tidal power the recent years. SmartMotor AS has engineered a tidal energy generator prototype, which is currently being deployed in the sea. The magnetic core in the generator's rotor must be relatively thick to avoid losses caused by induced eddy currents in the underlying steel carrying structure. A non-magnetic carrying structure can potentially reduce the thickness of this member, resulting in lower overall mass and inertia. The purpose of this study was to enable this reduction through a redesign of the rotor structure utilizing non-magnetic composite materials.

A non-magnetic composite rotor structure, which seems possible to manufacture, have been proposed and analysed implementing design philosophy from the DNV-OS-C501 Composite Components standard. The standard was not followed in detail, but the results can be used to indicate the feasibility of the proposed composite structure.

A bolted composite joint between the shaft and the rotor structure was designed and analysed in detail utilizing FEA including a contact analysis. Local stresses caused by the generator torque load were found acceptable, and alternative joints were discussed. Solutions for improving the stiffness of the structure were evaluated. FEA indicated that the stiffness of the proposed structure is sufficient to avoid resonance from relevant excitation sources, and to keep global displacements from static load cases within specifications. The local stress response of the structure to a set of static load cases was shown to be within material strength limits. Linear elastic buckling eigenvalue analyses indicated low risk of local and global buckling.

The proposed composite structure gives a reduction in weight (28%) and inertia (34%) compared to the original rotor with a steel structure. The use of a composite structure seems therefore possible, but testing and analyses with more realistic load cases following the standard are required for verification. Before deciding to go further with a composite structure, a cost comparison of the existing- the new- and alternative non-magnetic structures should be performed.

## Sammendrag

Mål om lavere klimagassutslipp samt behov for nasjonal energisikkerhet har de senere år ført til økt FoU av fornybare energikilder, blant annet tidevannsenergi. SmartMotor AS har utviklet en generator for en prototype tidevannsturbin, som er i ferd med å bli testet i sjøen. Jernkjernen i generatorens rotor må være relativt tykk for å unngå tap som følge av induerte virvelstrømmer i den underliggende bærestrukturen. En ikke-magnetisk bærestruktur vil muliggjøre en vesentlig reduksjon av denne tykkelsen, og dermed lavere samlet masse og treghet. Hensikten med denne studien var å muliggjøre denne reduksjonen gjennom et redesign av bærestrukturen med bruk av ikke-magnetiske komposittmaterialer.

En realiserbar ikke-magnetisk bærestruktur i komposittmateriale ble foreslått og analysert med bruk av designfilosofi fra standarden DNV-OS-C501 Composite Components. Standarden ble ikke fulgt i detalj, men resultatene kan brukes til å indikere muligheten for bruk av den foreslåtte strukturen.

En bolteforbindelse mellom aksel og bærestruktur ble utviklet og analysert i detalj ved hjelp av FE-analyser. De lokale spenningsnivåer i forbindelsen som følge av generatormoment ble funnet akseptable, og alternative forbindelser ble drøftet. Løsninger for forbedring av rotorstrukturens stivhet ble vurdert. FEA indikerte at den foreslåtte strukturen er stiv nok til å unngå resonans fra relevante eksitasjonskilder, og at globale forskyvninger fra statisk belastning er innenfor spesifikasjonene. Det ble vist at lokale spenninger i strukturen fra disse belastningene er innenfor valgte materialers styrkegrense. Lineære knekningsanalyser indikerte at strukturen ikke er utsatt for lokal eller global knekking.

Strukturen gir en reduksjon av masse (28%) og treghet (34%) for rotoren, sammenlignet med referanserotoren med stålstruktur. En komposittstruktur ser derfor anvendbar ut, men testing og analyser med mer realistiske laster som følger standarden behøves for verifikasjon. Før det besluttes å gå videre med en komposittstruktur bør kostnadskalkyler for den nye-, den originale, og alternative ikke-magnetiske strukturer sammenlignes.

# Preface

This work was carried out in the spring of 2014 as part of a master degree in mechanical engineering at the Department of Engineering Design and Materials, Faculty of Engineering Science and Technology at the Norwegian University of Science and Technology. The thesis covers 30 ECTS with a time limitation of 20 weeks, and is a continuation of a study made by the author during a preceding specialization project in the fall of 2013 [1].

The purpose of this study was to examine possibilities for redesign of a tidal turbine generator rotor carrying structure utilizing composite materials in a manufacturing friendly way.

Experimental approaches were considered inappropriate in such an early phase of the design process. Obligatory risk assessment is attached in Appendix K.

**This report is based on research done by SmartMotor AS and is therefore subject to delayed publication for three (3) years.**

A handwritten signature in black ink that reads "Jon Ivar Koa". The signature is written in a cursive, flowing style.

Jon Ivar Koa, Trondheim, June 2014

# Acknowledgements

I would like to thank my academic supervisor at the department Associated Professor Nils Petter Vedvik, and my supervisor Dr. Jørg Høyland and his colleagues at SmartMotor AS for their guidance and support. I would also like to thank my co-students in room 230, for their help and discussions on both relevant and not so relevant issues. Finally, thanks to the helpful staff at IPM.



# Table of Contents

<b>PROBLEM DESCRIPTION</b>	<b>I</b>
<b>ABSTRACT</b>	<b>III</b>
<b>SAMMENDRAG</b>	<b>IV</b>
<b>PREFACE</b>	<b>V</b>
<b>ACKNOWLEDGEMENTS</b>	<b>VI</b>
<b>TABLE OF CONTENTS</b>	<b>VII</b>
<b>LIST OF SYMBOLS</b>	<b>IX</b>
<b>LIST OF ABBREVIATIONS</b>	<b>XI</b>
<b>LIST OF TERMS</b>	<b>XII</b>
<b>LIST OF FIGURES</b>	<b>XIII</b>
<b>LIST OF TABLES</b>	<b>XVI</b>
<b>1 INTRODUCTION</b>	<b>1</b>
1.1 Background .....	1
1.2 Participants/stakeholders .....	3
1.3 Objectives .....	3
1.4 Outline of the report .....	3
<b>2 TIDAL TECHNOLOGY &amp; COMPOSITE MATERIALS</b>	<b>5</b>
2.1 Tidal Technology .....	5
2.2 Permanent magnet synchronous machines .....	8
2.3 Composite materials .....	11
<b>3 REFERENCE ROTOR AND CONCEPT DEVELOPMENT</b>	<b>15</b>
3.1 Reference rotor .....	15
3.2 Concept development .....	16
3.3 Chosen concept .....	18
<b>4 DESIGN PHILOSOPHY</b>	<b>19</b>
4.1 Design philosophy and design principles .....	19
4.2 Design input .....	19
4.3 Failure mechanisms .....	24
4.4 Material properties .....	26
4.5 Design criteria .....	28
<b>5 STRUCTURAL JOINTS IN COMPOSITES</b>	<b>31</b>
5.1 Laminated joints .....	31
5.2 Adhesive joints .....	32
5.3 Design approach .....	33
5.4 Joint selection for the structure .....	34
5.5 Yoke/disc structural joint .....	35
<b>6 BOLTED JOINT THEORY</b>	<b>37</b>
6.1 Configuration and geometry .....	37
6.2 Failure modes in bolted laminates .....	39
6.3 Effects of parameters .....	41
6.4 Design practice, failure criteria and factor of safety .....	44
6.5 Stress concentration .....	44
6.6 Fatigue performance .....	44
6.7 Summary .....	45

<b>7</b>	<b>BOLTED JOINT DESIGN</b>	<b>47</b>
7.1	Concept description.....	47
7.2	Bolt selection .....	47
7.3	Bolt contact analysis using FE .....	50
7.4	Alternative bolted joint concepts.....	63
7.5	Summary .....	68
<b>8</b>	<b>STRUCTURE STIFFNESS</b>	<b>69</b>
8.1	Approach.....	70
8.2	Forcing frequencies.....	70
8.3	Modal analysis and structure stiffness .....	71
8.4	Relationships between natural and forcing frequencies .....	82
8.5	Summary .....	83
<b>9</b>	<b>STATIC LOAD CASES</b>	<b>85</b>
9.1	Model.....	85
9.2	Results.....	88
9.3	Summary .....	100
<b>10</b>	<b>MANUFACTURING AND ASSEMBLY</b>	<b>101</b>
10.1	Manufacturing processes.....	101
10.2	Manufacturing and assembly of inner structure .....	104
10.3	Manufacturing of magnetic core and yoke.....	106
10.4	Final assembly.....	106
<b>11</b>	<b>DISCUSSION</b>	<b>109</b>
11.1	Design input.....	109
11.2	Joints .....	110
11.3	Structure.....	111
11.4	Manufacturing and feasibility .....	112
<b>12</b>	<b>CONCLUSIONS AND FURTHER WORK</b>	<b>115</b>
12.1	Conclusions.....	115
12.2	Further work.....	115
	<b>REFERENCES</b>	<b>I</b>
<b>APPENDIX A</b>	<b>PRODUCT REQUIREMENT SPECIFICATION</b>	<b>V</b>
<b>APPENDIX B</b>	<b>MORPHOLOGY MATRIX</b>	<b>VI</b>
<b>APPENDIX C</b>	<b>SN-CURVES AND DETAIL CATEGORY</b>	<b>VII</b>
<b>APPENDIX D</b>	<b>SURFACE-SURFACE CONTACT DEFINITION</b>	<b>VIII</b>
<b>APPENDIX E</b>	<b>CONSTRAINT IN BOLT CONTACT ANALYSIS</b>	<b>IX</b>
<b>APPENDIX F</b>	<b>BOUNDARY CONDITIONS</b>	<b>X</b>
<b>APPENDIX G</b>	<b>DIMENSIONS IN GLOBAL FE MODEL</b>	<b>XI</b>
<b>APPENDIX H</b>	<b>CONSTRAINTS ON PART LEVEL</b>	<b>XIII</b>
<b>APPENDIX I</b>	<b>HORIZONTAL VS. VERTICAL JIG ASSEMBLY</b>	<b>XIV</b>
<b>APPENDIX J</b>	<b>DETAILS OF MASS AND MOMENT OF INERTIA</b>	<b>XV</b>
<b>APPENDIX K</b>	<b>RISK ASSESSMENT</b>	<b>XVI</b>

# List of Symbols

## Arabic

$A$	Area
$a_{design}$	Design gravity
$a_{specified}$	Specified gravity
$d_n$	Specified maximum displacement
$d_{spec}$	Local displacement
$e$	Edge distance
$E_{1T}$	Tension Young's moduli in longitudinal direction
$E_{2T}$	Tension Young's moduli in transverse direction
$E_{3C}$	Compression Young's moduli in out-of-plane direction
$E_{3T}$	Tension Young's moduli in out-of-plane direction
$F_{bolt}$	Bolt load
$G_{12}$	In-plane shear moduli
$G_{13}$	Trough thickness shear moduli
$G_{23}$	Out-of-plane shear moduli
$I_p$	Second moment of area
$K_t$	Stress concentration factor
$l$	Length
$m$	Mass or SN-curve slope
$n$	Number of something, e.g. bolts
$N_R$	Design lifetime in cycles
$N_x$	Laminate load in longitudinal direction
$N_{xy}$	Laminate shear load in fibre plane
$N_y$	Laminate load in transverse direction
$^{\circ}$	Degrees, angle
$^{\circ}C$	Degrees Celsius
$P$	Pitch
$P_{back}$	Back pitch
$P_{circ}$	Circumferential distance
$r$	Radius
$R_{bolting}$	Bolting radius
$R_k$	Characteristic resistance
$S$	Side distance
$S_k$	Characteristic load effect
$t$	Thickness
$T$	Torque
$t_a$	Adherend thickness
$T_{design}$	Design torque corrected with partial factors
$T_g$	Glass Transition temperature
$t_g$	Adhesive thickness
$V_f$	Fibre volume fraction
$W$	Width

## Greek

$\hat{\sigma}_{12}^{shear}$	In-plane shear strength
$\hat{\sigma}_{1c}^{fibre}$	Ultimate tensile strength in longitudinal direction
$\hat{\sigma}_{1t}^{fibre}$	Ultimate compression strength in longitudinal direction
$\hat{\sigma}_{2c}^{matrix}$	Ultimate tensile strength in transverse direction
$\hat{\sigma}_{2t}^{matrix}$	Ultimate compression strength in transverse direction
$\hat{\sigma}_{3c}^{matrix}$	Ultimate compression strength in out-of-plane direction.
$\hat{\sigma}_{3t}^{matrix}$	Ultimate tensile strength in out-of-plane direction.
$\Delta\tau_C$	Detail category reference fatigue strength
$\Delta\tau_L$	Fatigue shear stress range cut-off limit
$\Delta\tau_R$	Fatigue strength shear stress range
$\gamma_{FM}$	Combined load effect and resistance factor
$\gamma_{Rd}$	Resistance model factor
$\gamma_{Sd}$	Load model factor
$\gamma_{distribution}$	Load sharing distribution
$\nu_{12}$	Longitudinal Poisson's ratio
$\nu_{13}$	Trough thickness Poisson's ratio
$\nu_{23}$	Out-of-plane Poisson's ratio
$\sigma_{nk}$	Local response in structure in each direction
$\rho$	Density
$\tau$	Shear stress
$\tau_{bolt\ ss}$	Bolt shear stress

# List of Abbreviations

AC	Alternating Current
BC	Boundary Condition
CAD	Computer Aided Design
COV	Coefficient Of Variation
CSM	Chopped Strand Mat, also used for chopped strands in general
DC	Direct Current
DNV	Det Norske Veritas
DOF	Degrees Of Freedom
EMEC	European Marine Energy Centre
EO	Engine Order
EV	Eigenvalue
FE	Finite Element
FEA	Finite Element Analysis
FRP	Fibre Reinforced Polymer
FW	Filament Winding
GFRP	Glass Fibre Reinforced Polymer, partially interchangeable with GRP
HAWT	Horizontal Axis Wind Turbine
HISC	Hydrogen Induced Stress Cracking
ISO	International Organization for Standardization
LRFD	Load and Resistance Factor Design
NR	Not Relevant
PM	Permanent Magnet
PMSM	Permanent Magnet Synchronous Machine
R&D	Research and Development
RP	Reference Point
TEC	Tidal Energy Converters
UD	Unidirectional
ULS	Ultimate Limit State

# List of Terms

Buckling	Unstable displacement of a structural part caused by excessive compression or shear.
Characteristic value	A nominal value to characterise a stochastic variable. Has a small probability of not being exceeded in a hypothetically unlimited test series.
Cogging	Torque due to the interaction between the permanent magnets of the rotor and the stator slots of a Permanent Magnet (PM) machine.
Condition	A particular state of existence.
Delamination	Separation or loss of bonds of plies.
Eddy currents	Electric currents induced within a conducting material by a changing magnetic field.
Environmental conditions	Environmental exposure that may harm or degrade the material properties.
Failure criterion	Criterion to define or identify when failure has occurred.
Failure mechanism	Underlying phenomenon at the material level that determines the mode of failure.
Failure mode	State of inability to perform a normal function, or an event causing and undesirable or adverse condition.
Fatigue	The cumulative and irreversible damage incurred by cyclic or static application of mechanical and/or thermal loads.
Global Response	Displacement and stability of a structure as a whole.
Laminate	Layers of plies bonded together to form a single structure
Load effect	Effect of a single load or combination of loads on the system, such as stress, strain, deformation, displacement, etc.
Local Response	Stresses, strains and deformations in every local part of a structure.
Magnetic core	A piece of magnetic material with a high permeability used to confine and guide magnetic fields in electric motors and generators.
Orthotropic	Having three mutually perpendicular planes of material symmetry
Partial Factor	Partial factors are assigned to basic variables in order to account for their inherent uncertainties or systematic errors
Ply	Basic building block of a laminate. Layer of reinforcement surrounded by a matrix
Ply level	Individual layers in a laminate
Prototype	Complete model to prove shape, function, performance and production process.
Resistance	Capability of a structure or part of a structure, to resist load effects.
S-N Curve	Graph showing the relationship between stress and cycles to failure.
Stacking sequence	A description of the orientation of plies in a laminate
Structure	General word for system, component or detail.

# List of Figures

Figure 1: Detailed section view of the reference rotor.....	1
Figure 2: The design space of the rotor structure (green) and connecting parts (blue).....	2
Figure 3: La Rance tidal power plant in France. Image adapted from Wikimedia commons.....	5
Figure 4: Morphology matrix showing tidal energy converter categories and fixing methods. ....	6
Figure 5: Commercial scale devices to be deployed the coming years.....	7
Figure 6: A hierarchy of electrical motors showing the PMSM's position. ....	8
Figure 7: PMSM nomenclature for a four-pole machine without magnetic core in rotor.....	9
Figure 8: Lines of magnetic fields in a four-pole PMSM machine.....	9
Figure 9: Stacking of electric steel laminations to form a magnetic core.....	9
Figure 10: Magnet configurations: a) Interior magnets. b) Surface mounted magnets.....	9
Figure 11: Basic types of composites. ....	11
Figure 12: Material orientation in the local material coordinate system for each ply.....	12
Figure 13: Composite failure modes.....	13
Figure 14: Exploded view of the reference rotor with essential component names.....	15
Figure 15: Illustration of the reference rotor with basic properties (CAD model by Høyland).....	15
Figure 16: Morphology matrix. Sub-functions on the vertical, solutions on the horizontal. ....	16
Figure 17: Illustrations of some proposed concepts. ....	17
Figure 18: Cross section of the proposed solution.....	18
Figure 19: Typical laminated joint with pad/backing. ....	31
Figure 20: Geometrical parameters for a single-lap adhesive joint. ....	32
Figure 21: Fracture modes in adhesive composite joints.....	32
Figure 22: Joints in the structure. ....	34
Figure 23: Bolt in single (left) and double shear (right). Image adapted from Wikimedia commons. ....	37
Figure 24: Geometry of a multi-row joint. One row joint (lower right) and one line joint (upper right). ....	38
Figure 25: Geometry parameters and notation used for this joint in this thesis.....	38
Figure 26: Failure modes in bolted composite joints.....	39
Figure 27: Illustrations of chosen layup. ....	42
Figure 28: Illustration of preliminary rotor concept and detailed views of bolted area.....	47
Figure 29: Part dimensions [m]. ....	51
Figure 30: Bolt partitioning and mesh.....	52
Figure 31: Disc partitioning, mesh and stack orientation. ....	52
Figure 32: Material and layup orientation for the composite disc. ....	53
Figure 33: Section view of the meshed parts. Steel disc in grey, composite disc in green.....	53
Figure 34: Surface to surface contact in the assembly.....	54
Figure 35: Coupling from RP to outer edge of the composite disc.....	55
Figure 36: BC; inner edge of disc fixed.....	55
Figure 37: Element-size convergence study for composite disc stress. ....	56
Figure 38: 22-tensile stresses in the bolthole. Coloured areas exceeds material strength.....	57
Figure 39: Rejected joint. The area exceeding 22 tensile strength (coloured) is too large. ....	58
Figure 40: Compressive stress in 22 direction. Area with stress above 50% of strength is coloured. ....	58
Figure 41: 12-shear stress. Area with stress above 50% of strength are coloured. ....	59
Figure 42: Through-thickness (33) compressive stress. Areas with stresses above 1MPa are coloured. .	59

Figure 43: Element-size convergence study for hub stress.....	60
Figure 44: Overview of von Mises stress in the hub. ....	60
Figure 45: Von Mises stress above 100 MPa in the hub bolthole.....	61
Figure 46: Element-size convergence study for bolt stress.....	61
Figure 47: Section views showing stress levels in a bolt.....	62
Figure 48: Single and double shear configuration. ....	63
Figure 49: Comparison between normal short bolt and through bolt concept.....	64
Figure 50: Pretension concept with through bolt and support pipe .....	64
Figure 51: Comparison of deformations.....	66
Figure 52: Reference composite structure with flat discs.....	69
Figure 53: Mesh stack direction for all parts .....	72
Figure 54: Material and layup orientation for the composite yoke.....	73
Figure 55: Normal definition and ply stack plot for the composite disc and stiffener ring .....	73
Figure 56: Nonstructural mass dialogue box. ....	74
Figure 57: Boundary conditions .....	74
Figure 58: Constraints shown in the complete assembly.....	75
Figure 59: Complete assembly without and with mesh ( 88 000 elements). ....	76
Figure 60: First dominant modes common for most of the studied structures.....	77
Figure 61: Illustration of two yoke flapping modes.....	78
Figure 62: Two of the investigated one-hub designs.....	78
Figure 63: Two-hub designs.....	79
Figure 64: Low stiffness in yoke allows discs to move independently.....	80
Figure 65: Campbell diagram for the preferred solution. ....	82
Figure 66: Illustrations of the preferred concept from this chapter. ....	83
Figure 67: Loads and BC's for three static load cases .....	86
Figure 68: Coupling between RP and outer surface of the yoke.....	87
Figure 69: Element size convergence study for gravity load cases. ....	88
Figure 70: Global displacement of the structure for the gravity load cases.....	89
Figure 71: Element size convergence for the torque load case.....	90
Figure 72: Detail view of the 22 tensile stress in a disc hole.....	91
Figure 73: 22 tensile stresses in both discs. The bottom disc is in the loaded end of the shaft.....	91
Figure 74: Comparison of stress fields for disc with (left) and without (right) holes.....	92
Figure 75: Tensile stress in 22 direction the stiffener rings.....	93
Figure 76: Max absolute shear stress (12) in the yoke.....	93
Figure 77: Von Mises stress shaft/hub part. Max is 146 MPa (red). ....	94
Figure 78: Mesh convergence for torque buckling load. ....	96
Figure 79: Mode shapes for torque buckling load. ....	96
Figure 80: Element size convergence for axial gravity hub buckling.....	97
Figure 81: Element size convergence study for the disc-warping mode. ....	97
Figure 82: Mode shapes for axial gravity buckling load. ....	98
Figure 83: Element size convergence for radial gravity buckling. ....	98
Figure 84: Eigenmodes for radial gravity buckling load. ....	99
Figure 85: Complete rotor on jig with 1.90 m mannequin for scale.....	101
Figure 86: Illustration of the spray-up process. ....	102
Figure 87: Illustration of the hand layup process.....	102



Figure 88: Illustration of vacuum bagging. ....	103
Figure 89: Illustration of the infusion process. ....	103
Figure 90: Shaft with welded onto hubs. ....	104
Figure 91: Areas with critical dimensions highlighted. ....	104
Figure 92: First disc bolted on to the shaft. Dark blue indicates applied adhesive. ....	105
Figure 93: Second disc entered and bolted. ....	105
Figure 94: Section view of a simple assembly jig with the magnetic core. ....	106
Figure 95: Sprayed up yoke (green) with joint backing in place (purple). ....	106
Figure 96: Shaft and structure in position inside the yoke. ....	107
Figure 97: Stiffener ring entered and three laminated joints completed. ....	107
Figure 98: Structure turned around with all joints completed. ....	107
Figure 99: Detailed view of the main joint. ....	108

# List of Tables

Table 1: Description of the rotor structure.....	20
Table 2: Design life phases and assigned safety classes.....	20
Table 3: Relevant functional requirements for operation phase. ....	21
Table 4: Evaluation of failure modes for the structure laminates .....	21
Table 5: Link between functional requirements and failure modes.....	22
Table 6: Characteristic loads for the rotor structure .....	22
Table 7: Description of the environment of the structure .....	23
Table 8: Link between failure modes and failure mechanisms for the structure laminates. ....	24
Table 9: Failure mechanism and failure type with target reliability level for operation phase. ....	25
Table 10: Material properties used in this thesis. ....	27
Table 11: Explanation of the factors in the general design criterion .....	28
Table 12: Factors used for the matrix and fibre failure criterion .....	29
Table 13: Factors used for the buckling criterion. ....	30
Table 14: Factors used for the displacement criterion. ....	30
Table 15: General guidelines for joint type selection. ....	34
Table 16: Values for simple stress analysis .....	35
Table 17: Summary of recommendations for bolted joints.....	45
Table 18: Results from fatigue stress range calculations for the bolts.....	48
Table 19: Minimum number of bolts for different bolting radiuses and bolt diameters .....	49
Table 20: Materials used in the parts.....	51
Table 21: Summary of stresses in all directions compared to corresponding strengths.....	57
Table 22: Input data for through bolt calculations. ....	65
Table 23: Results for through bolt calculations. ....	66
Table 24: Parameters in adhesive hybrid joint calculation. ....	67
Table 25: Bolted joint parameters resulting from this chapter.....	68
Table 26: Identified possible excitation frequencies and other frequency requirements. ....	71
Table 27: Materials used in the parts.....	72
Table 28: Overview of constraints used in the model.....	75
Table 29: Results from modal analysis for different models .....	81
Table 30: Loads and boundary conditions for three static load cases.....	86
Table 31: Maximum stresses in the structure. Percentage of limit in parenthesis. ....	89
Table 32: Comparison of stresses in structure with and without disc holes. ....	92
Table 33: Eigenvalues (EV) and mode shapes for the load cases.....	99
Table 34: Comparison of mass and inertia of reference structure and new proposed structure.....	113
Table 35: Compared to possible reductions with other non-magnetic materials .....	113

# 1 Introduction

## 1.1 Background

The world is currently on a trajectory for a long-term global temperature rise of 3.6 °C, well above the internationally agreed target of limiting the increase to 2 °C [2]. Renewable energy technologies, such as tidal energy is pointed out as one of the key mitigation technologies expected to be developed commercially before 2030 [3]. Amongst other, an EU target of 20% renewables by 2020, and a UK a target of 80% by 2050 have led to a push in tidal energy R&D the recent years.

SmartMotor AS is a company involved in tidal R&D and has delivered the generator for a tidal turbine prototype currently being deployed in the sea at the European Marine Energy Centre (EMEC). The rotor in this generator has a steel carrying structure illustrated in Figure 1.

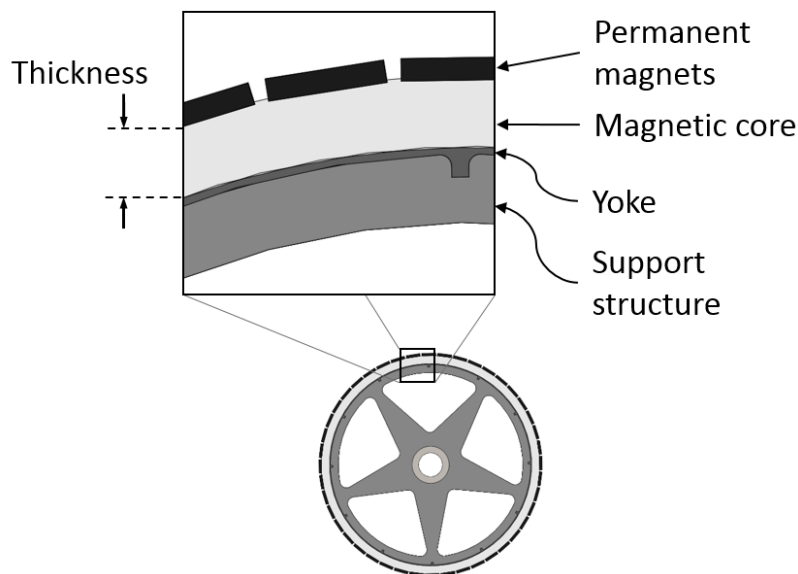


Figure 1: Detailed section view of the reference rotor.

A relatively thick magnetic core is needed to avoid losses from induced eddy currents in the underlying steel structure. This gives a rotor with high mass and inertia. Electromagnetic calculations have shown that with a non-magnetic rotor structure, the thickness can be halved from 60 mm to 30 mm [4]. This will give a significant reduction in mass and inertia. A report by Høyland [4] concluded that little further improvement can be gained from a structure optimization itself. The magnetic core, magnets and shaft accounts for

approximately 90% of the rotor's mass and moment of inertia. Therefore, any significant improvements lies in enabling the reduction in magnetic core thickness by using a non-magnetic material in the structure. Non-magnetic metals such as stainless steel or aluminium are assumed to result in roughly the same manufacturing costs as the steel design. Composite materials are well suited for corrosive environments, and it is assumed that manufacturing cost and time can be reduced compared to that of metals. An investigation in the use of composites in the rotor structure was therefore requested. E-glass should be used, as it is non-conductive and have a good balance between strength and cost. Knowing that the shaft and the outer surface of the magnetic core will be kept as-is, the design space for the new structure can be illustrated as in Figure 2.

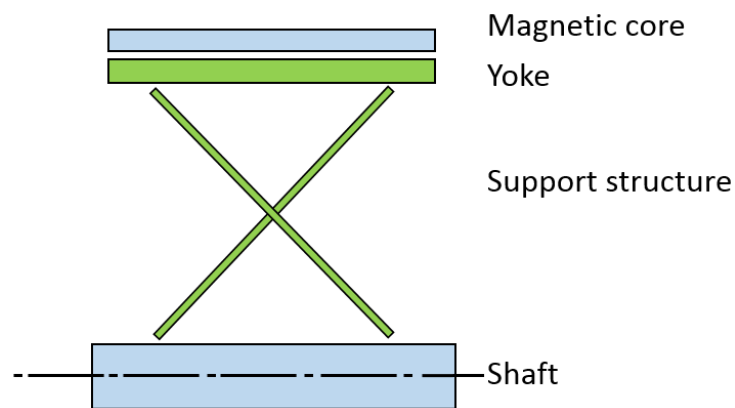


Figure 2: The design space of the rotor structure (green) and connecting parts (blue).

In the specialization project [1] preceding this master thesis, a concept was chosen and a preliminary composite structure design was developed. In this master thesis, the structure will be studied in more detail.

## 1.2 Participants/stakeholders

SmartMotor is based in Trondheim, Norway, and was acquired by Rolls-Royce Marine AS August 2013 [5]. The company specialise in customized, compact, highly efficient, high torque electrical machines with integrated drives and controls [6]. More specific, these are Permanent Magnet Synchronous Machines (PMSM), which finds a wide range of application within the renewable energy, oil & gas and marine industries.

## 1.3 Objectives

The overall objective is to enable reduced mass and inertia of the rotor through a redesign of its carrying structure utilizing non-magnetic composite materials and design for efficient manufacturing. Detailed objectives are:

- Use the standard DNV-OS-C501 Composite Components (C501) to establish a design philosophy.
- Develop and analyse a bolted joint between the structure and the shaft.
- Evaluate solutions for improving the stiffness of the preliminary structure.
- Study performance and integrity of the structure using FEA.

## 1.4 Outline of the report

Background information on tidal energy in general, the generator technology, and some basics on composite materials are provided in chapter 2. The chosen concept from the preceding specialization is described in chapter 3. Chapter 4 introduces a design philosophy for the structure based on the methods used in C501.

The joints of the structure are treated in general in chapter 5, followed by a literature review on composite bolted joints in chapter 6. Recommendations from the literature are used in chapter 7, where a bolted joint is proposed and analysed. Alternatives for the bolted joint are also discussed briefly.

The structure as whole is studied in chapter 8, where solutions for improving stiffness are evaluated using modal analyses. The preferred structure is further studied in chapter 9, where structural response to a set of load cases are investigated. In chapter 10, a manufacturing and assembly procedure for the structure is proposed.

Chapter 11 contains a discussion, followed by conclusions and recommendations for further work in chapter 12.



## 2 Tidal Technology & Composite Materials

This chapter describes basics on tidal energy, the generator and composite materials.

### 2.1 Tidal Technology

Tidal energy is the use of tidal streams to generate electricity. The industry is immature and prototype dominated, with costs among the highest of all energy sources [7]. However, the estimates vary widely, and the lack of commercial scale deployment makes it difficult to accurately assess the true cost of a large scale installation and operation [7]. There is large optimism among investors that the costs can be driven down to competitive levels [8]. Tidal energy is very site specific because the tidal flow needs to be constrained to either give a height difference between ebb and tide, or reach high velocity. Nonetheless, several “sweet spots” exist around the world, where this can prove to be a reliable and feasible source of energy. The predictability of the tides, the desire for energy independency, and an estimated 100 GW of global installed capacity potential [9] [10], has led to considerable investments and activity on this energy frontier the recent years. UK, France and Ireland have the largest potential in Europe [11], and the UK alone has some 10 GW of estimated resources, accounting for half of Europe’s tidal resources [10]. Essentially the kinetic energy of the tides can be harnessed in two ways. One is by building a barrage across a tidal estuary, and the ebb and flow of the water is used to turn turbines [11]. The principle is similar to conventional low head hydropower, and a classic example is the 240 MW La Rance Tidal Power Plant in the North-West of France, operating since 1966 (Figure 3).

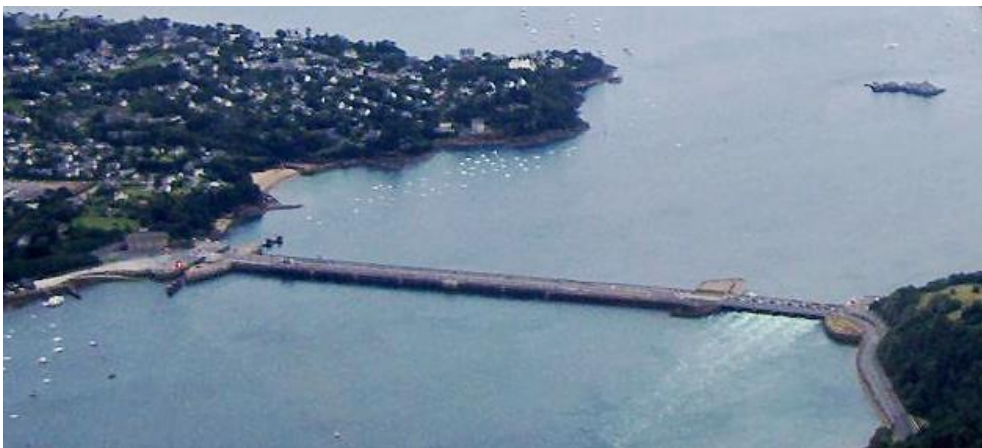


Figure 3: La Rance tidal power plant in France. Image adapted from Wikimedia commons.

The other, less researched way of harnessing tidal power is using underwater devices in fast flowing tidal streams, so called tidal energy converters (TEC). This can be cheaper and cause less environmental impact. There are six main types of TEC's, and four principal methods of fixing them to the seabed [12]. Possible combinations are shown in the morphology matrix in Figure 4 (based on [12]). The turbine connected to this project thesis marked with an x.

TEC type	Fixing method			
	Seabed mounted / gravity base	Pile mounted	Floating *	Hydrofoil inducing downforce
Horizontal axis turbine			x	
Vertical Axis Turbine				
Oscillating Hydrofoil				
Enclosed Tips (venturi)				
Archimedes Screw				
Tidal kite				

\* Three subdivisions: Flexible mooring, rigid mooring and floating structure.

Figure 4: Morphology matrix showing tidal energy converter categories and fixing methods.

Many concepts are currently being researched and tested, and so far, several failures have happened. Examples include the OpenHydro turbine in Bay of Fundy, Canada [13], blade failure of the AK1000 turbine at Orkney [14], and the abortion of Neptune Renewable Energy's concept after testing of a full scale demonstrator in 2012 [15]. This emphasises the harsh operating conditions, and the difficulty of creating robust designs. R&D hubs for tidal power worth noticing are The European Marine Energy Centre (EMEC) at the Orkney Islands, UK and FORCE in Nova Scotia, Canada.

The industry have previously consisted of relatively small and unknown companies. Recently larger players have entered the scene, mainly through acquisitions. Examples include Andritz Hydro (Hammerfest Strøm), Alstom (Tidal Generation Ltd.), Siemens AG (Marine Current Turbines), DCNS S.A. (OpenHydro), Lockheed Martin, Voith Hydro, and Kawasaki Heavy Industries. Some concepts have been tested with commercial scale devices (~1 MW). Deployment of small arrays of such devices is under way, and three such



plans are listed below. The images in Figure 5 are obtained from the respective companies' websites.

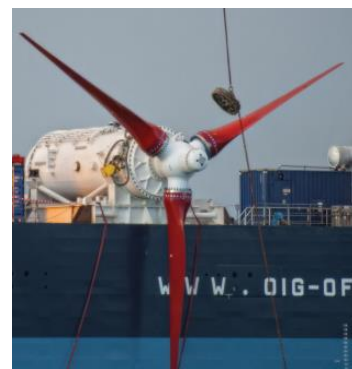
**Skerries Tidal Stream Array**, Wales, UK. Planned commercial operation in 2015. 10 MW array consisting of five SeaGen generators in Figure 5 a).

**Pentland Firth**, UK. An array of up to six 1MW turbines installed on a phased basis from 2014 until 2020 [16]. Two turbine technologies will be used, the AR1000 in Figure 5 d), and the HS1000 in Figure 5 b) [17].

**Sound of Islay**, UK. Four Alstom turbines in Figure 5 c) and four HS1000's. Planned start in 2015 and full site deployment during 2016. Operated by Scottish Power Renewables [18].



a) 2MW SeaGen TEC owned by Siemens.



b) 1MW HS1000 turbine from An-dritz Hydro Hammerfest.



c) 1MW Turbine from Alstom.



d) 1MW AR1000 turbine from Atlan-tis Resources Corporation.

Figure 5: Commercial scale devices to be deployed the coming years.

## 2.2 Permanent magnet synchronous machines

The generator studied here is Permanent Magnet Synchronous Machine's (PMSM). Its position in a hierarchy of electrical motors is shown in Figure 6.

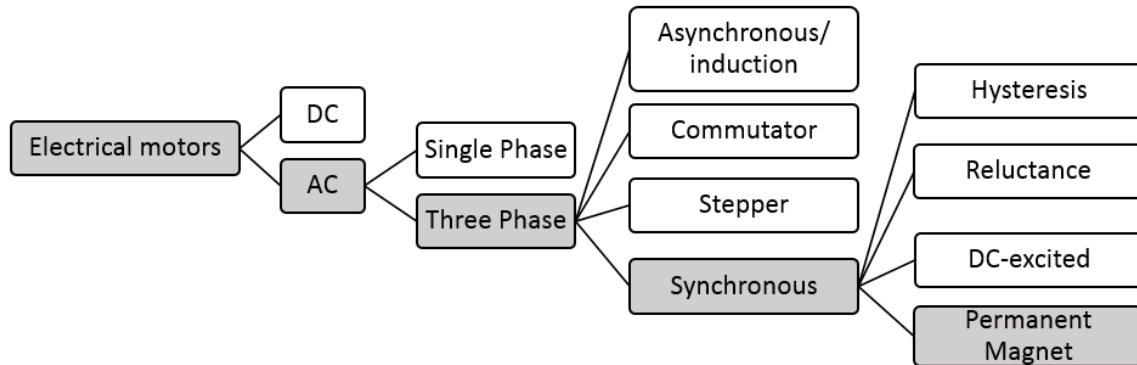


Figure 6: A hierarchy of electrical motors showing the PMSM's position.

Permanent Magnet AC (PMAC), Brushless AC and PMSM are synonymous terms [19], and the latter will be used here. The difference between a motor and a generator is essentially just a matter of which way power is converted (electrical - mechanical). Therefore, the term machine is used. Synchronous speed means that the rotor spins at the same speed as the motor's internal rotating magnetic field. The PMSM is closely related to the DC-excited synchronous machine used in large utilities. Both have a stator with three-phase windings. The rotor of the DC-excited has excitation windings (slip rings and bushes) to set up its rotor field. In contrast the PMSM rotor field is set up by its permanent magnets [20]. Figure 7 (adapted from [21]) shows a cross section of a typical four-poled radial PMSM machine with essential nomenclature.

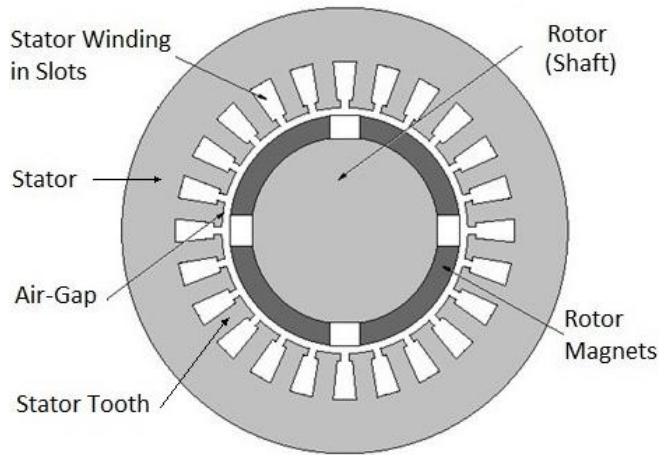


Figure 7: PMSM nomenclature for a four-pole machine without magnetic core in rotor.

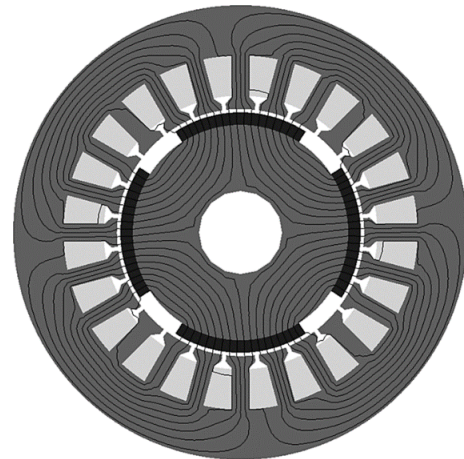


Figure 8: Lines of magnetic fields in a four-pole PMSM machine.

The stator is made of thin isolated electrical steel strips, i.e. electrical steel laminations (see Figure 9, adapted from [20] p. 530) stacked together to form a magnetic core. Isolated strips reduces induced eddy currents, which leads to losses. Stator windings, which sets up the rotating stator field, are put into the stator slots. Usually there is also a magnetic core in the rotor.

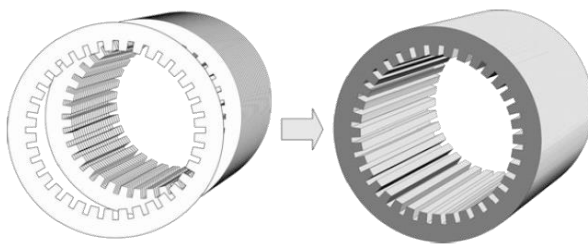


Figure 9: Stacking of electric steel laminations to form a magnetic core.

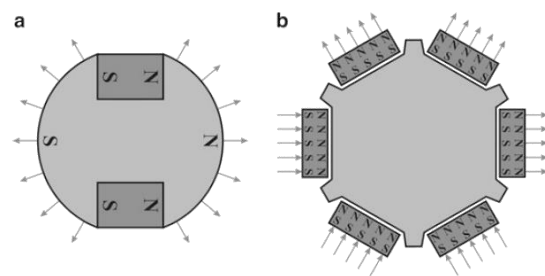


Figure 10: Magnet configurations: a) Interior magnets. b) Surface mounted magnets.

Permanent magnets can be mounted on the surface of the rotor magnetic circuit (surface mount) or within the interior part of the magnetic circuit [20] (Figure 10, adapted from [20] p. 536). The permanent magnets are made of sintered or bonded rare earth materials pressed into various shapes, of which the most used are rectangles or parts of arcs. The most common material is neodymium (NdFeB) because of its good magnetic properties compared to price.

PMSM's comes in radial- (cylinders), axial- (discs) and linear/translational configurations. The different names arise from the direction of magnetic flux in the air gap. The machine in this thesis belongs to the most common category; radial flux machines with iron in both rotor and stator and a slotted stator [22].

The PMSM works by interaction between the magnetic field set up by the stator windings and that of the permanent magnets. As illustrated in Figure 8 (adapted from [23]), the lines of magnetic field pass from the stator teeth into the air gap and enters the permanent magnet. They then move through the magnetic core of the rotor to the opposite magnetic pole, returning through the air gap and into the stator teeth [20]. The magnetic core is there to facilitate the magnetic field flux.

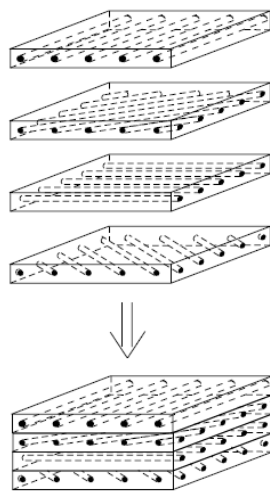
Having a permanent magnetic field in the rotor simplifies the design and gives less rotor losses, easier cooling and higher efficiency compared to other kinds of electrical machines [20]. On the downside, PM's can be challenging during assembly, and can lead to some degree of cogging in the machine. Cogging is unwanted jerking during motor spinning that occurs from repeatedly overcoming the attraction between the rotor magnets and stator structure.

The strength of a permanent rotor field cannot be controlled without so grid connection is done via power electronics, which increases upfront costs. However, with power electronics the machine is able to work over a wide speed range, with smooth speed and torque control [22]. For multi-pole machines, gearboxes can be omitted, resulting in a so-called direct drive. The simplified construction means lower weight and maintenance, which is of special importance in harsh marine conditions. These advantages together with recent developments in both magnet materials and power electronics have opened up possibilities for the construction and application of the PMSM [24].

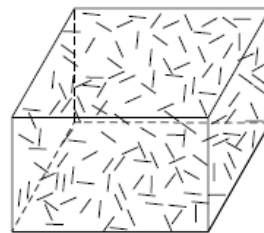
## 2.3 Composite materials

### 2.3.1 General

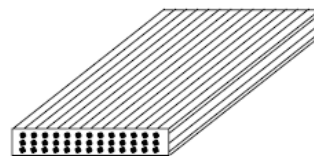
In this project thesis, the term *composite material* refers to a material consisting of reinforcing fibres embedded in a polymer matrix. The fibres give the material its strength, whereas the matrix binds, protects and transfers loads between the fibres. One layer of fibres is called a ply, and these can be stacked at different angles to form a laminate as illustrated in Figure 11 a). It is convenient to separate the properties of a ply into fibre and matrix dominated properties [25]. Depending on the combination of fibre type and orientation, resin and manufacturing method, a wide range of material properties can be achieved. An example from the lower range of properties is discontinuous fibre reinforced composites (Figure 11 b) [26]). In the higher end, we find high performance components made of unidirectional (UD) carbon fibre/epoxy (Figure 11 c)).



a) Stacking of several plies to form a laminate.



b) Discontinuous fibre reinforced composite.



c) Unidirectional ply

Figure 11: Basic types of composites.

Analyses to be performed later will study stresses in the local material coordinate system on the ply level. Figure 12 (adapted from [26], p. 19) illustrates the coordinate system used in this thesis. The fibre direction is referred to as 11, the matrix dominated transverse direction as 22, and through the thickness direction as 33. Max and min refers to tensile and compressive stresses respectively.

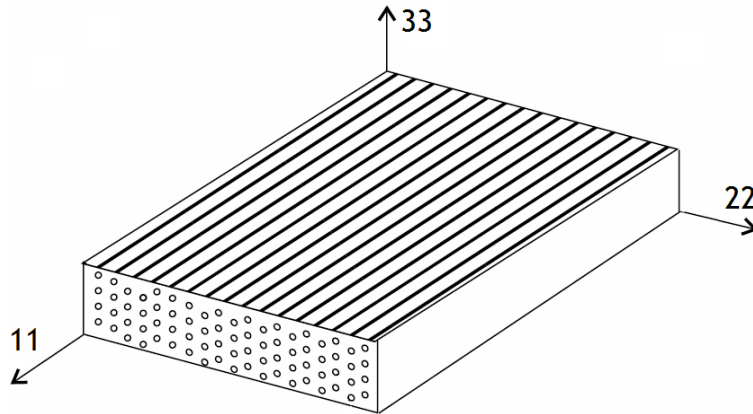


Figure 12: Material orientation in the local material coordinate system for each ply.

Common fibre materials are E-glass, carbon and aramid. Fibre controlled properties include strength and stiffness, toughness, impact resistance, fatigue and thermal properties [27]. Fibre volume fraction  $v_f$  is determined by manufacturing method and is measured in %. Higher fibre volume fraction means better mechanical properties.

For discontinuous fibre composites, there is a critical fibre length. For a given fibre diameter and resin, a certain fibre length is needed to utilize its strength. If fibres are shorter, the composite fails by interfacial failure or matrix cracking. With longer fibres the composite fails in tension, which is preferred [28].

The most common matrix materials are thermosetting polymer resins such as polyester-, vinyl ester- or epoxy. Resin controlled properties include fire retardancy, corrosion resistance, temperature resistance, hardness/abrasion resistance, thermal conductivity and electrical insulation [27]. Glass transition temperature  $T_g$  characterises a temperature where matrix dominated properties changes significantly [29].

Several mechanisms may contribute to local failure of a composite laminate, and they can be summarized as fibre failure, matrix cracking and delamination (see Figure 13 [30]). Matrix cracks often appears first, and a long lasting structure should not have stress levels leading to matrix cracking [31]. Fibre failure may arise in a number of ways from tension or compression overload, micro buckling or cracking from stress corrosion. Discontinuous fibre reinforced composites have similar failure processes except micro buckling and delamination [28]. The most frequent cause of failure in composite structures however, is not the composite material itself, but the assembly regions [32].

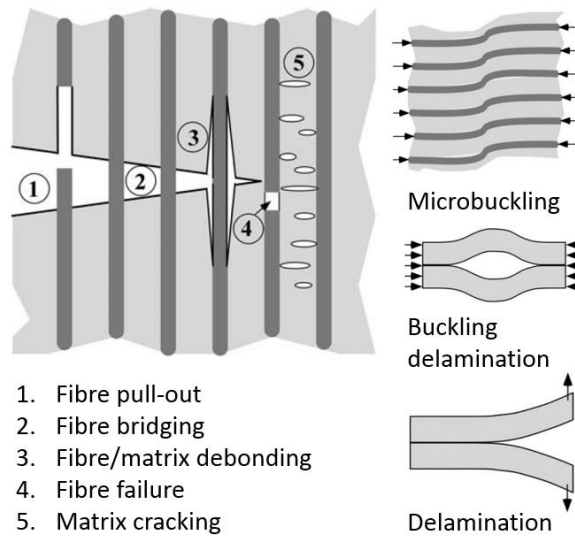


Figure 13: Composite failure modes.

More than 50 failure criteria for composites have been published, and principally they involve either the strain- or stress state, energy considerations, or a combination of these [33]. The most widely used ply failure criteria are maximum stress, maximum strain, Tsai-Hill and Tsai-Wu, and the first will be used here. Maximum stress is a relatively simple criterion commonly used for orthotropic and transversely isotropic materials. Normal stresses and shear stresses are compared to corresponding strengths, but interaction between stresses are not taken into account. Design criteria are further described in Section 4.5.1.

### 2.3.2 Composite materials for marine applications

Composites have been used for over 50 years by the small boat industry [32]. Large structures, such as boat hulls, are generally produced by wet hand layup or sprayup methods, using polyester resins formulated for room-temperature cure. Epoxy resins are used in applications requiring superior physical or mechanical properties. They may be cured at room temperatures, but for optimum properties, heat curing is necessary [34]. Infusion has become more common the recent years because of legislation to limit VOC [32].

Currently, the design methods for composite boats only take into account the quasi-static loading, and high safety factors are used to account for fatigue. For example, DNV recommends safety factors from 3-6 for the hull structural design for FRP and sandwich constructions [32].

Marine boring organisms do not attack GRP, and this may be ignored as a factor affecting the mechanical properties of these materials. However, like for all other materials, marine organisms will grow upon GRP surfaces, adding mass and increasing drag [34].

Composite materials are already widely applied for rotor blades in existing tidal turbine concepts, but there is a wide scope for expanding the use to include structural parts.

Even though this is not the case for the rotor studied here, the main motivation for using composite materials is often the mass reduction that follows from their high stiffness/mass ratio, and especially the high strength/mass ratio. Reduced mass in one component reduces the overall demands on the structure and thus further mass reductions are possible. Benefits of reduced mass in the rotor and turbine include:

- Smaller dynamic loads during braking and acceleration.
- Reduced need for buoyancy material
- Smaller lifting equipment and installation vessels



### 3 Reference Rotor and Concept Development

This chapter is based on the specialization project preceding this master thesis. A reference rotor and the result from the concept development process is presented.

#### 3.1 Reference rotor

The rotor provided by SmartMotor will be used as a reference for the work (Figure 14). Note that this illustration does not include stiffening plates inserted between the spokes of the support structure. Figure 15 shows the rotor assembly with some basic properties.

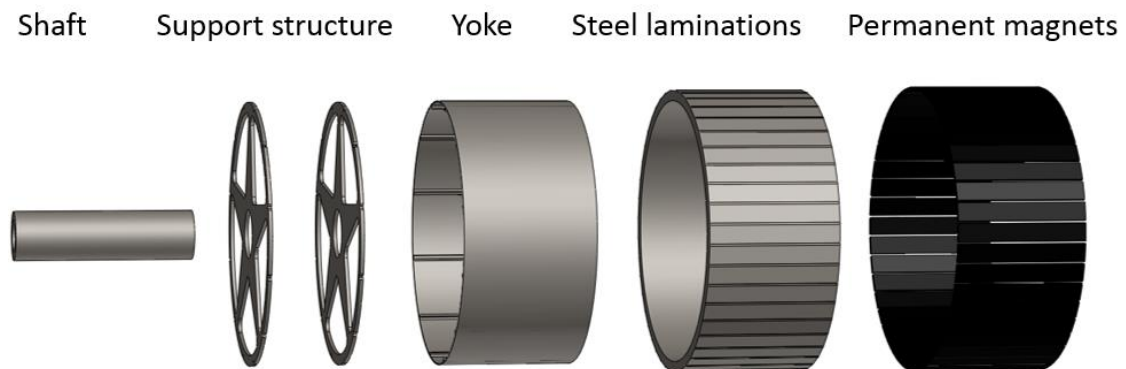


Figure 14: Exploded view of the reference rotor with essential component names.

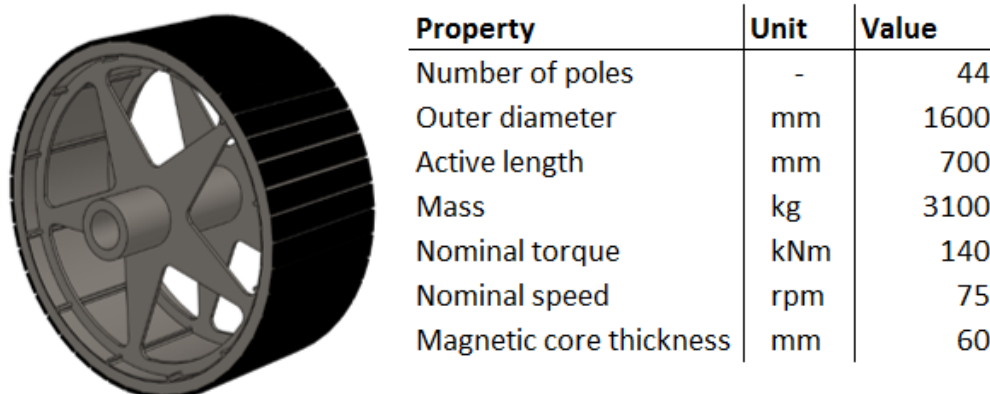


Figure 15: Illustration of the reference rotor with basic properties (CAD model by Høyland).

The structure, including shaft, support structure and yoke, is made of carbon steel. The shaft is turned to correct dimensions from a solid piece of steel. The support structure and stiffener plates are cut from steel plates. The yoke is made of a steel plate rolled into an annular (ring) shape. All parts are then welded together, and outer dimensions of the yoke are controlled by a final turning after welding.

The steel laminations are stacked on to the yoke and secured by slits and/or wedges. The laminations are covered with a thin layer of glue/isolation, which enables them to be adhered together by a heating process at 160 °C. Because of different thermal expansion factors, this cannot be done while stacked on a composite structure [4]. Finally, the permanent magnets are glued between the ribs in the magnetic core and retained by a wound layer of glass fibre.

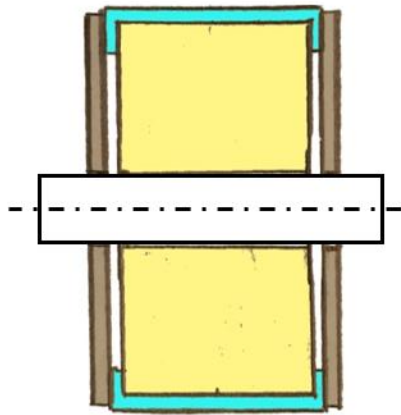
### 3.2 Concept development

A product requirement specification was made and used as input for the concept development (attached in Appendix A). Possible solutions to sub-functions were organized in a morphology matrix illustrated in Figure 16 (larger version in Appendix B).

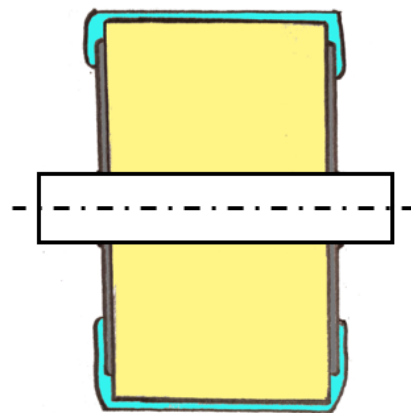
Solutions Sub-Functions	1	2	3	4	5	6	7	8	9	10
1. Yoke (and combined structures)	Harmonic wound or composite mounted	Polygon plates	Microcross infused	2 part infused and adhesive	Wound/infused	Partially wound outside lamination material of steel steel plates	Partially wound outside lamination material	Completely wound outside lamination material	Sprayed inside laminations	Radial enclosing
2. Yoke /structure interface	Adhesed oval brackets	Adhesed/infused radial brackets	Adhesed/infused radial brackets	Adhesed/infused radial brackets	Adhesed/infused radial brackets	Wound into ring	Wound into ring	Wound into ring	Adhesed to wound in support 2	Layer/terminated
3. Axial stiffness/ support structure	Infused disc	Adhesed rectangle	Adhesed T	Adhesed U or L	Sandwiched H, U or L	Sandwiched disc	Curved plates	Curved plates	Stiffer diameter plates	Circular struts
4. Axial stiffness/ support structure	Simple infused disc	Adhesed tapered disc	Tapered disc	Array of protruded profiles, (U, L)	Y-shaped	Y-shaped	Y-shaped	Y-shaped		
5. Support structure/ sub/shaft interface	Bolted/ adhesed simple	Bolted/ adhesed with disc	Bolted/ adhesed stress	Bolted/ adhesed, double shear disc	Screw/ adhesed, double shear plate	Bolted/ adhesed, double lap disc	Adhesed	Adhesed	Adhesed	
6. Yoke / lamination package interface	Concentric adhesed	Conically wound	Bolted keys	Axially sectioned yoke	Composed yoke	Sectioned laminations packages	Mounting in holes on yoke surface	Sprayed inside laminations		
7. Hole/ shaft interface	Splines	Keys	Interference, heat	Welded	Keyless fractional	Hubs				

Figure 16: Morphology matrix. Sub-functions on the vertical, solutions on the horizontal.

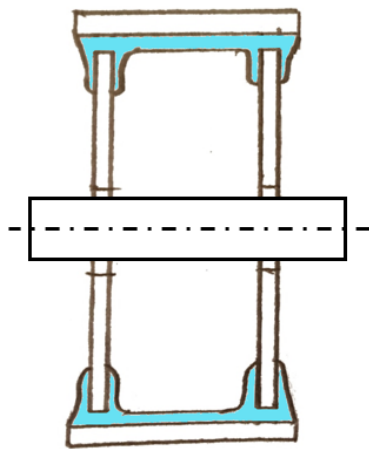
Solutions to sub-functions were put together into complete concepts, some of which are illustrated in Figure 17. These were evaluated, and it was determined to focus on the spray-up concept (Figure 17 c)).



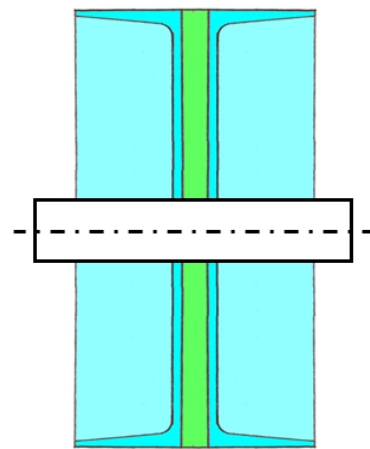
a) Fibres wound outside buoyancy material with discs adhered to the outside.



b) Fibres wound outside buoyancy material with discs inside winding.



c) Spray-up yoke inside magnetic core with disc lamination joints.



d) Two infused half-parts adhered together, possibly with a core for stiffness.

Figure 17: Illustrations of some proposed concepts.

### 3.3 Chosen concept

Simple analytical calculations indicated low stresses in the magnetic core/yoke interface, and this concept utilizes this fact by making the yoke of cheap chopped strand E-glass reinforced composite material. Figure 18 shows the chosen concept and part names.

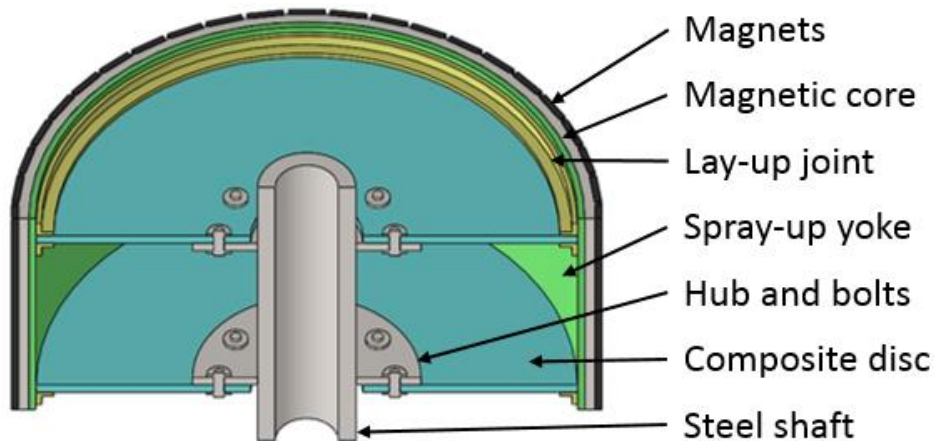


Figure 18: Cross section of the proposed solution.

In this concept, the magnetic core is used as a mould in which the yoke is made with spray-up, hand layup or a combination. The dimensions of the magnetic core must be correct at this point. The composite discs are made with a vacuum-bagged composite laminate of E-glass/epoxy (Figure 18). They are joined to the yoke with laminated joints, and to the shaft with a bolted connection via hubs. The spray-up parts of the process allows for some degree of automation as the assembly can be placed on rolls or a rotating table. A more detailed manufacturing and assembly procedure is proposed in chapter 10.

An initial FE-model was established to verify the feasibility of this structure concerning stiffness and strength. A yoke thickness of 20 mm and flat discs with 30 mm thickness were used. Generator torque and gravity loads were used. The results showed good margins for material strength, but low axial stiffness of the structure. Low stiffness caused large displacements in the axial direction, and an axial translation mode shape with a low natural frequency (approx. 10 Hz). The project report concluded that a better design philosophy must be established, and the stiffness of the structure must be improved to avoid large displacement and achieve a better structural efficiency. A more detailed structural analysis and engineering of the bolted joint is also needed.

## 4 Design Philosophy

Final design and verification of a composite rotor structure is likely to use DNV-standards such as DNV-OSS-312 Certification of Tidal and Wave Energy Converters [35] and DNV-OS-C501 Composite Components [25]. The latter will therefore be used in order to adapt a basic design philosophy and correct terminology. Following the standard in detail is outside the scope of this thesis and simplifications will be done.

### 4.1 Design philosophy and design principles

The basic approach used is the limit-state design method, with the following workflow:

1. Identify the functional requirements of the structure.
2. Consider possible failure modes for all the functional requirements.
3. Assign a limit state to all failure modes, which beyond the structure no longer satisfies the functional requirements.
4. Identify all failure mechanisms for all failure modes, and define a design equation for each failure mechanism. These are formulated in the so-called *Load and Resistance Factor Design (LRFD)* format, where partial safety factors are applied to the load effects and the resistance variables.

### 4.2 Design input

This section describes the input needed for the analysis of the composite structure, based on data provided by SmartMotor, results from the concept development phase and other assumptions. The substructure in question is the rotor structure for a tidal energy generator, as described in section 3.3. Components were named in Figure 18, and some properties are given in Table 1.

Table 1: Description of the rotor structure

Property	Value
Outer diameter	1600mm
Working length	770mm
Shaft diameter	280mm
Type of fibre in structure	E-glass
Type of resin in structure	Polyester and epoxy
Maximum composite surface temperature	60 °C
Nominal torque	140kNm
Design life	20 years
Yoke laminate	Hand/spray layup isotropic ply
Disc and stiffener ring laminate	UD/Quadrax vacuum bagged

#### 4.2.1 Phases and safety class definitions

The design life is divided into phases, and two phases are presented here. Only the operation phase will be considered further, but additional phases should be taken into account in future work. For each phase, the structure is assigned a safety class based on the consequences of failure. Safety class assignments are presented in Table 2.

Table 2: Design life phases and assigned safety classes.

Phase	Duration	Safety class	Comment
Construction	NR	Low	Small risk of human injury or environmental, economic and political consequences.
Operation	20 years	Normal	Small risk of human injury. Risk of significant economic consequences (potentially large number of devices).

## 4.2.2 Functional requirements

A functional requirement is defined as a requirement that the global structure has to fulfil. Functional requirements relevant for the operation phase are listed in Table 3.

Table 3: Relevant functional requirements for operation phase.

Functional requirement	Operation	Comments
Load carrying capacity	X	The structure must handle all loads in all phases.
Dimensional stability	X	The integrity of the generator relies heavily on dimensional stability.
Environmental resistance	X	Temperature range and aerated marine environment during construction and maintenance. Operation submerged in seawater.
Maximum vibrations	X	Excessive deformation caused by resonance must be avoided.
Electrical resistance or insulation	X	E-glass composite material is chosen for its non-magnetic properties. Not discussed further.

## 4.2.3 Failure modes

A failure mode is the manner in which one or several functional requirements fail. Table 4 presents an evaluation of possible failure modes for the structure laminates.

Table 4: Evaluation of failure modes for the structure laminates

Failure mode	Evaluation
Fracture (local and global)	Relevant
Buckling (local or global)	Relevant
Burst	NR
Leakage	NR
Impact	NR
Excessive deformation	Relevant
Wear	NR

Table 5 links the relevant failure modes to the functional requirements of the structure.

Table 5: Link between functional requirements and failure modes

Functional requirement	Failure mode	Comments
Load carrying capacity	Fracture	Shall always be checked
	Global, local buckling	Shall always be checked if compressive loads are present.
Dimensional stability	Excessive deformation, ovalization, excessive displacement.	Displacement, ovalization and eccentricity may lead to vibrations, lack of efficiency and/or stator collision.
Environmental resistance	Linked to all other functional requirements	Resistance to the environment is treated as a possible change to material properties that shall be considered in the evaluation of all other functional requirements.
Maximum vibrations	Excessive deformation. Part of general structural analysis.	Excessive deformation due to resonance leading to generator breakdown.

Failure modes shall also be linked to limit states, and here all failures modes are considered Ultimate Limit States (ULS). Access to a submerged tidal turbine is difficult, and maintenance should therefore minimised.

#### 4.2.4 Loads and environment

Loads are divided into functional, environmental and accidental loads. Only functional loads will be considered here. Loads provided SmartMotor are presented in Table 6, and these are assumed to be known with a COV = 0%. In other words, they are assumed exactly known without any statistical variation, and actual loads cannot under any circumstance exceed those values.

Table 6: Characteristic loads for the rotor structure

Load	Char. value	COV	Fatigue value	Fatigue cycles
Nominal Torque	140 kNm	0	0/140 kNm	$3 \cdot 10^4$
Radial gravity	2g	0	2g	$10^3$
Axial gravity	2g	0	2g	$10^3$

The design lifetime in cycles ( $N_R$ ) for the torque load was calculated assuming that the turbine exploits the tides in both directions. This particular turbine moves to position itself towards the tide, and the stress magnitude is therefore not reversed. The time between low and high tide is set to 6h 12.5m, and the design life in years is 20.  $N_R$  is then given by equation (1).



$$N_R = \frac{(365 \text{ d/y}) * (20\text{y}) * 24 \text{ h/d}}{6.2083 \text{ h}} = 28220 \approx 3 * 10^4 \quad (1)$$

The environment is the surroundings that impose no direct load on the structure. It is generally considered for its effect on the degradation of material strength. The environment is described in Table 7.

Table 7: Description of the environment of the structure

<b>Environment</b>	<b>Char. value</b>	<b>COV</b>	<b>Sustained value</b>
<b>Natural</b>			
Temperature external, construction	-20 °C to +30 °C	0	NR
Temperature external, operation	-2 °C to +30 °C	0	NR
<b>Functional</b>			
Temperature on composite surface	60 °C	0	NR
Exposure to seawater	-	-	Permanent

### 4.3 Failure mechanisms

A failure mechanism is the underlying phenomenon at the material level that determines the failure mode. Failure mechanism can be regarded as the cause of failure and failure mode as the effect. All failure mechanisms on the material level shall be identified, and those relevant for this structure are identified in Table 8. Failure mechanisms that are linked to critical failure modes shall be analysed, other failure mechanisms can be ignored.

Table 8: Link between failure modes and failure mechanisms for the structure laminates.

<b>Failure modes</b>	<b>Relevant failure mechanisms</b>	<b>Evaluation/comment</b>
Fracture, (local/global)	Fibre failure	Is assumed to cause fracture. Shall always be checked
	Matrix cracking	Is assumed not to cause fracture in isotropic and multi axial laminates. However, matrix cracks will accumulate and compromise long-term performance.
	Delamination	Delamination will not initiate before matrix cracks have formed. It is therefore a conservative choice to model the onset of delamination with the matrix cracking criterion (C501, Section 6, E201).
	Buckling	May cause fracture. Shall always be checked if compressive and/or significant in-plane shear loads are present.
	Unacceptably large displacement	It shall be checked that excessive displacement cannot cause fracture. No excessive displacements are expected for this structure.
	Stress rupture	Effect shall be checked for all failure mechanisms mentioned above. However, this is outside the scope of this thesis.
	Fatigue	
Buckling (local or global)	Buckling	Needs special analysis methods and special design criteria.
	Unacceptably large displacements	May lead to violation of displacement requirements. Only relevant if buckling can happen.
Excessive deformation	Unacceptably large displacements	May be caused by loads or resonance. Shall be checked to ensure air-gap is not closed, and magnets are kept aligned with stator windings.

Based on these tables the following failure mechanisms for the structure will be checked:

- Fibre failure – short term static
- Matrix cracking – short term static
- Buckling
- Unacceptably large displacements
  - From loads
  - From resonance

The critical failure mechanisms shall be linked to a failure type. Failure types are divided into plastic, ductile and brittle, based on the degree of pre-warning intrinsic to a given failure mechanism. Table 9 shows links for the failure mechanisms to be checked. The target reliability level shall be determined for each relevant failure type to obtain the right partial safety factors for the design criteria. Target reliability levels as specified in Section 2, C500 in C501 are also included in the table.

Table 9: Failure mechanism and failure type with target reliability level for operation phase.

<b>Failure mechanisms</b>	<b>Failure type</b>	<b>Target reliability level</b>	<b>Comments</b>
Fibre failure	Brittle	C	Table A2 Section 6
Matrix cracking	Plastic	B	Cracks bridged by fibres. Table A2 Section 6
Elastic buckling	Brittle	C	May lead to unacceptably large displacements or fracture (S6 A202).
Unacceptably large displacements	Brittle	C	The structure should never touch the neighbouring structure. S6 I103.

## 4.4 Material properties

The material properties used shall be the appropriate properties for the point of time where the analysis is carried out. This means that the effects of permanent static loads-, cyclic loads- and environmental effects should be taken into consideration. All strength properties are assumed to have a  $COV \leq 15\%$ .

The main disc and stiffener ring laminates are assumed made of E-glass/epoxy, and material properties was obtained from [29]. The yoke is assumed made of chopped strand E-glass/polyester, and material properties was obtained from Mullick [28] and some assumptions. The shaft and hubs are assumed made of weldable S355 construction steel. Degradation of the composite material properties will now be considered using C501.

The strength of a laminate exposed to permanent stress will be reduced to new residual strength, which may be estimated from stress rupture curves. This will not be considered here.

The modulus of elasticity tends to reduce under the effect of cyclic fatigue. The main reason for this is the formation and accumulation of matrix cracks. Fibre-dominated modulus is expected to drop by 10%. Matrix dominated modulus may drop to zero in tension, but with no change in compression. Fibre dominated static strength is not changed. Other properties are also expected to drop. Degradation of properties will happen after extensive cyclic fatigue exposure (about  $10^6$  cycles). This structure is only exposed to cyclic fatigue in the order of  $10^4$  cycles, so this is omitted.

Long-term exposure to water (more than 10 years) affects material properties. It is recommended that fibre dominated strength be reduced by 10%. Matrix dominated strength properties will have “some reduction” which should be measured, and elastic constants will have a “slight reduction”. Here, these are all reduced by 10%.

Temperatures up to  $20\text{ }^{\circ}\text{C}$  below the glass transition temperature ( $T_g$ ) causes no change to static elastic constants and strengths. The turbine will operate submerged in seawater ( $-2\text{ }^{\circ}\text{C}$  to  $+30\text{ }^{\circ}\text{C}$ ) and the yoke will reach a maximum temperature of  $60\text{ }^{\circ}\text{C}$  under operation. It is assumed that these temperatures will have no effect on material properties.

End-of life properties resulting from the preceding discussion are listed under “20 y water” in Table 10. The properties in the “new” columns are those obtained from the literature.

Table 10: Material properties used in this thesis.

Property	Unit	E-Glass/Epoxy		E-glass chopped strand/polyester		Steel
		<i>New</i>	<i>20y water</i>	<i>New</i>	<i>20y water</i>	
$\rho$	kg.m <sup>-3</sup>	1990	1990	1500	1500	7850
$v_f$	%	56.8	56.8	25	25	-
$E_{1T}$	GPa	44.6	40.1	7.0	6.3	210
$E_{2T}$	GPa	17.0	15.3	7.0	6.3	-
$E_{3T}$	GPa	16.7	15.0	4.0	3.6	-
$E_{3C}$	GPa	14.2	12.8	-	-	-
$G_{12}$	GPa	3.49	3.14	2.7	2.4	-
$G_{13}$	GPa	3.77	3.39	2.0	1.8	-
$G_{23}$	GPa	3.46	3.11	2.0	1.8	-
$v_{12}$	-	0.262	0.262	0.3	0.3	0.33
$v_{13}$	-	0.264	0.264	0.3	0.3	-
$v_{23}$	-	0.350	0.350	0.3	0.3	-
$\hat{\sigma}_{1t}^{fibre}$	MPa	980	882	83	74	355
$\hat{\sigma}_{1c}^{fibre}$	MPa	625	562	124	111	-
$\hat{\sigma}_{2t}^{matrix}$	MPa	28.1	25	83	74	-
$\hat{\sigma}_{2c}^{matrix}$	MPa	109	98	124	111	-
$\hat{\sigma}_{3t}^{matrix}$	MPa	21.2	19.1	-	-	-
$\hat{\sigma}_{3c}^{matrix}$	MPa	157.5	141.7	-	-	-
$\hat{\sigma}_{12}^{shear}$	MPa	51.9	46	70	63	-

## 4.5 Design criteria

A design criterion shall be assigned to each relevant mechanism of failure. The general form of the design criterion used in this thesis, and an explanation of its factors are given in equation (2) and Table 11.

$$S_k \cdot \gamma_{FM} \cdot \gamma_{Sd} \cdot \gamma_{Rd} \leq R_k \quad (2)$$

Table 11: Explanation of the factors in the general design criterion

Factor	Name	Explanation
$S_k$	Characteristic load effect	E.g. stresses from an analysis
$\gamma_{FM}$	Combined load effect and resistance factor	Accounts for the uncertainties in load effects and resistance. Simplified set (Section 3 I304) will be used because the loads were assumed exactly known without any statistical variation
$\gamma_{Sd}$	Load model factor	Accounts for inaccuracies, idealisations, and biases in the engineering model used for representation of the real response of the structure.
$\gamma_{Rd}$	Resistance model factor	Accounts for differences between true and predicted resistance values.
$R_k$	Characteristic resistance	E.g. material strength

Note that the design equation has been rearranged to have all factors on the left hand side for the ease of use. For example, some stresses ( $S_k$ ), obtained from a structural analysis are multiplied with the partial factors ( $\gamma_{FM} \cdot \gamma_{Sd} \cdot \gamma_{Rd}$ ). The product should then be less than or equal to the corresponding strength ( $R_k$ ).

Only linear analyses are to be performed, therefore all partial factors will be used to scale analysis input loads. I.e. the loads are increased in advance of an analysis, rather than load effects resulting from the analysis.

#### 4.5.1 Fibre and matrix failure – short term

C501 recommends using a strain criterion to check for fibre failures, but here a stress criterion will be used both for fibre and matrix failure to evaluate static strength. The criterion is given in equation (3), and partial factors in Table 12.

$$\gamma_{FM} \cdot \gamma_{Sd} \cdot \gamma_{Rd} \cdot \sigma_{nk} < \hat{\sigma}_k \quad (3)$$

Table 12: Factors used for the matrix and fibre failure criterion

Partial factor	Symbol	Value	Explanation
Local response of the structure in each direction.	$\sigma_{nk}$	-	Largest stress in each direction
Stress to failure in each direction	$\hat{\sigma}_k$	-	Strength values from Table 10.
Simplified partial safety factors	$\gamma_{FM}$	1.96	S8 B400. Safety class normal, failure type brittle. Strength COV $\leq 15\%$ .
Load model factor	$\gamma_{Sd}$	1.0/1.1	1 if FE methods are within assumptions, 1.1 if boundary conditions does not exactly represent the real conditions.
Partial resistance-model factor	$\gamma_{Rd}$	1.0	Linear analysis with degraded properties (S6 C202). Simple matrix criterion (S6 D201).

The criterion will be used for the bolted joint contact analysis and all global load cases. For isotropic materials such as the bolts, hubs and the shaft, the von Mises yield criterion will be used. This is readily available in the literature, e.g. [36].

Matrix and fibre failure must be checked at the ply level, not the laminate level, for both tensile and compressive stresses in all directions parallel to the fibres. In the FE-program, stress results will be displayed as contour envelope plots, showing the section point with the critical value in the selected direction for each element [37]. This is then checked for tensile (max) and compressive (min) value for all directions.

The bolt contact analysis will have a stress singularity in the bolt/bolthole contact point, and matrix cracking and delamination will occur. Special design criterions exists for these situations (see Section 6, C600 [25]), but this is outside the scope of this thesis and the criterion above will be used.

## 4.5.2 Buckling

C501 recommends using criteria applied at the level of local stress or strain to assess buckling-induced failure. Because only simple linear analyses will be performed here, a global buckling criterion proposed in equation (4) will be used. The partial factors used for fibre and matrix failure will be added to the loads in the analysis. The resulting eigenvalues (EV) from the analyses should then be higher than 1.

$$\gamma_{FM} \cdot \gamma_{Sd} \cdot EV > 1 \quad (4)$$

Table 13: Factors used for the buckling criterion.

Factor	Symbol	Value	Explanation
Lowest eigenvalue of the structure	$EV$	-	Resulting from the buckling analysis
Partial load effect factor	$\gamma_F$	1.96	S8 B400. Safety class normal, failure type brittle. Strength COV $\leq$ 15%.
Load model factor	$\gamma_{Sd}$	1.0	FE methods within assumptions.

## 4.5.3 Unacceptably large displacements

Collision between the yoke and the stator must be avoided, and the magnets must be in correct position for the generator to work. A maximum displacement criterion is defined to use for the yoke in the gravity load cases in equation (5).

$$\gamma_F \cdot \gamma_{Sd} \cdot d_n < d_{spec} \quad (5)$$

Table 14: Factors used for the displacement criterion.

Factor	Symbol	Value	Explanation
Local displacement in structure	$d_n$	-	Displacement results of the yoke
Specified maximum displacement	$d_{spec}$	2 mm	Chosen as a reasonable limit
Partial load effect factor	$\gamma_F$	1.96	S8 B400. Safety class normal, failure type brittle. Strength COV $\leq$ 15%.
Load model factor	$\gamma_{Sd}$	1.0	FE methods within assumptions, C501, Section 8 Table C1.

Avoiding unacceptably large displacements from resonance will be treated in Chapter 8.



## 5 Structural Joints in Composites

It is beneficial to design the joints first, and fill in the basic structure afterwards [38]. Joints are defined as load bearing connections between structures, components or parts, and there are three composite joint categories: laminated, adhesive and mechanical joints [25]. The latter includes fasteners, such as bolts, and these treated in chapter 6.

### 5.1 Laminated joints

Laminated joints are fabricated from the same constituent materials as the laminates that are jointed. The interface will have resin dominated strength properties, but it may differ from the through-thickness matrix properties of the laminate. This is because the joint may be a resin rich layer and the joint may be applied to an already cured surface instead of a wet on wet condition. These joints are very sensitive to peel conditions. Figure 19 shows a such a joint in a boat and provides some basic vocabulary (adapted from [39]). Pad/backing creates a radius, spreading the load and gives larger bond area.

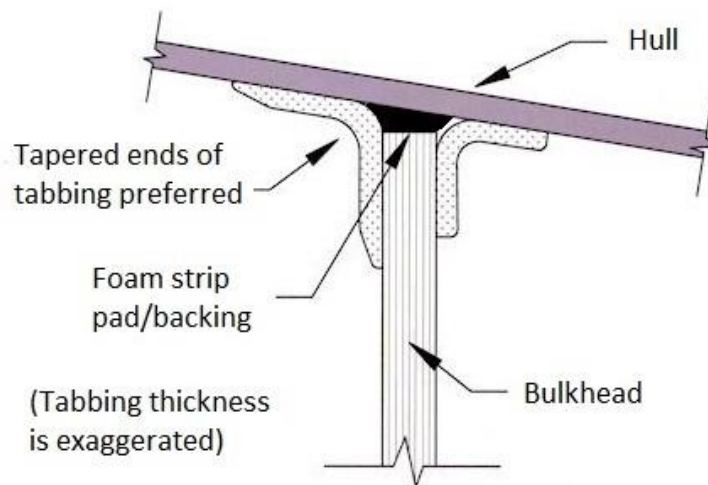


Figure 19: Typical laminated joint with pad/backing.

## 5.2 Adhesive joints

Adhesive joints are joints between laminates, cores or between laminates and other materials, which use an adhesive other than the laminate resin. These joints have the same issues as laminated joints. Adhesive bonding has potential of mass saving compared to mechanical fastening, and makes smooth surfaces possible. Figure 20 illustrates geometrical parameters in a single-lap adhesive joint: length of overlap ( $l$ ), adherend thickness ( $t_a$ ), adhesive thickness ( $t_g$ ). Other important parameters are adherend strength and elastic moduli, adhesive strength and elastic moduli, adhesive strength stress/strain characteristics.

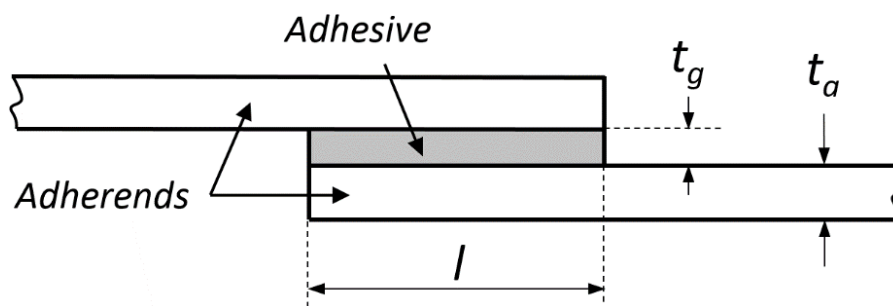


Figure 20: Geometrical parameters for a single-lap adhesive joint.

Figure 21 illustrates the three general failure modes: adhesive and cohesive debonding, and failure in the adherends (interlaminar failure, transverse and tensile). These can also occur in combinations [40].

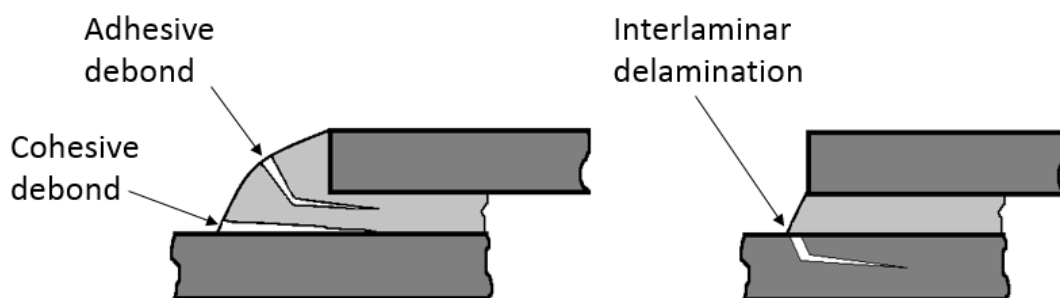


Figure 21: Fracture modes in adhesive composite joints.

Some general recommendation for adhesive joints are listed below.

- Joint strength is improved with higher adherent stiffness, and lower adhesive moduli [41]. A ductile adhesive is preferable to a brittle adhesive as this increase static and fatigue strength [41].
- Plies parallel to the load should be placed on the outside of the adherents [41].
- Fatigue resistance is increased with overlap length and using double overlap over single overlap [40].
- Stress concentrations at the ends of lap joints can be reduced with fillets and reverse taper at the end of the adherents [40].

Matthews et al. conducted a comprehensive review of adhesively bonded joints in FRP, and presents several analysis methods including classical- and FEA- linear and nonlinear, and experimental [41]. There is however, no general agreement about the method that should be used to predict failure, and safety considerations often require that adhesively bonded structures include mechanical fasteners as an additional safety precaution [42]. The use of results from small test specimens to design large joints are problematic, because all dimensions scale-up except the adhesive thickness. This increases stress concentrations and causes a change in failure mode and lower strength than expected. It is therefore not recommended to use design methods based on mean allowable adhesive shear strength [41].

### **5.3 Design approach**

The accepted design approach depends on the type of joint. The most practical approach regardless of joint type is likely to use a combination of analysis and testing, which is also needed for a valid assessment [25]. Effects of the environment should also be included in such tests [34]. The structure is now in an early design phase, and analytical approaches are therefore used.

Effects of thermal stresses and strains and displacements shall be considered for all joints and interfaces [25]. The temperature changes under production and operation of the rotor structure is small, and this will not be considered here.

## 5.4 Joint selection for the structure

Table 15 shows general guidelines for joint type selection [40]. The joints in the rotor are illustrated in Figure 22.

Table 15: General guidelines for joint type selection.

Bolted joints are used when	Adhesive bonding is used when
<ul style="list-style-type: none"> <li>• The structure is relatively thick</li> <li>• Service load level is high</li> <li>• Disassembly is required for inspection and repair</li> </ul>	<ul style="list-style-type: none"> <li>• The structure is thin or a large area is to be joined</li> <li>• Service load levels are low</li> </ul>

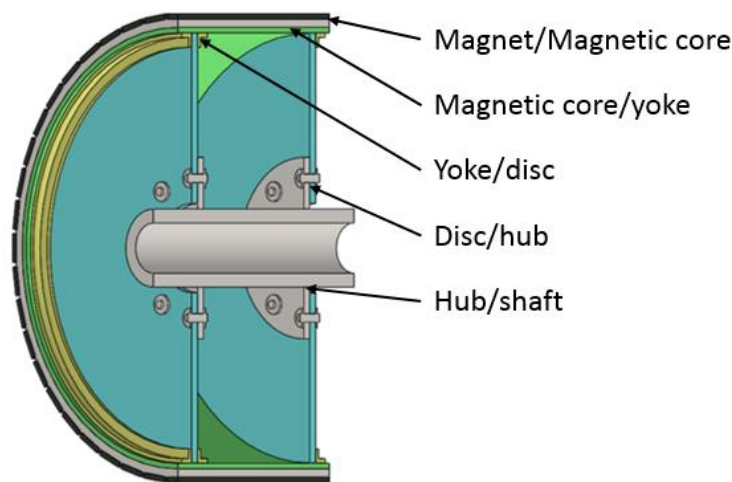


Figure 22: Joints in the structure.

Magnet/magnetic core joining procedures are already developed and not treated here

The magnetic core/yoke interface is made during layup of the yoke. The large surface area gives low shear stresses for this resin-dominated joint.

Yoke/disc joints have low stresses because of the large area sharing the load, and a laminated joint is chosen for this interface. This is discussed briefly in the following section.

The disc/hub joints transfers high loads between relatively thick members, therefore a bolted joint is selected as the main approach for this joint. A hybrid joint is also considered. This is treated in more detail in Chapter 7.

The hub shaft/joint can be made by welding, which will also ensure electric contact between the shaft, and the bolts if cathodic protection is used. Further details is not treated in this thesis.

## 5.5 Yoke/disc structural joint

A simple calculation based on elastic theory [36] is performed to predict the stress levels in the laminated joint. Maximum shear stress from torsion for a thin walled pipe is given by equations (6) and (7). Thickness ( $t$ ) is here the radial thickness of the laminated joint. It is assumed that only one laminated joint (one side of one disc) transfers 2 x nominal torque, effectively giving a factor of safety of 4 for a structure with two joints.

$$\tau_{max} = \frac{T}{I_p} r \quad (6)$$

$$I_p = 2\pi r^3 t \quad (7)$$

Table 16: Values for simple stress analysis

Property	Symbol	Value	Unit
Design torque	$T_{design}$	280 000	Nm
Radius	$r$	0.77	m
Thickness	$t$	0.05	m
Max shear stress	$\tau_{max}$	1.50	MPa

Maximum stress was found to be 1.5 MPa. This is low and a laminated joint seems feasible.



## 6 Bolted Joint Theory

The behaviour of bolted joints in composites differs considerably from what occurs with metals. Composites are brittle and stress concentrations will dictate the part static strength to a larger degree than for metals (no local yielding). As a result, composite joint design is more sensitive to edge distances and hole spacing's than metal joint designs [38]. There is no fundamental difference in the behaviour of the composite part in a composite-metal joint compared to a composite-composite joint, except the coefficient of friction and wear properties [40].

### 6.1 Configuration and geometry

Bolted joints can be made in a single- or double shear configuration (Figure 23). The latter halves the shear stress in the bolts and avoids out-of-plane bending moment, giving a better bearing load distribution over the boltholes. When one of the bolted members is very stiff, the effect of the out-of-plane load is minimized [43].

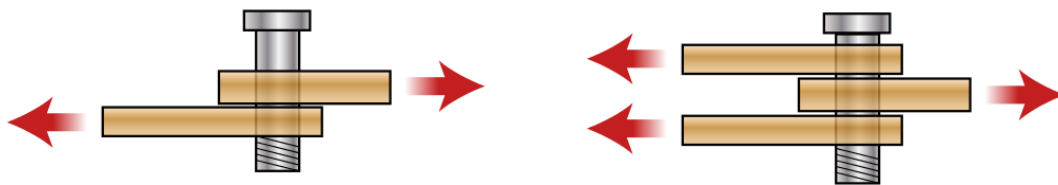


Figure 23: Bolt in single (left) and double shear (right). Image adapted from Wikimedia commons.

Bolted joints are divided into single- and multi row designs [38]. A multi row joint is illustrated with parameters in Figure 24. The nomenclature used here is the same as that used by Godwin and Matthews [44]. The bolted joint in the rotor differs from that of a standard lap joint. In a multi row lap joint, the shear force is different for each row of bolts because of buy-pass loads. In this joint, the shear forces from the torque load are transferred by an equal amount by each bolt from hub to the structure. A new set of geometry parameters for this joint are proposed in Figure 25. Further discussion of general theory will use the nomenclature from Figure 24, but links will be made to those presented in Figure 25.

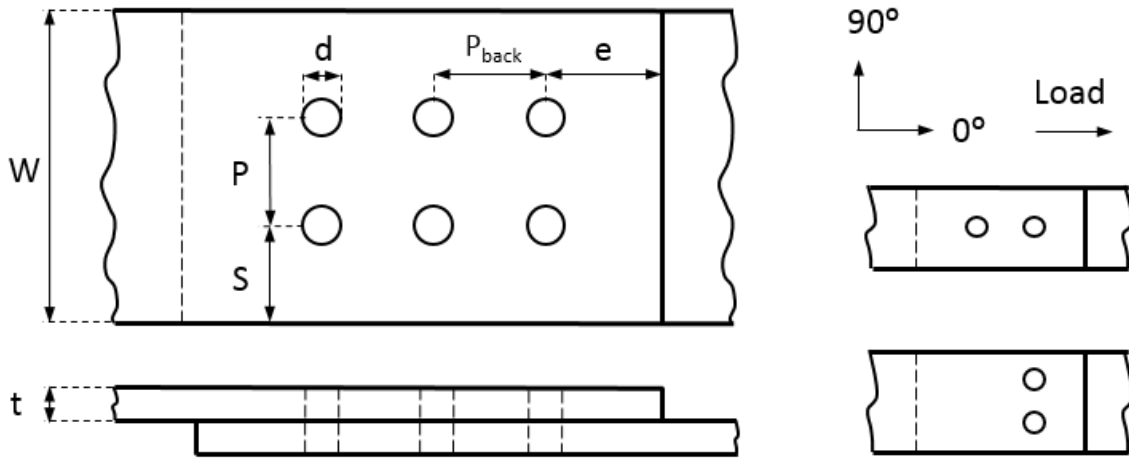


Figure 24: Geometry of a multi-row joint. One row joint (lower right) and one line joint (upper right).

$d$	Bolt/hole diameter
$t$	Thickness of laminate
$S$	Side distance, distance from side edge of laminate to first bolt centre.
$P$	Pitch, distance between bolt lines centre-centre.
$P_{back}$	Back pitch, the distance between rows.
$W$	Width
$e$	Edge distance, distance from centre of bolt to the edge of the laminate along the loading direction

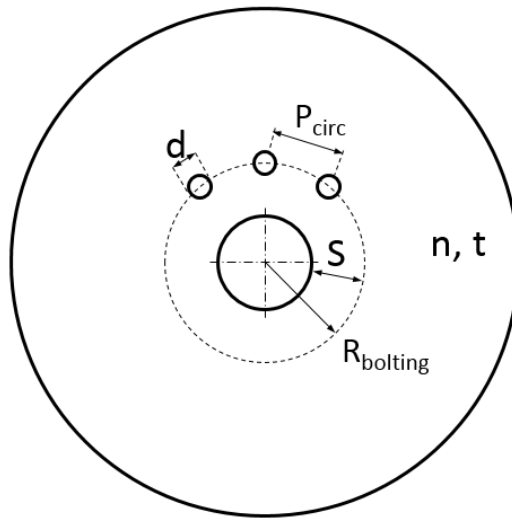


Figure 25: Geometry parameters and notation used for this joint in this thesis.

$d$	Bolt/hole diameter
$t$	Thickness of laminate
$S$	Side distance, distance from side edge of laminate to bolt centre
$P_{circ}$	Circumferential distance between bolts, determined by $R_{bolting}$ and $n$
$n$	Number of bolts
$R_{bolting}$	The radius of bolting



## 6.2 Failure modes in bolted laminates

Failure modes for a standard composite joint are illustrated in Figure 26. The predominant failure mode is usually determined by the geometric factors ( $W$ ,  $e$ ,  $d$ ,  $t$ ). These failure modes will be discussed in the following sections, together with simplified formulas (adapted from [45]) for calculating laminate loads. These formulas are applicable only to one-bolt joints (see Figure 26 for an illustration).

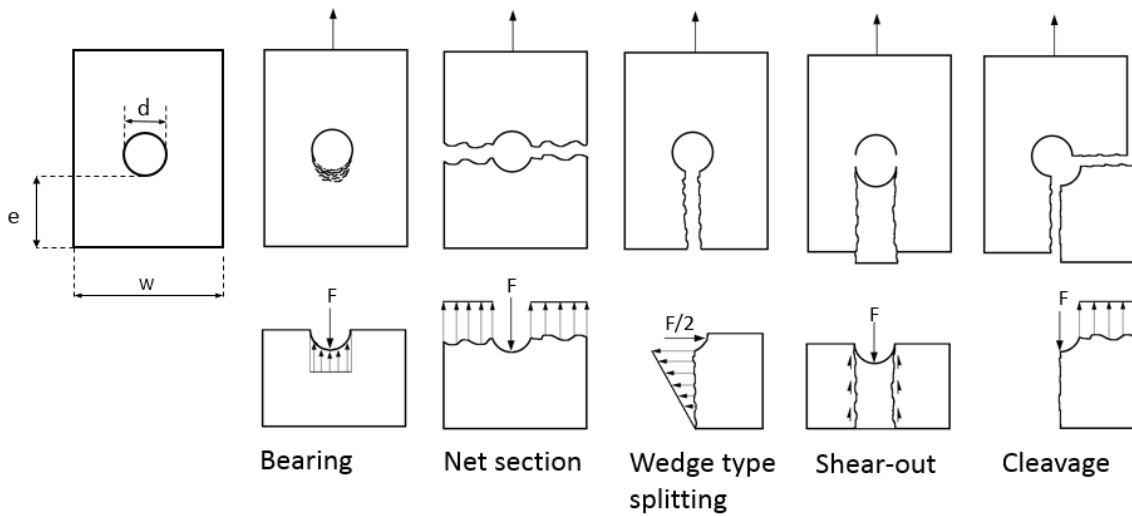


Figure 26: Failure modes in bolted composite joints.

Bearing failure modes are characterized by a local laminate compressive failure caused by the bolt diameter which tends to crush the composite material [45]. Laminate crushing gives mushrooming and delamination of the laminate [46]. This is a common failure mode for one-row joints. Equation ( 8 ) gives a simple estimation of the local bearing load.

$$N_x = \frac{F_{bolt}}{d} \quad (8)$$

A more conservative approach is to use a cosine distribution of the load across the bolt hole, as given by equation ( 9 ).

$$N_x = \frac{\pi F_{bolt}}{2 d} \quad (9)$$

Net section is failure in tension or compression in the cross section between the bolts. Net-section strength is a function of both joint geometry and composite material strength. The laminate load can be calculated using equation ( 10 ), where  $K_t$  is a stress concentration factor.

$$N_x = \frac{F_{bolt}}{(w - d)} K_t \quad ( 10 )$$

Wedge-type splitting is characterized by laminate splitting, which starts at the local bearing point and propagates to the free edge. These failure modes are caused by the lateral pressure of the bolts against the laminate [45]. The laminate transverse load is given by equation ( 11 ).

$$N_y = \frac{2F_{bolt}}{(2e - d)} \quad ( 11 )$$

Shear out failures are characterized by a shear-out part of the laminate ahead of the bolt [45]. It occurs because the bolt is too close to the edge [44], and joints are usually designed to avoid this brittle mode of failure. The laminate load is given by equation ( 12 ).

$$N_{xy} = \frac{F_{bolt}}{2e} \quad ( 12 )$$

Tension with shear-out failure is a combination of net-section and shear out failure. This mode can be avoided by selecting an appropriate edge distance and layup [47].

Bolt failure is a result of high shear stresses acting in the bolt shank. This is avoided by selecting a sufficient bolt diameter. An additional failure mode is bolt pull-out, which is characterized by the bolt being pulled through one laminate, and can be avoided by choosing a sufficient washer diameter.

## 6.3 Effects of parameters

The strength of a load-carrying joint in composites is affected by a large number of variables. Joint parameters such as end distance ( $e$ ), width ( $W$ ) and pitch distance ( $P$ ) are usually measured in ratios showing their dimensions relative to the diameter of the hole. Recommendations of these and other parameters are collected from the literature.

### 6.3.1 Thickness of laminate

Small  $d/t$  values will give failure of the bolts in shear. Large values decrease the bearing strength of the joint, leading to bearing failure [47]. Some recommendations from the literature are: Higher than 1 [48], higher than 1.2 [47], 0.75-1.25 [38], less than 2 [46], 1 for GFRP thicker than 2-29mm [34]. It is chosen to use a  $d/t > 1$ .

### 6.3.2 Width of joint

As the width of the specimen decreases, there is a point where the mode of failure changes from bearing to net section. Minimum values of  $w/d$  ratios reported from the literature are 3 [47], 3.2 [48] and 4 (0/+45 layup) [44]. These values are not directly transferable to the joint in question, but will be used as a guide for choosing the inner and outer radius of the bolted area. There should be at least  $2d$  radial distance to each side, written as  $S/d > 2$ .

### 6.3.3 Edge distance

As the edge distance decreases, the failure mode changes from bearing to shear-out. The layup will also affect this, and not only the end distance [47]. Recommendations for  $e/d$  from the literature: optimum value of 4 [49], 1.2-3 [47], higher than 3 [44] higher than 4.5 (0/±45 layup) [38]. It is assumed that edge distance is comparable to the circular pitch distance between the bolts for the joint in question. This would be very conservative, and an  $e/d > 3$  is chosen, here written as  $P_{\text{circ}}/d > 3$ .

### 6.3.4 Pitch distance

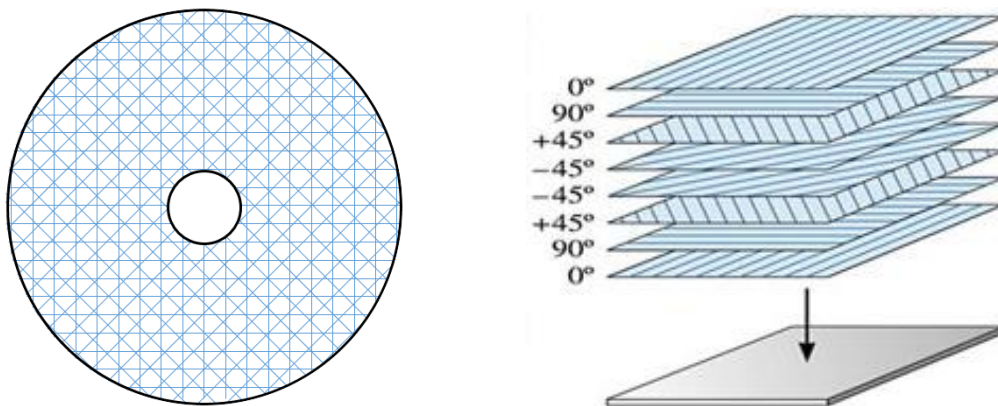
A minimum spacing between adjacent bolts is necessary to prevent premature net section failure. Like  $w/d$  ratios, typical pitch distance ( $p/d$ ) ratios for structural composites are 4-6 [46], and up to 5 [47]. This ratio is for multi-row joints, and is therefore not applicable to this joint.

### 6.3.5 Layup

Layup affects both the joint strength and the mechanism of failure [48]. The most efficient layups for mechanical fasteners are those that are nearly quasi-isotropic [47]. Mosallam suggests max 40% in each direction [47]. Tsai recommends 30-64% ±45°, 25-60% 0° and

minimum 10%  $90^0$ . The best fibre patterns are fully interspersed (parallel plies not bunched together) and have at least 12.5% of the plies in each of the four directions  $0^0$   $+45^0$ ,  $90^0$  [47].

A practical way of manufacturing the laminate for this joint is a vacuum infused hand layup. A  $[0, 90, +45, -45]_s$ , fully interspersed, quasi-isotropic layup, with an equal ratio of fibres in all directions is chosen (see Figure 27. Figure 27 b) is adapted from www.quartus.com). This sequence is repeated until target thickness.



a) Flat disc with a  $[0, 90, +45, -45]$  layup. b) Stacking of a  $[0, 90, +45, -45]_s$  quasi-isotropic laminate.

Figure 27: Illustrations of chosen layup.

### 6.3.6 Clamp-up force/pretension

Increasing bolt pretension, or clamp-up force, increases the bearing strength [44], as a larger part of the applied force can be transferred by friction between the joined parts. This capacity increase is attributed to the effect of the lateral restraint provided by the washer and the frictional resistance against joint slip [47]. There is however an upper limit at where above the washers will dig into the face of the laminate and cause damage. Positive effects of clamp-up are even more clear under fatigue loading [38]. However, in the design, pins should be used (non-clamped), because the clamp up force may be relaxed with service usage [38].

### 6.3.7 Washers and bolt hole clearance

Washers are used to reduce the risk of bolt pull out, and reduce contact pressures on the laminate from clamp up and bending moments [46]. Washer size is also called head/tail

restraint [38]. For pultruded composites, a washer size of  $2d$  is recommended for bolts in shear [50], and it is assumed that this is also suitable for this application. The washer size can influence strength but it is more important that the hole in the washer (ideally, reamed) should be a close fit to the bolt [44]. Any variation in clearance between the different holes implies that load is shifted to the fastener where the smallest clearance occurs [51]. A sleeve/bushing is sometimes used between the bolt and the composite borehole, which can deform and distribute the load better.

### **6.3.8 Hybrid joints**

A bolted joint combined with an adhesive can gain mechanical resistance of 20-30% [46]. This because stress concentration at the bolt/hole zone are minimized due to better stress distribution between the connected elements [47]. However, considering the cumulative strength of fasteners with different stiffness is not advisable, and is for example explicitly forbidden in the Eurocode for timber structure design [52]. Another advantage of combined joints is that the clamping force exerted by the bolt/nut/washer system can be used for the curing process of the adhesives [47]. Naturally, this comes with the penalty that the joint cannot be disassembled. A hybrid joint solution will be discussed in section 7.4.3.

## **6.4 Design practice, failure criteria and factor of safety**

According to [38], accepted design practice is to select edge distance, plate thickness, and fastener diameters, so that only net section and bearing remains as probable failure modes. There is no consensus whether the joint should fail in net section or bearing, but bearing failure is much less catastrophic. If it can be showed a margin against both failure modes, then the joint is sufficiently strong.

For this joint net section is judged less likely, and therefore only bearing failure should remain as a possible failure mode. A commonly used failure criterion for bearing strength is bearing yield, defined either as the load at either 0.02d or 0.04d displacement of the bolt/pin [38].

DNV-OS-C501 offers no detailed guidance on the design of bolted joints. It is however recommended that the joint be designed in a way that its performance is independent of the matrix. This way matrix cracking or degradation of matrix properties are not important for the performance of the joint. The design here will be based on judging the stress field around the bolthole calculated by FE models.

Practical approaches exists for specific applications such as structural design with pultruded FRP profiles. The manufacturer Fiberline offers a guide [50] based on EUROCOMP design code [53], where straightforward tables are provided for the most common bolt configurations. These are however not directly transferable.

## **6.5 Stress concentration**

Introducing holes creates stress concentration factors, and for composite parts, this reduces the fracture resistance of 40-60% in tension, and 15% in compression, compared to a region without holes, depending on layup and hole size [46].

## **6.6 Fatigue performance**

With few exceptions, bolted composite joints have excellent performance under tension-tension fatigue loading conditions. The major exception to this is in the case of joints with loose boltholes, particularly under reversed cyclic loading conditions. Well-designed bolted composite joints are not sensitive to cumulative damage under fatigue loads [47]. Protruding heads are preferred over countersunk heads [40]. Metallic bolted joints are usually more critical in fatigue than in ultimate static strength. The reason is that local yielding redistributes the loads and therefore alleviates local stresses. In contrast, bolted composite joints are more critical in static strength, with little degradation from fatigue loads. Gentle

tensile-tensile fatigue of interference fit bolts may even increase residual strength because of the progressive relief of stress concentrations [47]. As the applied fatigue load approaches the quasi-static strength, the failure mode will become the same in fatigue as in quasi-static loading. As the applied fatigue load decreases the failure mode of the changes to bolt failure.

## 6.7 Summary

Literature on bolted joint theory was reviewed and relevant issues presented. The most important findings are as following:

- Double shear configurations gives better bearing load distribution in the boltholes than single shear.
- Geometry recommendations for simple joints are not directly transferrable to this joint. Adaptations have been suggested.
- Classical analytical approaches was found inapplicable to the bolted joint in this structure. An FE-analysis seems like an appropriate option.
- Hybrid joints have increased mechanical resistance, but one should not calculate with cumulative strength.
- Bolted composite joints with interference fit have excellent performance under tension fatigue loading conditions.

Table 17 summarises other recommendations for bolted joints.

Table 17: Summary of recommendations for bolted joints

Parameter	Value	Comment
d/t	min. 1	Laminate thickness equal to or smaller than bolt diameter
S/d	min. 2	Determines inner and outer radius of bolted area
P <sub>circ</sub> /d	min. 3	Bolts to be spaced more than 3d apart
Layup	[0, 90, +45, -45]s	Repeated for maximum interspersion
Clamp-up	beneficial	Not to be included in analyses
Washers	2d	Include in analysis
Bolthole fit	snug fit	Tight, snug-fit, also for washer hole





## 7 Bolted Joint Design

### 7.1 Concept description

A bolted joint in single shear configuration without adhesive joining, bushings and pre-tension will be analysed. This is considered the worst case for the joint geometry, and will be investigated before considering concepts that are more complicated. Some alternative concepts for the joint will be discussed towards the end of this chapter. Figure 28 illustrates the preliminary structure with detailed views of the bolted joint area.

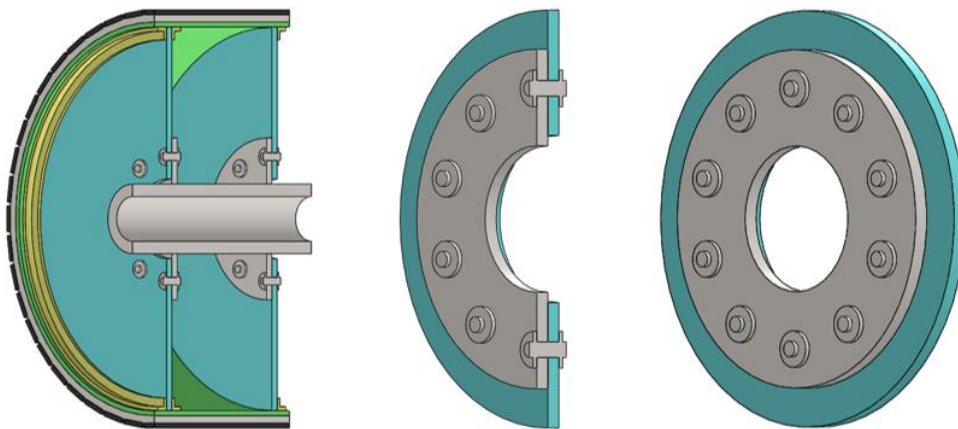


Figure 28: Illustration of preliminary rotor concept and detailed views of bolted area.

### 7.2 Bolt selection

#### 7.2.1 Material

Highly dynamically stressed connections in similar applications such as wind turbines often use pretensioned bolts of grade 8.8 or 10.9 [54]. Bolts for submerged structural applications shall not exceed ISO 898 [55] strength class 8.8, because of susceptibility to HISC under cathodic protection [56]. Therefore, carbon steel bolts of strength class 8.8 with yield strength and ultimate tensile strength of 640MPa and 800 MPa respectively are chosen for this joint. This must later be verified for compatibility with the chosen means of corrosion protection.

#### 7.2.2 Bolt fatigue

The bolts must survive the torque-load fatigue cycles. Eurocode 3, Part 1-9 [57] is used to calculate their fatigue limit. For constant amplitude nominal shear, fatigue shear-stress

ranges,  $\Delta\tau_R$ , can be obtained from equation (13). A fatigue stress range is the algebraic difference between the two extremes of a particular stress cycle.

$$\Delta\tau_R^m * N_R = \Delta\tau_C^m * 2 * 10^6 \quad (13)$$

The cut-off limit  $\Delta\tau_L$  is the shear stress range for which below the component can withstand an unlimited number of cycles. This is obtained from equation (14).

$$\Delta\tau_L = 0.457 * \Delta\tau_C \quad (14)$$

$N_R$  is the design lifetime expressed as number of cycles related to a constant stress range (calculated in section 4.2.4). The detail category for bolts in single shear has a reference fatigue strength,  $\Delta\tau_C = 100$  and  $m = 5$ . Results are presented in Table 18. See Appendix C for S-N curves and detail category description.

Table 18: Results from fatigue stress range calculations for the bolts.

Property	Symbol	Value	Unit
Cut off limit shear stress range	$\Delta\tau_L$	45	MPa
Fatigue strength shear stress range	$\Delta\tau_R$	231	MPa

The bolt shear stress is zero at the turn of a tide, and must be limited to a maximum of 231 MPa. This equates to a resolved von Mises stress of 400 MPa. The fatigue limit will determine the necessary bolt cross sectional area at a given bolting radius. Any pretension/clamp up will only offset the stress range, and not change its magnitude and is therefore not included here. The resolved von Mises stress in the bolts from shear and pretensions must however be checked for yielding.

### 7.2.3 Diameter and number

Diameter and number of bolts will be determined by the calculated fatigue shear stress range and the bolting radius, while respecting the previously discussed geometric parameters such as p/d, s/d and t/d ratios. Bolting radius is a trade-off between bolt loads, bolt dimensions, accessibility to the bolts, side distance and mass of the hub.

The nominal torque load is multiplied with partial factors to obtain the design torque load.

Torsional flexibility in the shaft between the hubs causes considerable difference in the stresses experienced by the discs. A 75% - 25% torque load distribution between the two discs is assumed, and accounted for using  $\gamma_{distribution} = 0.75$ . Simplified partial safety factor  $\gamma_{FM} = 1.96$  from section 4.5.1. A load model factor ( $\gamma_{Sd}$ ) of 1.1 is used as the boundary conditions does not exactly represent the real conditions. The design torque ( $T_{design}$ ) for the highest loaded disc is then obtained from equation (15):

$$T_{design} = T_{nominal} * \gamma_{distribution} * \gamma_{FM} * \gamma_{Sd} \quad (15)$$

$$T_{design} = 140kNm * 0.75 * 1.96 * 1.1 = 227 kNm$$

The relation between bolt load ( $F_{bolt}$ ) design torque ( $T_{design}$ ), bolting radius ( $R_{bolting}$ ), and the number of bolts ( $n$ ) is given in equation ( 16 ).

$$F_{bolt} = \frac{T_{design}}{R_{bolting} * n} \quad (16)$$

The relation between shear stress in bolts in single shear ( $\tau_{bolt ss}$ ), bolt load ( $F_{bolt}$ ) and the bolt shank area ( $A_{bolt}$ ) is given in equation ( 17 ).

$$\tau_{bolt ss} = \frac{F_{bolt}}{A_{bolt}} = \frac{4F_{bolt}}{\pi d^2} \quad (17)$$

Results for three bolting radiuses and five bolt diameters are given in Table 19. Bolt diameters were chosen from the ISO 261 list of preferred sizes [58].

Table 19: Minimum number of bolts for different bolting radiuses and bolt diameters

Bolting radius R [m]	Bolt diameter d [mm]				
	16	20	24	30	36
R = 0.20	24	16	11	7	5
R = 0.25	20	13	9	6	4
R = 0.30	16	10	7	5	3

## 7.3 Bolt contact analysis using FE

Classical laminate theory provide tools for predicting the strength of laminates, and this can be combined with formulas presented in section 6.2 for simple one-bolt problems. These methods are not applicable here. The local response of the structure in the bolted joint area will be studied using a linear static FE contact analysis.

The objective of the analysis was to obtain a joint geometry, which handles the stresses from the generator torque. The angle between load direction and fibre orientation will change along the circumference, and therefore the whole disc will be modelled.

### 7.3.1 Approach and assumptions

- Simulation tool: Abaqus /CAE 6.12-1 run on a Windows 8 operative system.
- Model type Standard & Explicit, with linear elastic materials based on engineering constants.
- Large deformations are ignored in this analysis.
- The design torque of 227 kNm calculated in section 7.2.3 is added separately in a single load step of type linear perturbation, static, general.
- Failure criterion from section 4.5.1.
- This analysis will have a stress singularity in the bolt/bolthole contact point and matrix cracking may occur locally. The design will be accepted when its extent is sufficiently small.
- Snug fit between bolts and boltholes.
- Layup as concluded in section 6.3.5.
- No pretension of bolts as discussed in section 6.3.6.
- Washers modelled as part of the bolts with an outer diameter of  $2d$  as described in section 6.3.7.
- Hub welded on to the shaft with a through the thickness weld, modelled with a fixed BC.

Several combinations of bolt number (12-16), bolt diameter (24 -30mm) and composite disc thicknesses (20-30mm) were investigated. Only the final model will be presented.

### 7.3.2 Units, dimensions, mesh and material

Only SI-units were used in the model. Part dimensions in meters are shown in Figure 29.

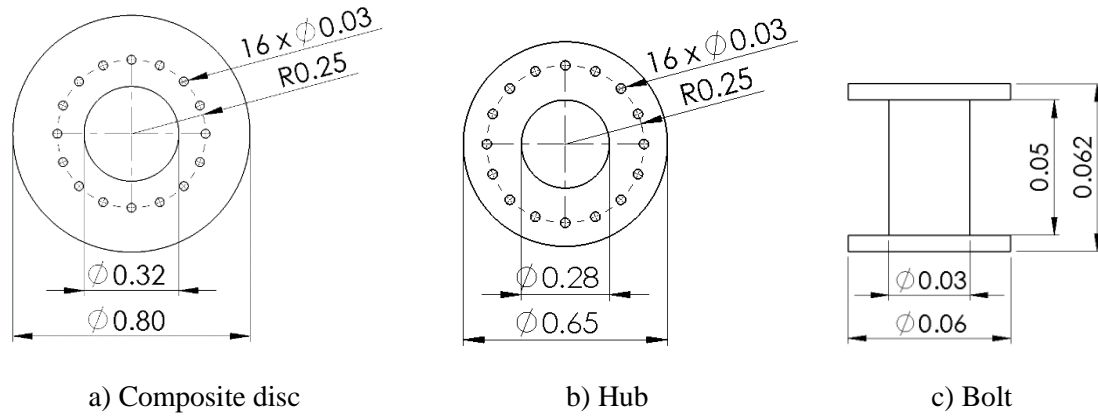


Figure 29: Part dimensions [m].

### 7.3.3 Mesh and material

The disc and the bolts were modelled as solid isotropic steel parts. The composite disc were modelled as a solid part with a  $[0, 90, +45, -45]$ s layup. Material assignment is summarised in Table 20.

Table 20: Materials used in the parts

Part	Material	Property assignment	Comment
Discs	E-glass/epoxy	Composite layup	$[0,90,+45,-45]$ s
Hub	Steel	Homogeneous section	
Bolts	Steel	Homogeneous section	

Solid element were used as detailed through the thickness-results are needed. C3D6 linear wedge elements with sweep technique were used for the centre part of the bolt (yellow colour in Figure 30 a)). The rest of the bolt was meshed with C3D8R linear hexahedral elements with structured technique.

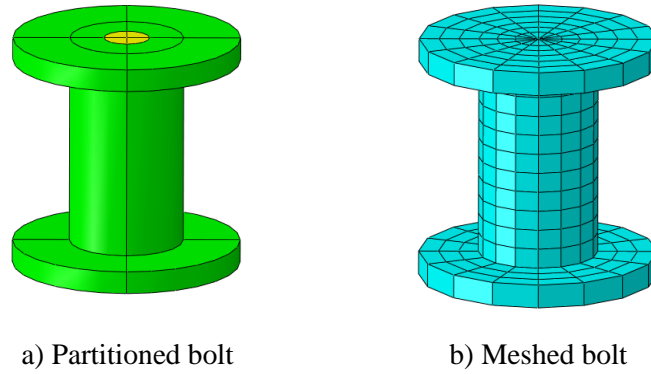


Figure 30: Bolt partitioning and mesh

Both discs were meshed with C3D8R linear hexahedral elements with sweep technique with advancing front (yellow in Figure 31 a)), and structured technique around the holes (green in Figure 31 a)). Partition circles with 40 mm diameter were made around the bolt-holes to enable local mesh refinement. Figure 33 shows mesh details in a section view of the assembly. Both discs has some mesh distortion in the area between the partitioning around the boltholes. It is assumed that this will not influence the results close to the bolt-holes, which are of interest here.

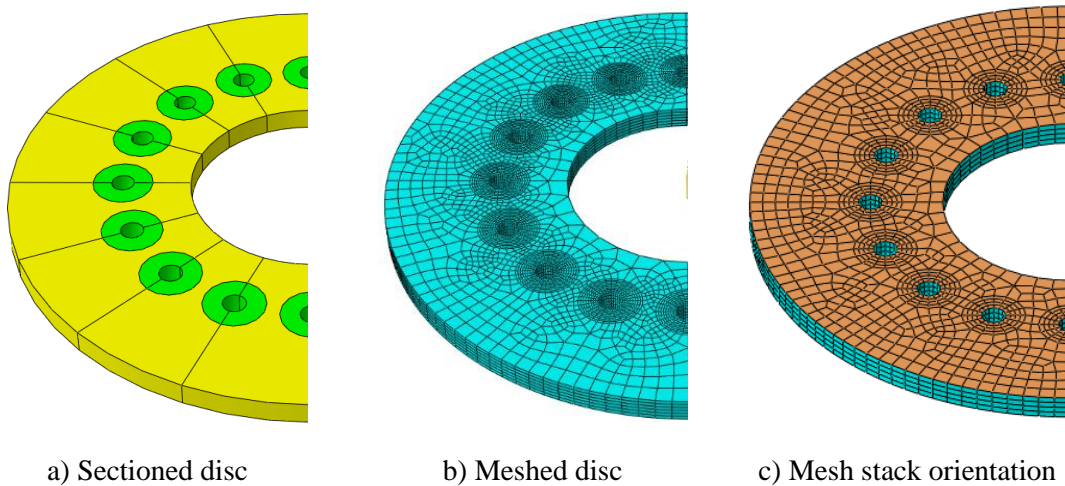
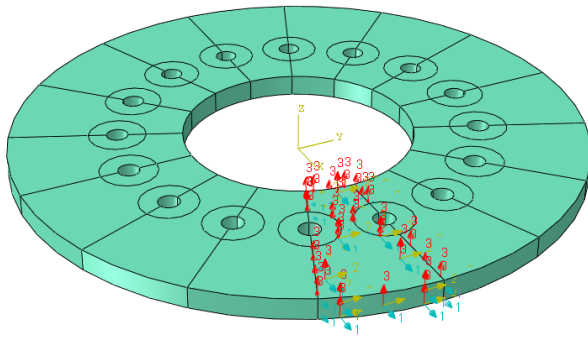
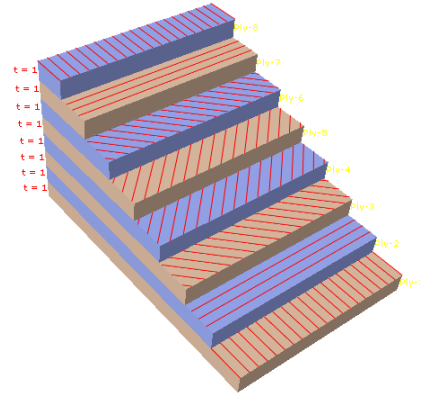


Figure 31: Disc partitioning, mesh and stack orientation.



a) Layup orientation



b) Ply stack plot.

Figure 32: Material and layup orientation for the composite disc.

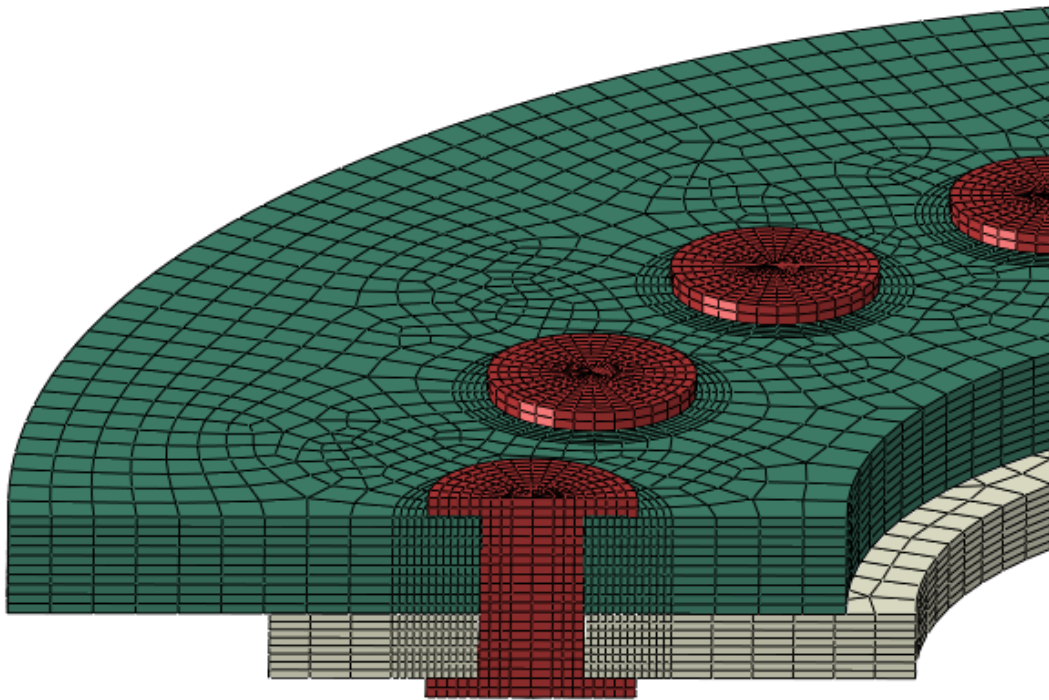


Figure 33: Section view of the meshed parts. Steel disc in grey, composite disc in green.

Solid composite layups are expected to have a single element through the entire thickness of the regions specified in the composite layup. When several elements are used through the thickness, each element contains the multiple plies defined in the ply table [59]. This is acceptable here because the layup is quasi isotropic, and a real laminate would also contain several repeated layers of the specified layup.

### 7.3.4 Interactions, loads and boundary conditions

A surface-to-surface contact interaction was defined between the bolts and the composite disc (see Figure 34 and details in Appendix D). This type of interactions describe contact between two deformable surfaces [59]. When specifying contact interaction properties there is a trade-off between accuracy (accurate transmission of forces from one component to the other) and solution robustness (avoiding solution convergence issues). Recommendations from [60] were used, and these are summarized below.

- Interaction type: surface-to-surface contact. Using the bolt surface as the “master surface” and the composite laminate surface as the “slave surface”. This prevents over-closure issues when the bolt is pressed into the softer composite laminate.
- Sliding formulation: small sliding. This gives better convergence behaviour in exchange of some loss of accuracy. With little relative tangential movement, as is the case for bolted joints, this gives minimal loss of accuracy.
- Slave adjustment: adjust only to remove over-closure. This will adjust the nodes on the slave surface to avoid initial over-closures.
- Contact properties – Tangential behaviour – Penalty. This prevents the bolt from spinning about its axis. A typical metal-composite friction coefficient of 0.2 were used.
- Contact properties – Normal Behaviour – Hard contact. This is the most accurate normal behaviour contact property for the interaction between a bolt and a composite laminate.

An additional surface-to-surface interaction was defined to prevent the steel and the composite disc from overclosing. The steel disc was chosen as the hard surface, and the same interaction properties as above were used.

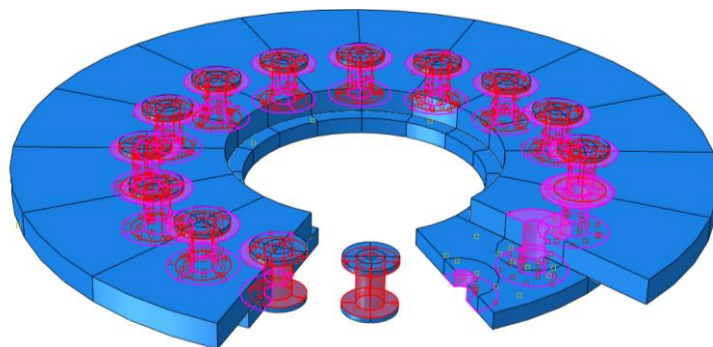


Figure 34: Surface to surface contact in the assembly.



The outer surface of the composite disc was coupled to a RP to which the design torque load was applied as a point moment (Figure 35, details in Appendix E).

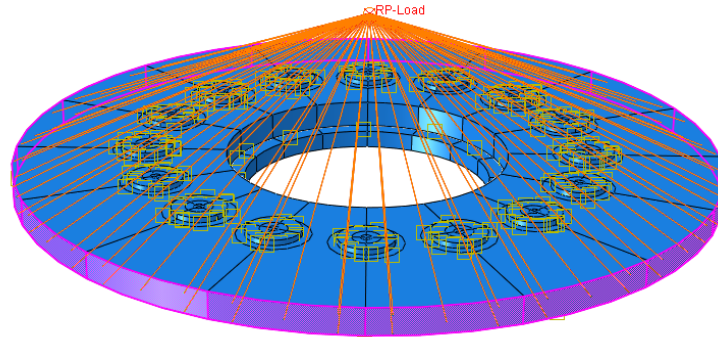


Figure 35: Coupling from RP to outer edge of the composite disc.

The inner edge of the steel disc was fixed to represent the hubs welded onto the shaft (see Figure 36, details in Appendix F).

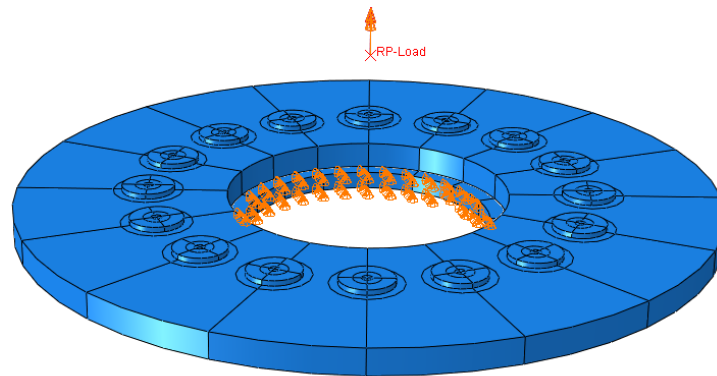


Figure 36: BC; inner edge of disc fixed.

### 7.3.5 Results

The results for the final design are presented using the direction definition in section 2.3.1.

Element-size convergence studies were performed for all parts in the assembly. The number of elements for each part was plotted against its highest stress (22-tensile for the composite part, and von Mises for hubs and bolts). For each data point, the mesh was changed in all parts, with focus on achieving a good mesh compatibility in the contact zone. Small unavoidable changes in the mesh compatibility will cause some strange behaviour in the plots, as the relative position of contact surfaces nodes affects calculated stress.

#### 7.3.5.1 Composite disc

Figure 37 shows max tensile stress in the 22-direction of the composite disc plies plotted against total number of elements in the disc. 22-tensile stress was used here because it is the most critical stress direction.

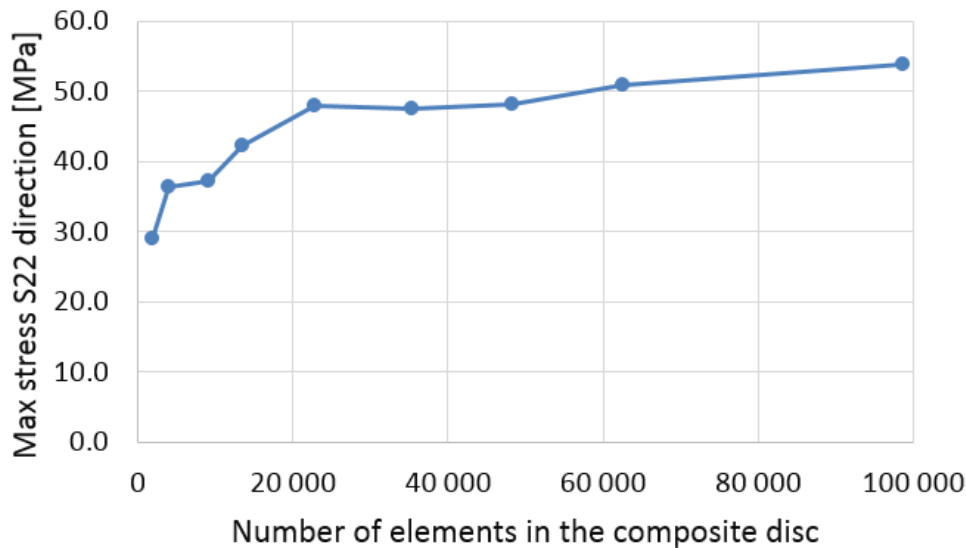


Figure 37: Element-size convergence study for composite disc stress.

A steady slope is seen after approximately 20 000 elements. The stresses are expected to rise further due to the singular contact point. The model with the highest element density will be used in the following discussion as it gives higher resolution of the stress field. Table 21 compares maximum stresses in all directions with their corresponding material strengths from Table 10.

Table 21: Summary of stresses in all directions compared to corresponding strengths.

Stresses	Explanation	Strength [MPa]	Max stress [MPa]	Utilization
11max	Fibre tensile	882	166.4	19 %
11min	Fibre compressive	562	154.8	28 %
22max	Matrix tensile	25	53.9	216 %
22min	Matrix compressive	98	97.0	99 %
12	Shear	46	36.0	78 %
33max	Matrix tensile	19.1	7.5	39 %
33min	Matrix compressive	141.7	18.0	13 %

The matrix dominated 22-tensile strength is exceeded, but only locally as we shall see. 22-compressive and 12-shear are also close to their limits. Through-the thickness compressive stresses will also be studied.

Figure 38 shows a detailed view of the highest stressed bolthole in 22-tensile.

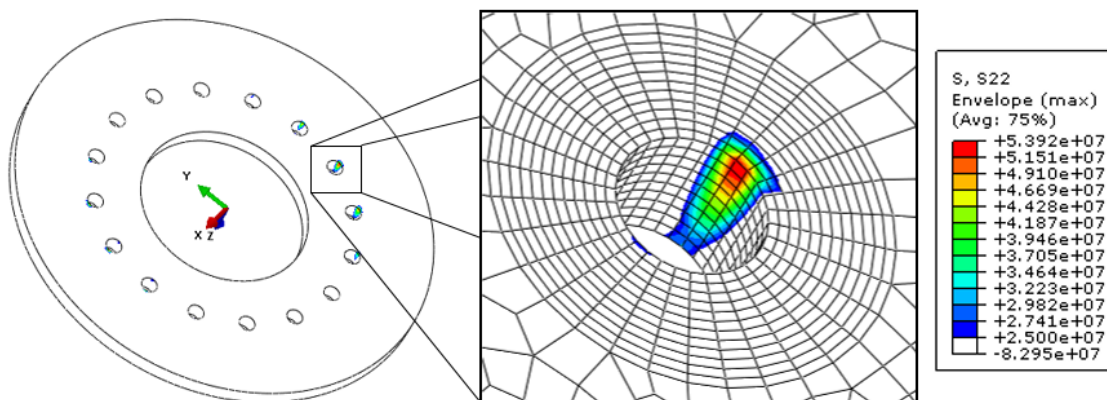


Figure 38: 22-tensile stresses in the bolthole. Coloured areas exceeds material strength.

The coloured area in Figure 38 have exceeded the material strength, and matrix cracking will occur. This area is considered small enough to be acceptable. For scale, the radial size of the small elements in the figure is about 2.1 mm. Rotation of the bolts due to secondary bending causes a higher stress at the upper side of the hole. This side is in the plane where the discs shears the bolts. A double shear joint would give a smoother stress distribution through the bolthole. The size of the area exceeding material strength in Figure 38 can be compared with that of a rejected 20 mm composite disc with 16x24 mm bolts shown in Figure 39.

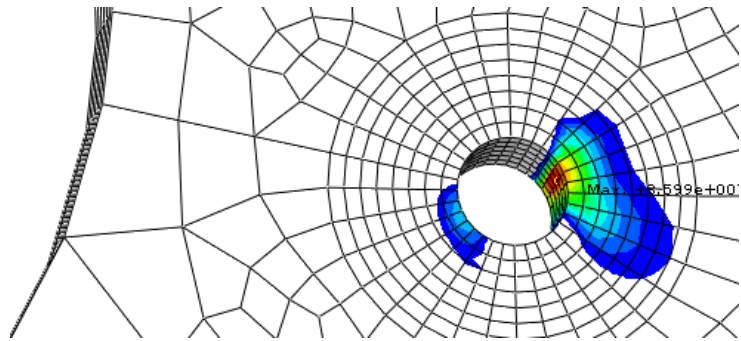


Figure 39: Rejected joint. The area exceeding 22 tensile strength (coloured) is too large.

Figure 40 shows a detailed view of the hole with the highest compressive stresses in the 22-direction. The bolts are bent against the bolthole causing compressive stresses in the matrix close to its strength limit. Some local matrix crushing on the edge of the bolthole may occur.

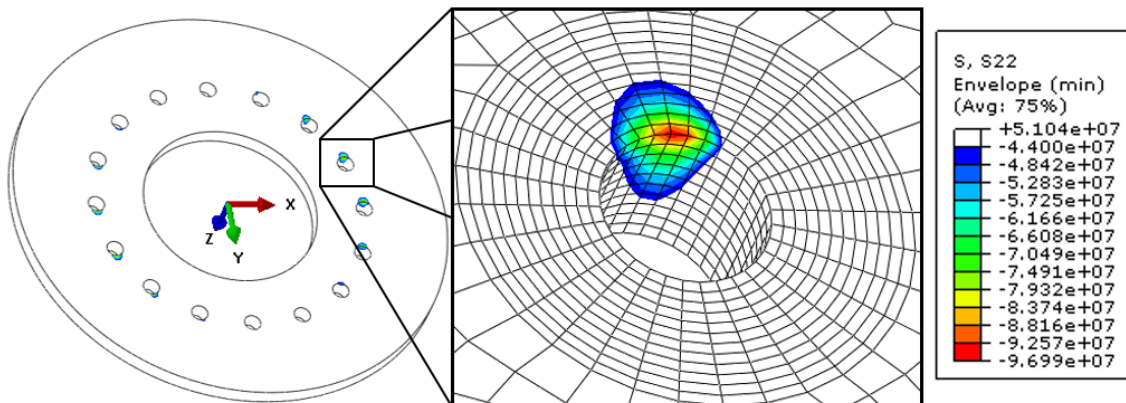


Figure 40: Compressive stress in 22 direction. Area with stress above 50% of strength is coloured.

Figure 41 shows a detailed view of hole with the highest shear stress. Maximum shear stress is within strength limits.

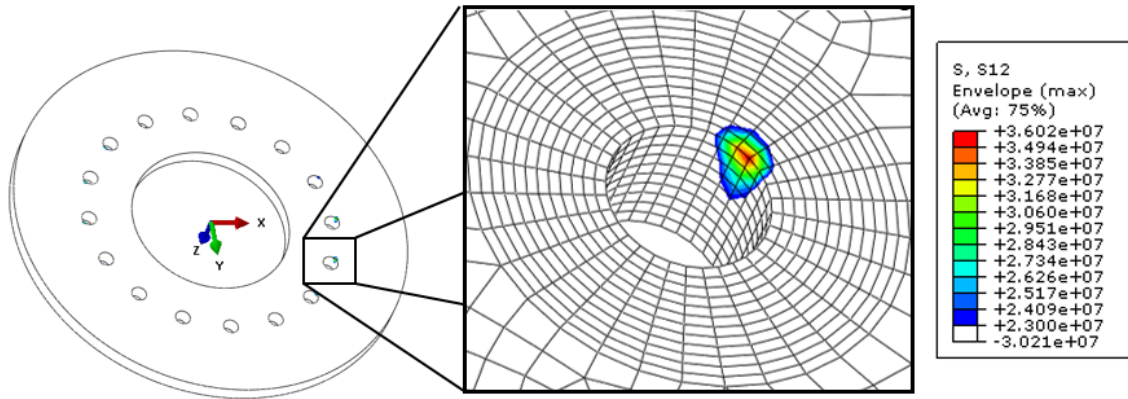


Figure 41: 12-shear stress. Area with stress above 50% of strength are coloured.

Figure 42 shows the compressive stresses in 33-direction. A footprint from the washer pressing down on the surface is clearly seen. Similar for all holes and well within strength limits.

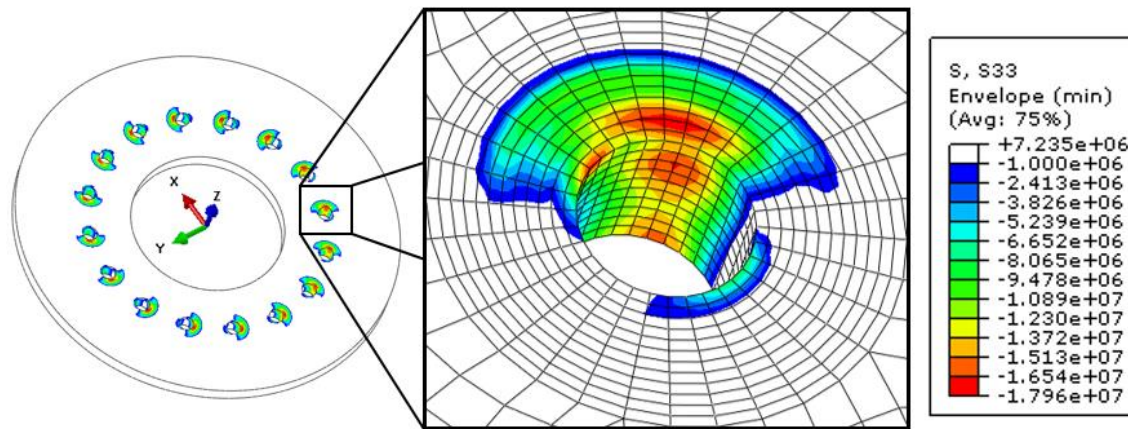


Figure 42: Through-thickness (33) compressive stress. Areas with stresses above 1MPa are coloured.

### 7.3.5.2 Hub

Figure 43 shows the results of an element-size convergence study. Max von Mises stress is plotted against number of elements in the hub.

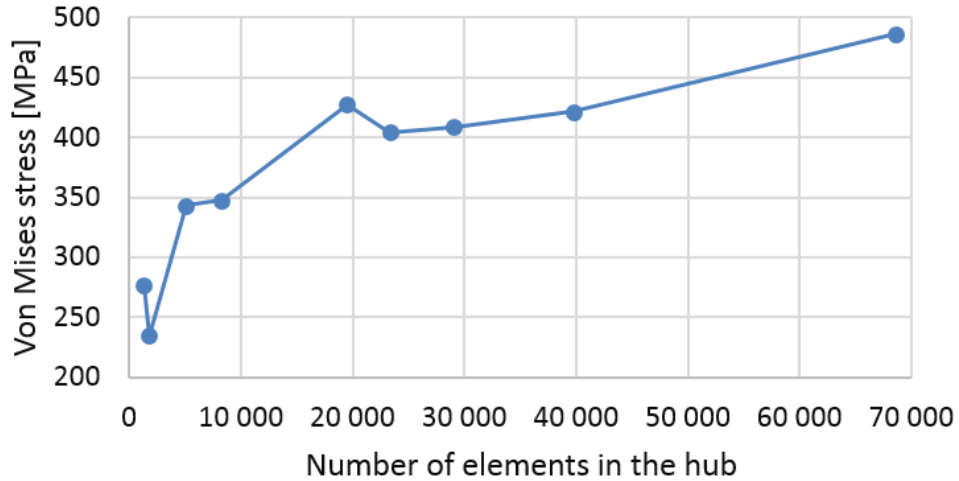


Figure 43: Element-size convergence study for hub stress.

An initially sharp increase is followed by a steady increasing slope due to the stress singularity. Figure 44 shows an overview of the stress levels in the hub.

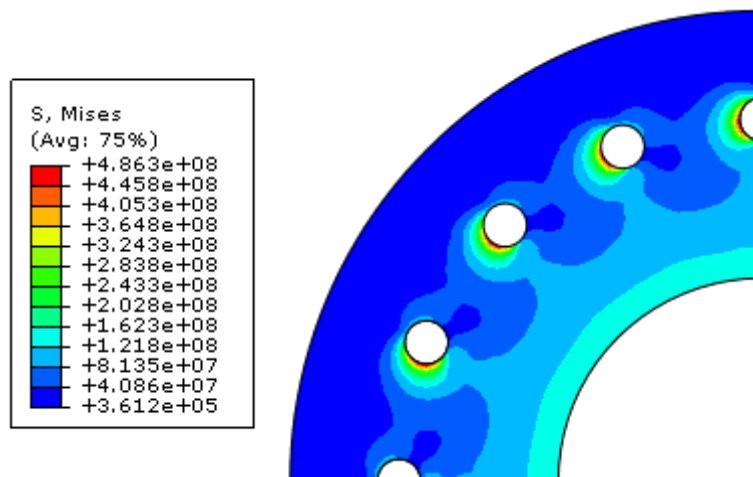


Figure 44: Overview of von Mises stress in the hub.

The stress in the hub-shaft interface is below 150 MPa. The higher local stresses at the edge of the boltholes are shown in detail in Figure 45.

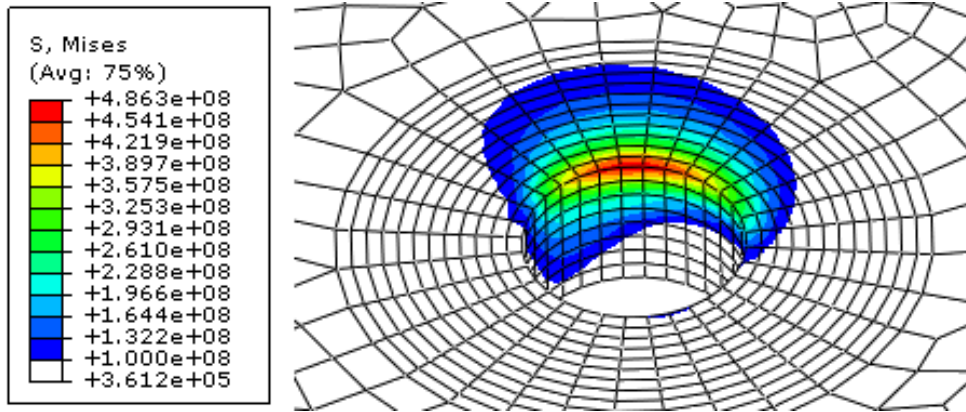


Figure 45: Von Mises stress above 100 MPa in the hub bolthole.

As for the composite disc, the stresses are concentrated on the side of the bolthole in the shear plane. At the edge of the bolthole, local yielding will redistribute the stresses. From these results a hub thickness of 20 mm made of standard weldable construction steel ( $R_y = 355$  MPa) is considered sufficient for this bolted connection.

### 7.3.5.3 Bolts

Figure 46 shows max stress in the bolts plotted against number of elements in one bolt.

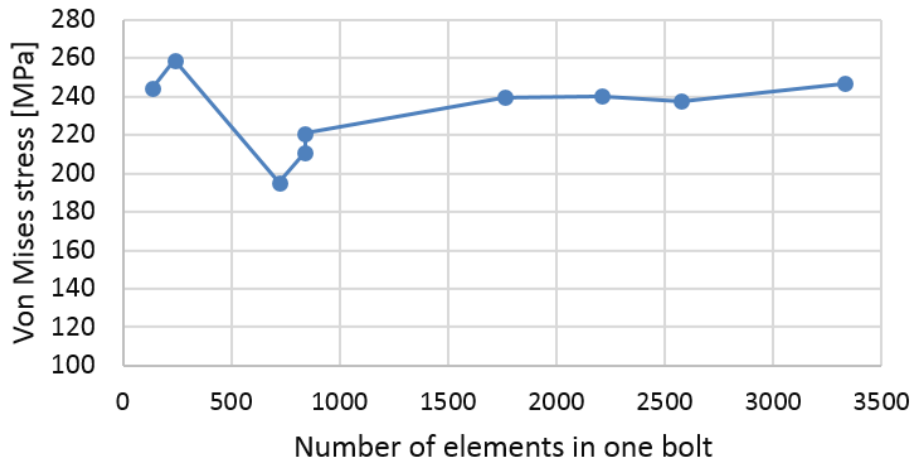


Figure 46: Element-size convergence study for bolt stress.

Max stress is relatively stable around 240 MPa, except for the first course meshes where low number of elements makes mesh compatibility in the contact area difficult. The stress

will not converge due to stress concentration. This maximum stress might be too high because of the way the bolt is modelled here. Figure 47 shows section views of a deformed and undeformed bolt.

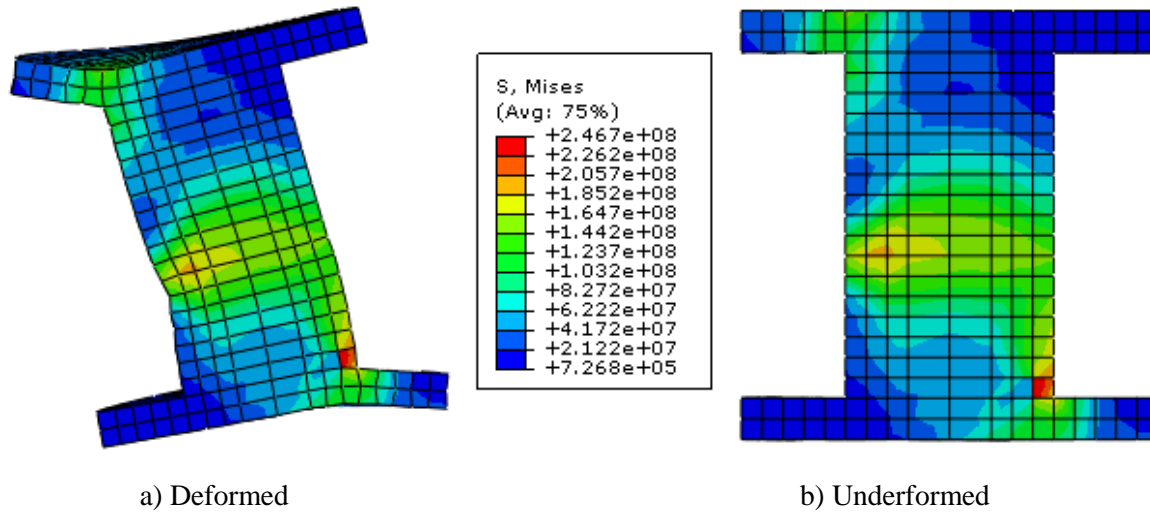


Figure 47: Section views showing stress levels in a bolt.

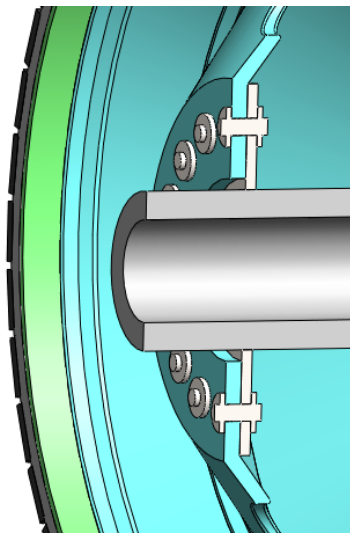
Secondary bending is clearly seen in the deformed bolt. The composite disc pulls the upper part of the bolt to the left, and it is held back by the stiffer steel disc at the bottom. A band of high stress forms where the discs shear the bolt. The highest stress occurs in the washer/bolt corner due to high stress concentrations. This would be different with a more realistic free washer. However, even this maximum stress is acceptable as it is lower than the fatigue limit of 400 MPa from 7.2.2.



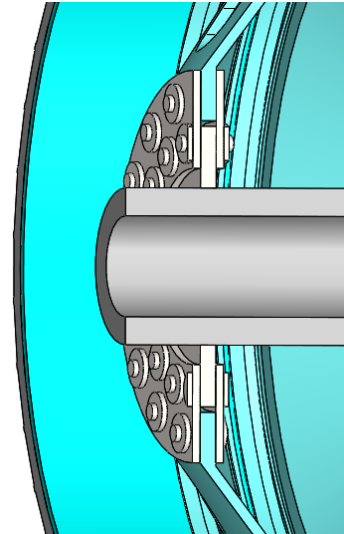
## 7.4 Alternative bolted joint concepts

### 7.4.1 Double shear configuration

As discussed in section 6.1, a double shear configuration does not give secondary bending of the bolts, resulting in a more even stress distribution in the bolt. Such a solution for this structure is compared to a single shear joint in Figure 48.



a) Single shear



b) Double shear with overlap discs

Figure 48: Single and double shear configuration.

### 7.4.2 Pretensioned through bolts

Stress introduced in the composite laminate from pretension/clamp-up in the bolts will make the laminate creep over time. Creep deformation will lead to a reduction in pretension, and if large enough, a complete loss of pretension. If this is the case then the joint will become a pinned bolt connection with considerable lower strength.

An alternative joint concept that deals with this problem will be discussed. This concept, which use long bolts running through both joints, is compared to the normal short bolt concept in Figure 49. Figure 50 provides more details.

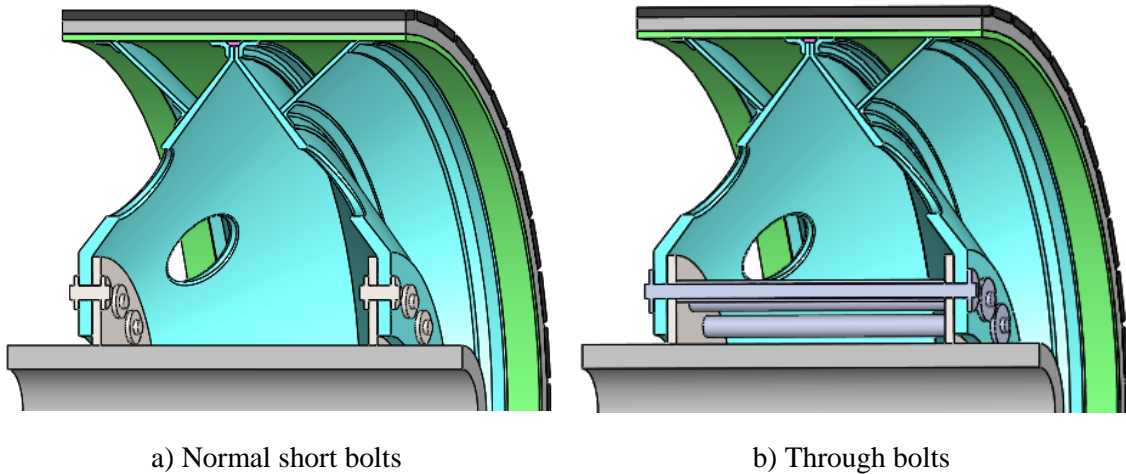


Figure 49: Comparison between normal short bolt and through bolt concept

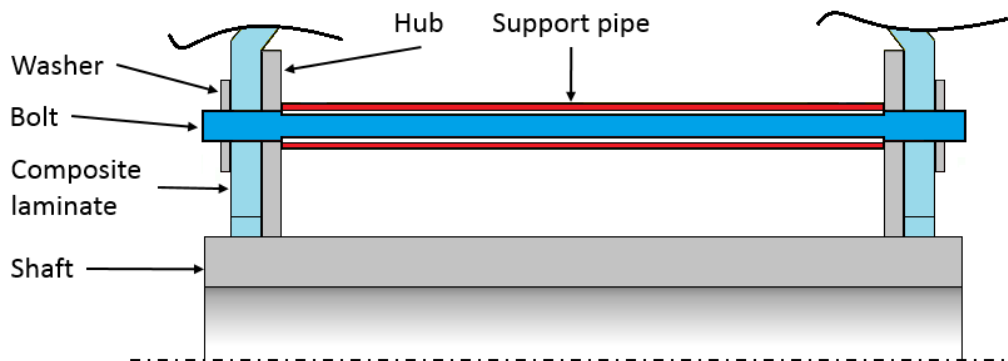


Figure 50: Pretension concept with through bolt and support pipe

The main point of this concept is that when the bolts are long in comparison to the laminate thickness, the laminate deformation over time will be small compared to the initial deformation in the bolts from the pretension force. After the creep-deformation of the composite there will still be some pretension left in the bolts. To increase this effect, the bolts can be turned down to a smaller diameter between the hubs, later referred to as the working length of the bolts. The concept requires a support pipe to counteract the pretension forces, and avoid excessive hub bending.

A calculation was done using classical stress analysis. Normal pretension force for 8.8 M30 bolts is in the order of 209-290 kN depending on the friction coefficient in threads and between the nut/washer/composite surfaces [61]. Pretension of this magnitude causes no crushing of the laminate if washers of  $\text{Ø}60$  mm are used. Washer size can be increased to  $\text{Ø}90$  mm without practical problems, and further improvement is possible if discs with boltholes are used rather than washers. This because of an increased contact area, and reduced problems with high stress gradients at the perimeter of the washers. Pretension is limited by tensile stress in the turned down part of the bolts. It was assumed that the support pipe and hubs are rigid enough to keep the hubs aligned at the same position through the creep/relaxation deformation process. Based on this it was assumed that the deformation of the composite could be subtracted from the pretension deformation of the working length of the bolt. Actual creep strain data would be needed to qualify this concept. For these calculations, two conservative creep strains (0.01 and 0.02) were assumed. These were coupled with two bolt diameters at 25 mm and 20 mm in their working length, and two pretensions of 250 and 200 kN. The diameter in the boltholes are kept at 30 mm to handle the torque load shear. Input data is summarised in Table 22, and results from the calculation in Table 23.

Table 22: Input data for through bolt calculations.

Property	Unit	Value
Composite laminate young's modulus, $E_{3C}$	GPa	12.8
Steel bolt young's modulus, $E_{\text{steel}}$	GPa	210
Composite laminate compressive strength, $\hat{\sigma}_{3C}^{\text{matrix}}$	MPa	141
Yield strength steel	MPa	640
Bolt working length	m	0.64
Support pipe outer diameter	m	0.04
Support pipe inner diameter	m	0.03
Washer outer diameter	m	0.06
Washer inner diameter	m	0.03
Total composite thickness	m	0.06

Table 23: Results for through bolt calculations.

Property	Unit	Strength	0.01 creep, 25mm bolts		0.02 creep, 20mm bolts	
			Initial	After creep	Initial	After creep
Bolt pretension	kN	-	250	153	200	76
Bolt stress	MPa	640	509	313	637	243
Compressive stress under washer	MPa	141	118	72	94	36

The initial and post-creep deformation in the bolts are compared in Figure 51, in addition to the composite deformation caused by the assumed creep/relaxation.

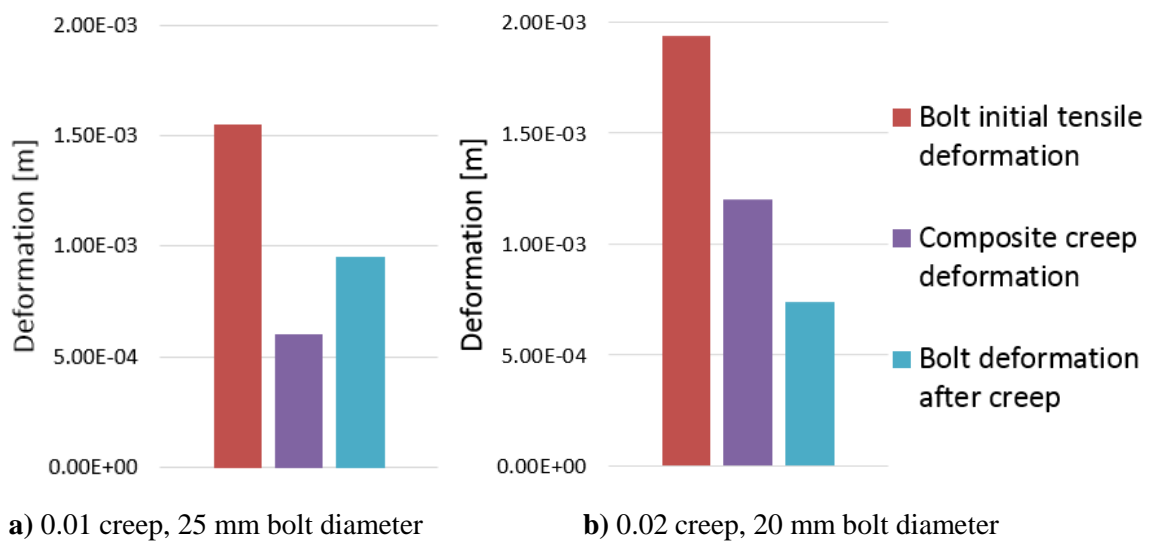


Figure 51: Comparison of deformations

The results indicates that with the assumed creep strains a considerable amount of pretension can remain in the bolts. The total mass penalty of this solution is in the order of 75-85 kg depending on the turned down bolt diameter.

### 7.4.3 Bolt/adhesive hybrid

The possibility of using an adhesive to handle the shear stresses in combination with bolts to avoid peel stress of the adhesive joint was investigated. It was assumed that the whole contact area between hubs and the composite discs are adhered.

Classic elastic stress theory [36] was used to predict the shear stress. Maximum shear stress from torsion for a thick walled pipe is given by equations (18) and (19). The design torque from section 7.2.3 was used.

$$\tau_{max} = \frac{T}{I_p} r \quad (18)$$

$$I_p = \frac{\pi}{2} (b^4 - a^4) \quad (19)$$

Table 24: Parameters in adhesive hybrid joint calculation.

Property	Symbol	Value	Unit
Design torque	$T_{design}$	227	kNm
Outer diameter of adhered surface	$b$	0.32	m
Inner diameter of adhered surface	$a$	0.17	m
Max shear stress	$\tau_{max}$	4.78	MPa

A maximum shear stress of less than 5MPa is sufficiently low to make further investigation of this concept worthwhile.

## 7.5 Summary

A single shear composite to steel bolted joint without bolt pretension, bushing and adhesive joining was studied using FE contact analyses. The final joint presented in this chapter fulfils geometry and layup recommendations from the literature. The local stresses caused by the torque load was considered acceptable. Parameters of the joint is summarised in Table 25.

Table 25: Bolted joint parameters resulting from this chapter

Parameter	Symbol	Value	Unit
Bolting radius	$R_{bolting}$	0.25	m
Bolt shank diameter	$d$	0.03	m
Number of bolts	$n$	16	-
Design torque	$T$	227 000	Nm
Bolt load	$F_{bolt}$	56 750	N
Bolt shear stress, classical	$\tau_{bolt, ss}$	80	MPa
Bolt von Mises stress, FEA	$\sigma$	247	MPa
Laminate thickness	$t$	0.03	m
Circular pitch	$P_{circ}$	0.098	
d/t ratio	$d/t$	1	-
S/d ratio	$S/d$	2.3	-
$P_{circ}/d$ ratio	$P_{circ}/d$	3.27	-
Minimum hub thickness	$t_{hub}$	0.02	m

## 8 Structure Stiffness

This chapter investigates possibilities for improving the stiffness of the preliminary structure. There is room for improvement, especially in the axial direction, where a low stiffness of the flat discs has been shown to cause low natural frequencies and large displacements [1]. The joining of the structure discs to the yoke and the shaft were treated in previous chapters, but still a lot of freedom remains in the choice of disc geometry. Several disc geometries will be considered, and they will be judged on their performance in an FE modal analysis. The preliminary structure from the specialization project is illustrated in Figure 52.

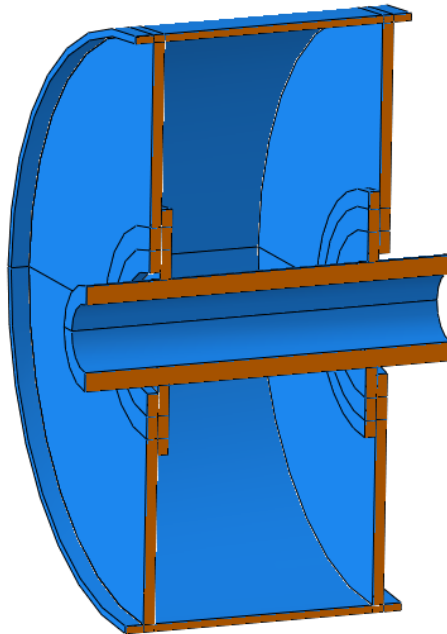


Figure 52: Reference composite structure with flat discs.

## 8.1 Approach

The structure must avoid operating at a natural frequency (resonance). EMEC standards [62] provide guidance on this, and three common approaches are discussed:

1. Ensure low stiffness of the structure, so that natural frequencies occurs below forcing frequencies.
2. Ensure high stiffness of the structure, so that natural frequencies occurs above forcing frequency
3. Ensure sufficient damping in the structure so that the response to forcing frequencies will not result in significant stresses.

Approach 2. is the simplest method and it is chosen here. Because the identified forcing frequencies are relatively low, it is assumed that necessary stiffness will be achieved relatively easy.

This analysis comprises three parts:

1. Identifying forcing frequencies.
2. Identifying natural frequencies and mode shapes.
3. Clarify the relationship between forcing- and natural frequencies.

Part 2 above will be expanded in this chapter to include evaluation of different solutions for the structure. According to [62], there should be a margin of at least  $\pm 20\%$  between natural frequencies and operating speed range.

## 8.2 Forcing frequencies

The structure may pass by a natural frequency through its operating speed range of 0-75 rpm. One possible local excitation source is cogging torque due to the interaction between magnet poles and stator teeth. Specific cogging frequencies have not been provided but should be considered in a final design. The most relevant global excitation source is loads on the rotor shaft from the attached turbine. Assuming a four bladed turbine will give a blade order frequency (also known as blade pass frequency) of four times the rotational speed. Other relevant applications of SmartMotor's electric machines include ship machinery, where it is often required that electrical equipment shall be *constructed to withstand a vibration frequency range from 5 to 50Hz* [63]. This will be kept in mind. Identified global and local excitation frequencies are summarised in Table 26.



Table 26: Identified possible excitation frequencies and other frequency requirements.

Excitation source	Data	Frequency [Hz]
Nominal speed range	0-75 rpm	1.25
Blade pass frequency/engine order, number of blades	4	5
Cogging	?	?
With margin of safety	20%	6
Additional requirement for ship machinery	-	50
With margin of safety	20%	60

The tidal turbine requirements are met with the reference structure (lowest natural frequency is 10Hz). However, analyses in the specialization project shows that this structure has a large displacement (16mm) for the axial gravity load case. Mass savings should also be possible with a better structure.

### 8.3 Modal analysis and structure stiffness

A modal analysis is performed using FE-software to predict the natural frequencies and corresponding mode shapes of the structure globally. Several structures will be analysed and modified, until a structure with sufficient stiffness is achieved. Only the FE model of the final preferred solution will be presented in detail.

#### 8.3.1 Assumptions, dimensions and units

- Simulation tool: Abaqus /CAE 6.12-1 run on a Windows 8 operative system.
- All models are Standard & Explicit, using linear elastic materials based on engineering constants.
- Procedure type for steps are linear perturbation, frequency.
- Joints modelled by a tie interaction.
- Magnets and magnetic core are modelled as an equivalent non-structural mass.

Only SI-units were used. Dimensions of the shaft and yoke are as measured on a CAD model of the reference rotor. Disc thickness in the bolted area is set to 30 mm as concluded in Chapter 7. Dimensions of all parts are attached in Appendix G.

### 8.3.2 Mesh and material

Parts are modelled as solids and meshed on part level with hex shaped elements using sweep technique. Edges are seeded separately when needed to ensure a symmetric and even mesh. All parts are meshed with general-purpose SC8R continuum shell elements. These elements are suitable for modelling shell-like solids and gives greater accuracy than conventional shell elements. These have only displacement DOF's [37]. Stacking directions for layups are shown in Figure 53 on some initial course meshes. In a modal analysis, the mesh only need be sufficiently fine in order to capture the first few modes shapes of interest. Thus, the no element-size convergence study is performed.

The discs have some mesh distortion in the area between the holes. It is assumed that this is acceptable for a sufficiently fine mesh. No other parts have mesh distortions.

The materials used for each part are the degraded properties from Table 10, summarised in Table 27. The discs are modelled as a symmetric 8-layer laminate layup as concluded in Chapter 7. Material orientation and ply stack plots for the composite discs, stiffener rings and the yoke are shown in Figure 54 and Figure 55.

Table 27: Materials used in the parts

Part	Material	Assignment	Comment
Yoke	E-glass/polyester	Composite layup	1 ply, 15 mm thick
Discs	E-glass/epoxy	Composite layup	[0/90/+45/-45]s
Stiffening discs	E-glass/epoxy	Composite layup	[0/90/+45/-45]s
Shaft with hubs	Steel	Homogeneous section	

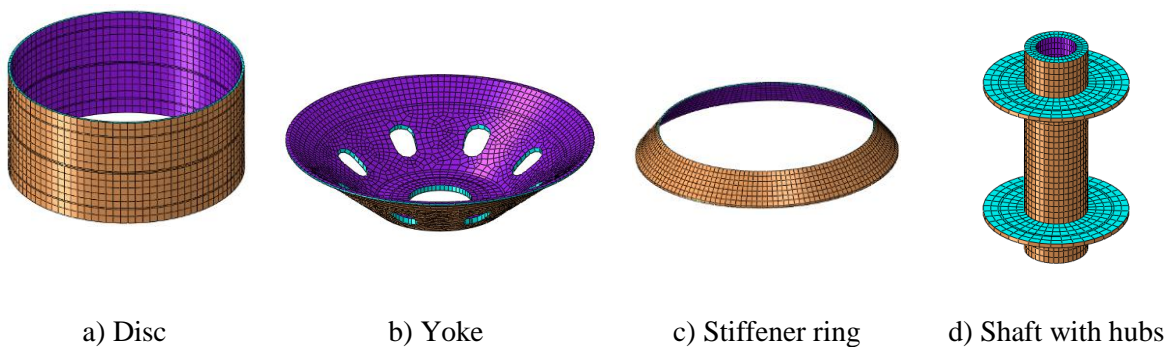
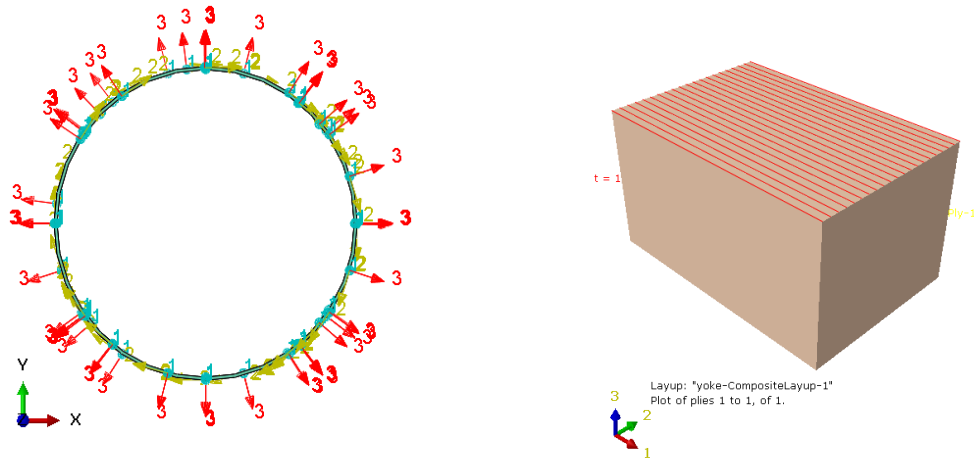


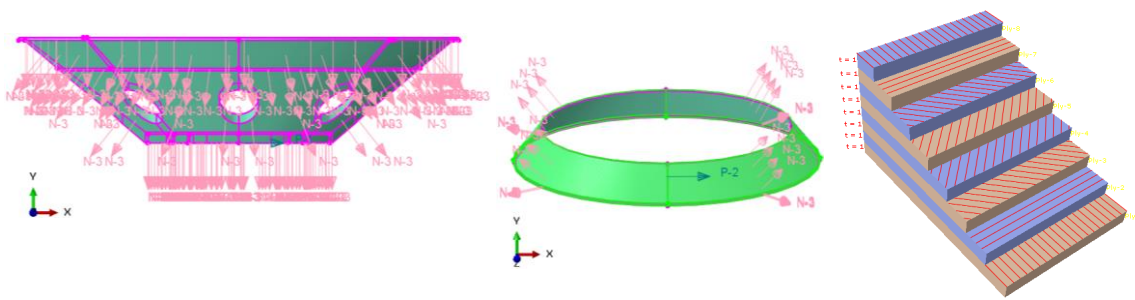
Figure 53: Mesh stack direction for all parts



a) Material orientation

b) Ply stack plot

Figure 54: Material and layup orientation for the composite yoke.



a) Composite disc normal

b) Stiffener ring normal

c) Ply stack plot

Figure 55: Normal definition and ply stack plot for the composite disc and stiffener ring

Continuum shell composite layups are expected to have a single element through the entire thickness of the regions specified in the composite layup. When several elements are used through the thickness, each element contains the multiple plies defined in the ply table [59]. This is acceptable here because the layup is quasi isotropic, and the actual laminate will also contain several repeated layers of the specified layup.

### 8.3.3 Boundary conditions, connections and interactions

The magnets and the magnetic core were modelled as an equivalent non-structural mass distributed as a volume proportional total mass on the volume of the yoke (see Figure 56). The equivalent mass was calculated by halving the magnetic core thickness (60mm to 30mm) from the reference rotor and adding the original magnet mass. Equivalent mass was estimated to be 1439 kg. A mass sensitivity study will also be performed to study the

effects of extra mass from e.g. layup joints, magnet retention, bolts/washers and coatings. This mass is added as percentages (10% = 144kg and 50% = 720kg) of the non-structural mass.

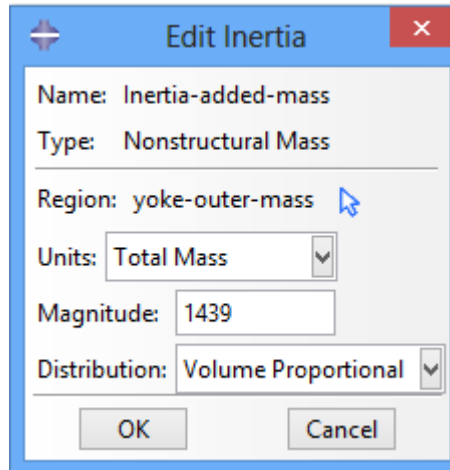


Figure 56: Nonstructural mass dialogue box.

Boundary conditions were used to fix the ends of the shaft, leaving one end free in the axial direction (Figure 57) to represent bearings. The boundary conditions were applied to two RP's which were tied to the ends of the shaft.

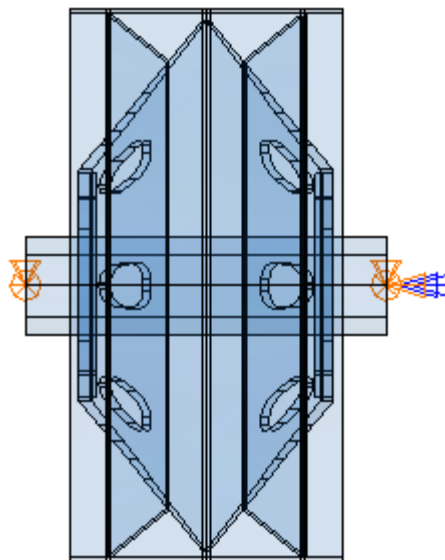


Figure 57: Boundary conditions

Joints in the assembly was modelled as tie constraints. A tie constrains ties two separate regions together so that there is no relative motion between them [59]. Constraints used in the model are summarised in Table 28 and illustrated on the assembly level in Figure 58. Appendix H contains illustrations on the part level. The complete assembly is illustrated in Figure 59.

Table 28: Overview of constraints used in the model

Description	Type
Shaft to disc	Tie
Disc to yoke	Tie
Disc to disc	Tie
Disc to stiffener ring	Tie
Stiffener ring to yoke	Tie
Shaft ends to RP	Coupling, U1, U2, U3

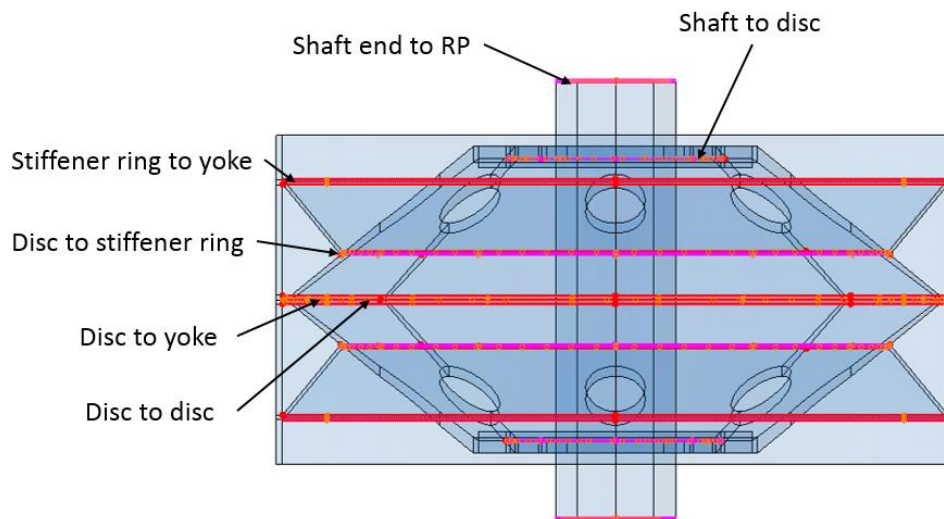


Figure 58: Constraints shown in the complete assembly

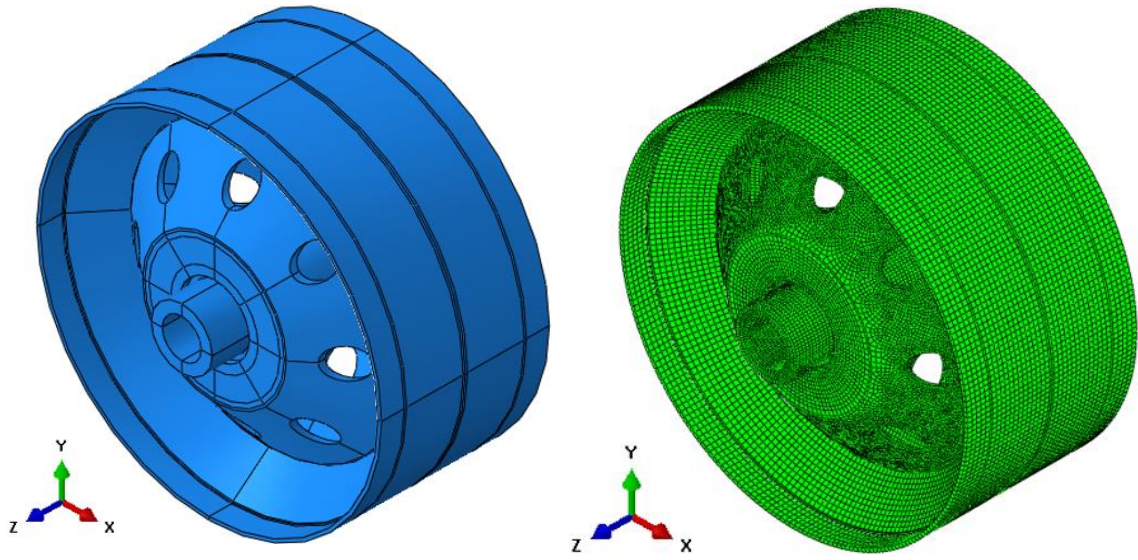


Figure 59: Complete assembly without and with mesh ( 88 000 elements).

### 8.3.4 General mode shapes

Common mode shapes for most of the structures are presented to facilitate further discussion of alternative structures. The mode shapes are normalized vectors and do not represent actual magnitudes of deformation. The actual magnitudes of deformation depends on excitation strength and damping. The explanations below refers to Figure 60.

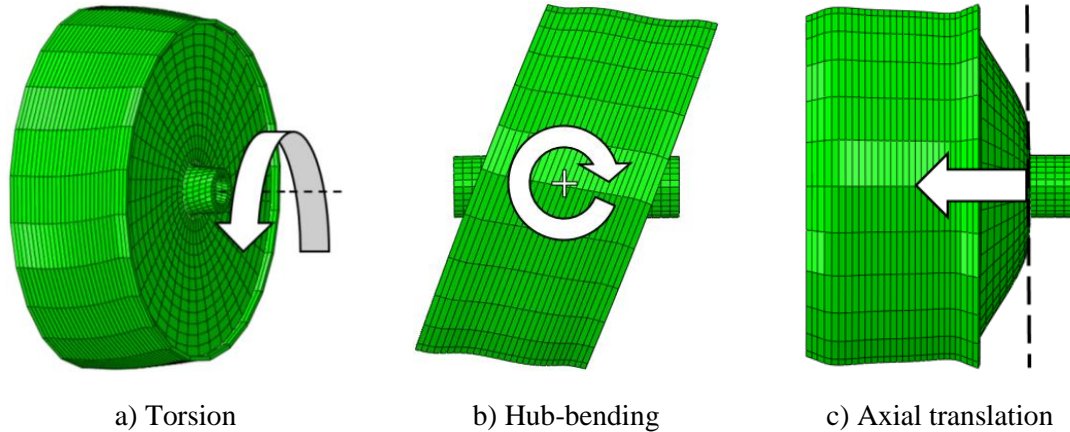


Figure 60: First dominant modes common for most of the studied structures.

The *torsion* mode depends on the shaft torsional stiffness, and the distance between the shaft end and the first hub. This mode can be excited by cogging and variations in torque load.

The *hub-bending* mode is influenced by hub spacing, disc stiffness and yoke stiffness. This is regarded as a critical mode as it may lead to rotor/stator collision.

The *axial translation* mode is influenced by the axial stiffness of the hubs and discs, and to a less degree the yoke stiffness. This mode can be excited by axial components of the attached load. The mode is regarded as critical as it may cause peel stresses in the structure joints.

In addition there are several yoke flapping modes (see examples in Figure 61), but these occur at higher frequencies and are not the main concern at this point.

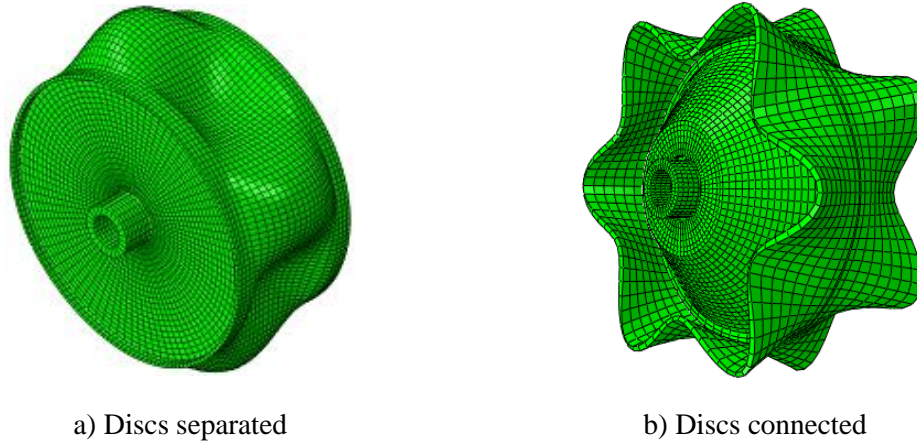


Figure 61: Illustration of two yoke flapping modes

A model to investigate the factors affecting the torsion mode was created. With very thick discs, and large hub spacing, the natural frequency for this mode was still around 48 Hz. In other words, the frequency of this mode is kept low by limited shaft torsional stiffness.

### 8.3.5 Evaluation of structure stiffness

Using only one hub would have several advantages such as equal load sharing between the discs, better joint configuration for the bolts, simplified bolting operation, less mass needed for bolts and hub and easier access to both sides of the joint. Disadvantages are larger loads in the hub (especially bending moment), and the resulting loads at the middle of the shaft. As for all the studied structures, a one-hub design will satisfy the frequency requirements of a tidal turbine. E.g. for the structure shown in Figure 62 a) (30mm hub thickness), the mode with the lowest natural frequency is hub bending mode at 23Hz. This is a good improvement from the reference structure, and it means that this type of structure is feasible for a tidal turbine rotor.

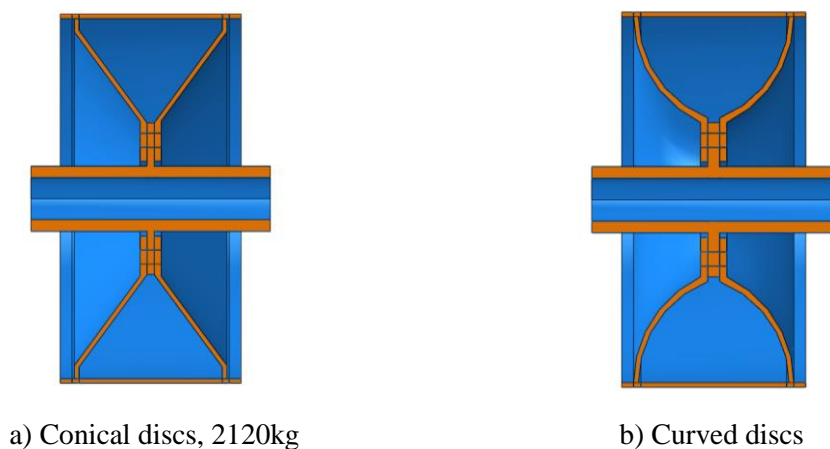


Figure 62: Two of the investigated one-hub designs.



However, it is chosen to look further into structures with two hubs, as these outperform one-hub designs in the hub bending mode, can give better stiffness with less material and will also enable the special pretensioned through bolt solution. It is also of interest to develop a structure that can be used for other applications with higher requirements w.r.t. stiffness. Figure 63 shows some of the structures that have been studied.

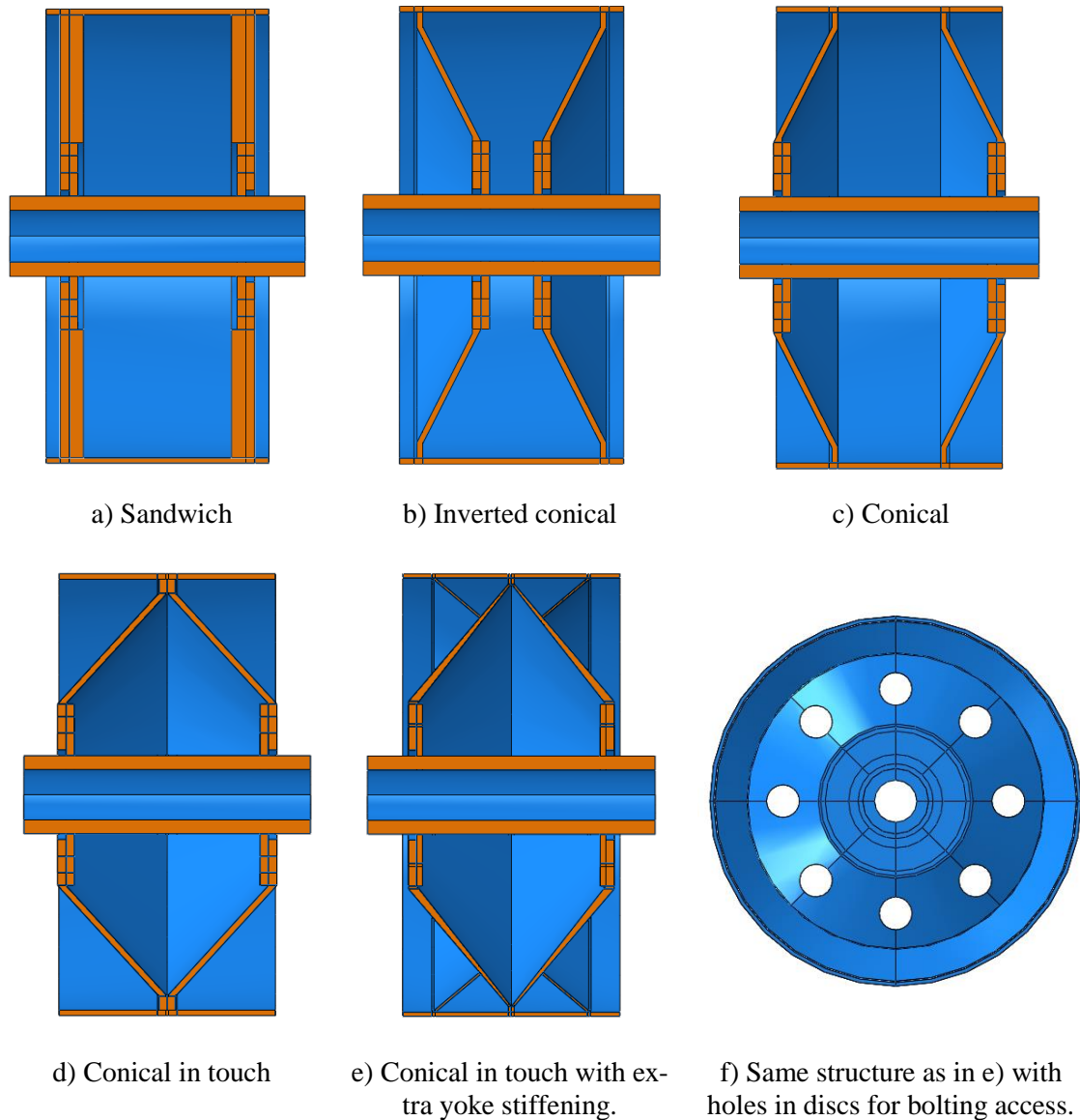


Figure 63: Two-hub designs.

Figure 63 a) illustrates an investigated structure with sandwich discs. A core thickness of 60mm and skin thickness of 10mm were used. The core was assumed isotropic and made of Divinycell H80. For this structure, the natural frequency of the axial translation mode was low. Increasing hub thickness to 50 mm only improved it to 15 Hz. This is attributed

to low stiffness in the discs, and partially to low stiffness in the yoke (see Figure 64), which allows the discs to move independently of each other. Sandwich discs introduces new failure modes due to the interaction between the skins and the core (p. 67, [25]), water intrusion, and possible compression of the core when submerged in water. Sandwich discs was therefore considered unsuited for this application.

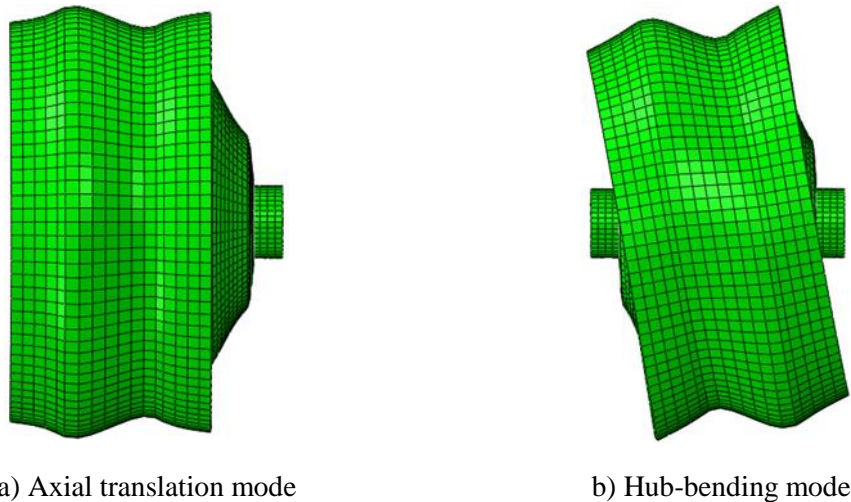


Figure 64: Low stiffness in yoke allows discs to move independently

Joining the discs as shown in Figure 63 d) increased performance in the axial translation mode and hub-bending mode. This is because the discs are locked in place by each other, independent of the yoke stiffness. However, this introduced several yoke flapping modes (see Figure 64) because of the lack of support towards the yoke ends. This was solved with additional stiffening discs as shown in Figure 63 e). These additional discs can be manufactured in the same way as the main discs, and joined with laminated joints. Finally, holes in the main discs were introduced to enable bolt assembly (Figure 63 f)), and the discs were tapered down towards the outer radius (Figure 63 e)). This is the preferred structure from this chapter, and it was studied in more detail.

### 8.3.6 Results

Results for some variations of the preferred structure are summarized in Table 29. The variations are hub thickness, size of hub-disc tie area, and added mass. The results are commented below.

Table 29: Results from modal analysis for different models

Model	A: Big tie 50mm hubs	B: Big tie 20mm hubs	C: Small tie, 20mm hubs	C, added mass +10%	C, added mass +50%
Model mass [kg]	2226	2103	2103	2247	2823
Mode	Frequency [Hz]				
Axial translation	81	33	22	21	18
Torsion	47	46	44	42	36
Hub-bending	77	59	54	52	45
Yoke flapping	75	74	73	70	61

The thickness of the hubs had a large influence on the performance in axial translation- and hub bending modes.

20 mm hub thickness, as needed from the bolted joint analysis, is sufficient for the tidal turbine requirements.

Using 50 mm hubs, big tie, and increasing shaft outer diameter from 280 mm to 360 mm raised the lowest natural frequency to 61 Hz. This is just above the requirements for ship machinery. The lowest mode for this structure was the torsional mode.

The size of the tied area between the hubs and the discs to represent the bolting connection has an effect on the stiffness. “Big tie” refers to tying the whole area between radiuses 0.2 - 0.3 m. This is necessary to prevent the surfaces of the composite disc and the steel hub from overclosing in the analysis. This will overestimate the stiffness of the connection. Therefore, the effects of a “small tie” was studied, using the area between radiuses 0.245 - 0.255 m. The size of this area ( $0.0157 \text{ m}^2$ ) is closer to the actual bolt cross section area ( $0.0113 \text{ m}^2$ ). However, this allows surface overclosing and will underestimate the stiffness of the joint.

The results from the mass sensitivity studies indicates that structure also has sufficient stiffness to handle these extra masses.

## 8.4 Relationships between natural and forcing frequencies

The relationship between natural frequencies and forcing frequencies can be identified by means of a Campbell diagram [62]. Such a diagram for the preferred solution (model C with +10% mass from Table 29) is shown in Figure 65.

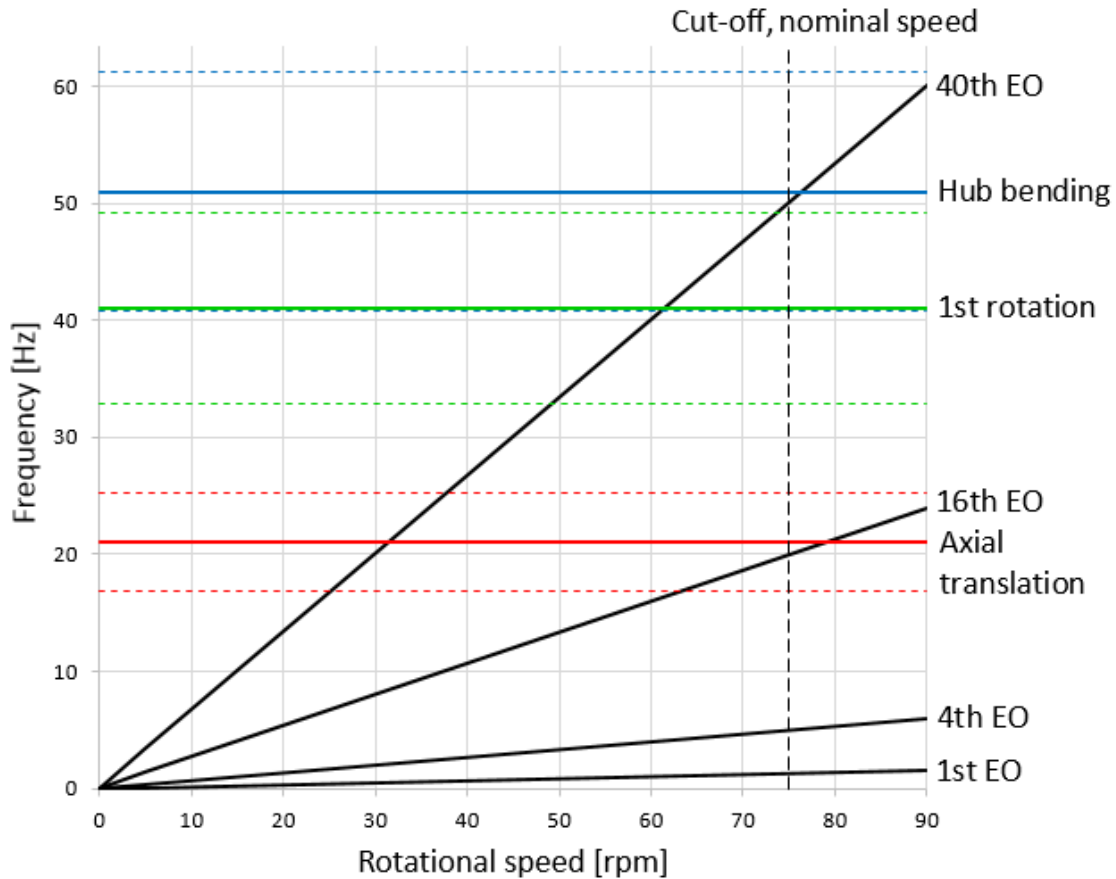


Figure 65: Campbell diagram for the preferred solution.

The diagram shows the natural frequencies corresponding to a mode shape plotted vertically. The  $\pm 20\%$  frequency band for each mode are drawn in dashed lines. The black fan lines are the rotational speed and its harmonics (also known as engine order, or EO lines) through the relevant speed range. The rotational speed is the 1<sup>st</sup> EO line. For this case a four bladed turbine is attached to the shaft, and thus the 4<sup>th</sup> engine order is of interest. Any intersection of a natural frequency line and an engine order line show a possible resonant condition. As can be seen from the diagram, the natural frequencies are all far away from the identified exiting frequencies (with the 4<sup>th</sup> engine order as a maximum). The 16<sup>th</sup> EO is included to illustrate that any excitation caused by the 16 bolts would break the lower 20% frequency band within the relevant speed range. It should be noted that the 11<sup>th</sup> EO is the highest EO that does not break the lower 20% frequency band (not shown in the figure). Any cogging at say the 40<sup>th</sup> EO, would also have to be considered further.

## 8.5 Summary

Several alternatives were evaluated using FE modal analysis. The lowest natural frequency of the preferred solution (Figure 66) from this chapter was 21 Hz. This gives a large margin to the highest identified excitation frequency of 5 Hz for the tidal turbine generator rotor. By increasing shaft diameter and hub thickness, the lowest natural frequency was raised to 61 Hz, meeting the 50Hz requirement of ship machinery. The yoke displacements under static gravity load cases must be studied before the stiffness of the structure can be approved.

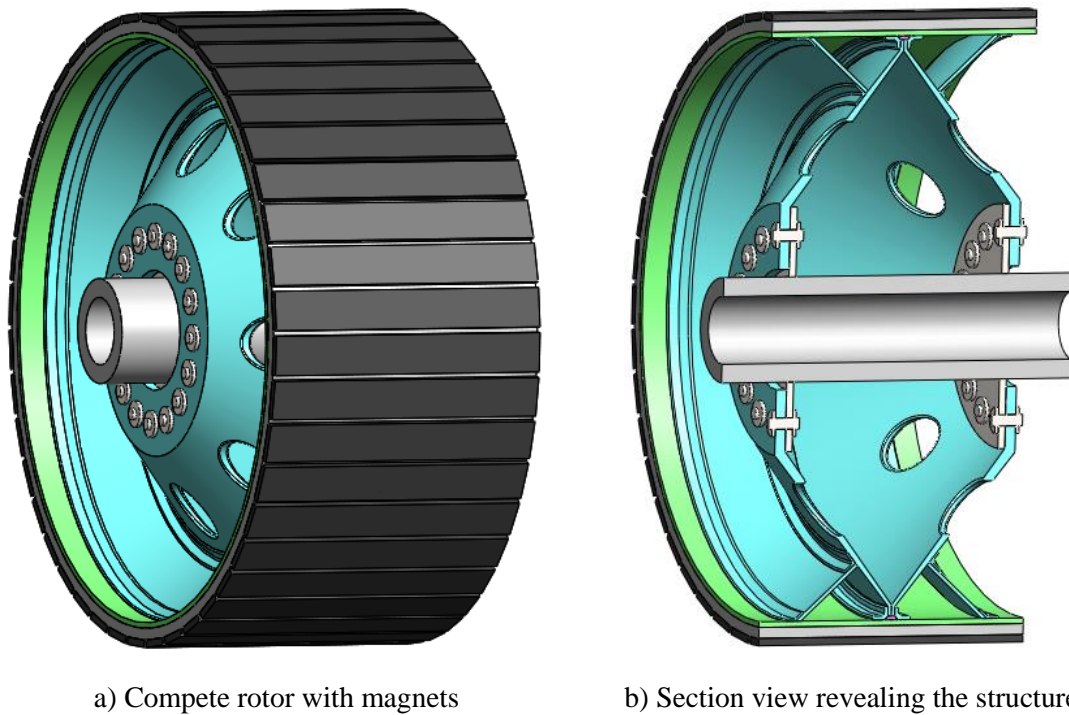


Figure 66: Illustrations of the preferred concept from this chapter.



## 9 Static Load Cases

### 9.1 Model

The objective of this structural analysis is to obtain the global and local response of the preferred structure from the load cases described in section 4.2.4. These load cases will also be used for linear elastic eigenvalue buckling analyses.

#### 9.1.1 Approach and assumptions

The same assumptions as for the modal analysis in chapter 8 apply, but with the following additions and changes:

- Partial factors for each relevant design criterion from section 4.5 are implemented by increasing the specified loads to get design loads. A load model factor ( $\gamma_{sd}$ ) of 1.0 is used, as the boundary conditions are assumed to represent the real conditions well.
- Procedure type for static loads are static; general. For the buckling analysis: linear perturbation; buckle. Static loads are added separately in a single load step for each load case.
- For the buckling analysis, the Lanczos eigenvalue solver was used, as it is faster for extracting more than 20 eigenmodes [37].
- Large deformations are ignored in this analysis.
- Mesh and material are the same as for the modal analysis in chapter 8. It is worth noting that the mesh distortion in the disc may influence some results.
- Loads and BC's differ. Description below.

### 9.1.2 Loads, boundary conditions, connections and interactions

The design torque load and design gravity acceleration are calculated in equations (20) and (21) with partial factors from section 4.5.

$$T_{design} = T_{nominal} * \gamma_{FM} * \gamma_{Sd} = 140 \text{ kNm} * 1.96 * 1 = 275 \text{ kNm} \quad (20)$$

$$a_{design} = a_{specified} * \gamma_{FM} * \gamma_{Sd} = 2 * 9.81 \text{ m.s}^{-2} * 1.96 * 1 = 38.5 \text{ m.s}^{-2} \quad (21)$$

The loads and boundary conditions are illustrated in Figure 67 and summarized in Table 30.

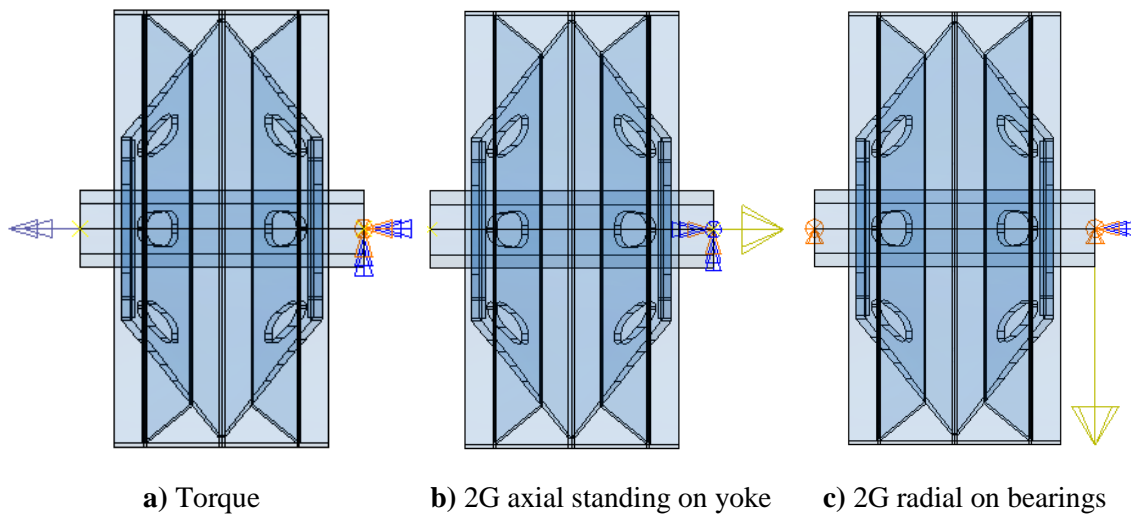


Figure 67: Loads and BC's for three static load cases

Table 30: Loads and boundary conditions for three static load cases

Load case	Torque	Axial gravity standing on yoke	Radial gravity on bearings
BC	Fixed RP coupled to the outer surface of the yoke	Shaft end fixed	RP's coupled to shaft ends
Load	275 kNm applied in RP coupled to one end of the shaft	38.5 $m.s^{-2}$ in axial direction	38.5 $m.s^{-2}$ in radial direction



The design torque is applied to a RP, which is coupled to one end of the shaft to represent the torque transferred from the tidal turbine. The outer surface of the yoke is coupled to another fixed RP to represent the resistance from the magnetic fields in the generator (see Figure 68). The nonstructural added mass is not included in the torque load analysis.

The gravity load cases use the same nonstructural mass as in the model named “C, added mass +10%” from Table 29 in section 8.3.6.

For the shaft-disc tie, the “big tie” version (see section 8.3.6) was used in order to avoid stress concentrations in the connection. These issues have already been treated in Chapter 7, and these models assume that the bolted connection is fit for purpose.

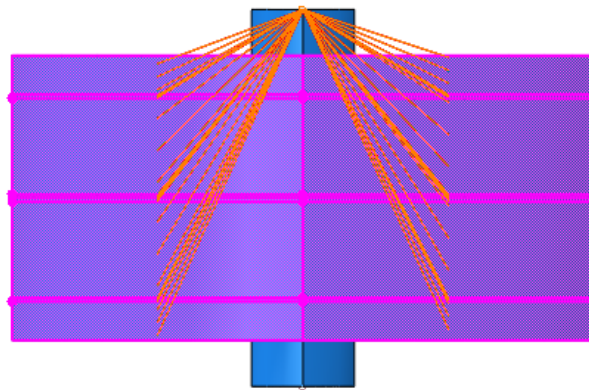


Figure 68: Coupling between RP and outer surface of the yoke.

## 9.2 Results

### 9.2.1 Gravity load cases

The maximum displacement and the max stress criterion applies here. Results from element-size convergence studies are presented in Figure 69.

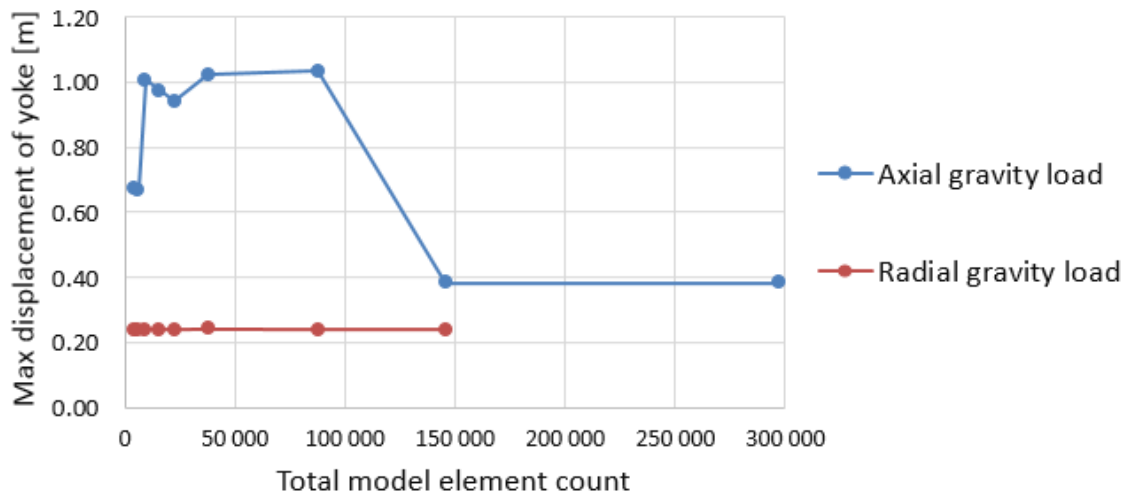


Figure 69: Element size convergence study for gravity load cases.

The displacement of the yoke for the radial gravity load is about 0.25 mm for all element sizes. For the axial gravity load, the displacement is unstable for the coarser meshes, but not higher than approximately 1 mm. This is well within the specified 2 mm. Figure 70 shows the global displacement of the structure for the two load cases with a high scale factor.

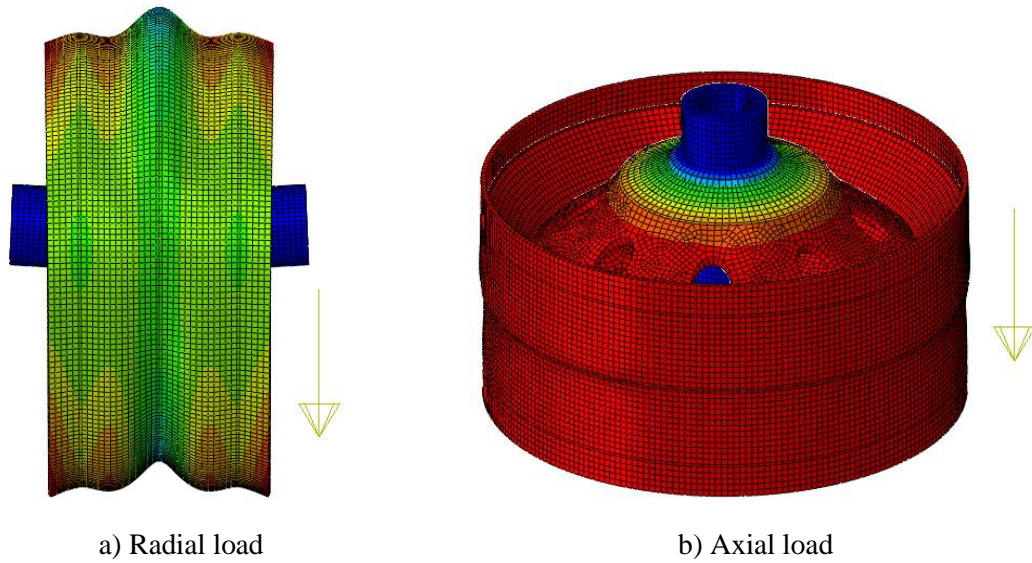


Figure 70: Global displacement of the structure for the gravity load cases.

Table 31 summarises the maximum stress levels, and yoke displacement. Tensile and compressive stresses are equal in magnitude, so only absolute values are shown.

Table 31: Maximum stresses in the structure. Percentage of limit in parenthesis.

Load case	Max displ. [mm]	11 [MPa]	22 [MPa]	12[MPa]	Location
Radial	0.25 (5%)	7.1 (1%)	2.7 (11%)	0.8 (2%)	Vicinity of disc hole
Axial	1 (20%)	13.7 (3%)	5 (20%)	1.5 (3%)	Inner radius of disc

These values are taken from the model where displacement shows convergence. Stresses are low and further studies are considered unnecessary.

The maximum von Mises stresses in the shaft and hubs were:

- Radial load case, 4.5 MPa in the middle of the shaft because of shaft bending.
- Axial load case, 28.5 MPa in the hub root because of hub bending.

## 9.2.2 Torque

An element-size convergence study was done for the highest stressed composite disc. The holes in the discs introduce stress concentrations, and the highest stresses near the holes are plotted against number of elements per disc in Figure 71.

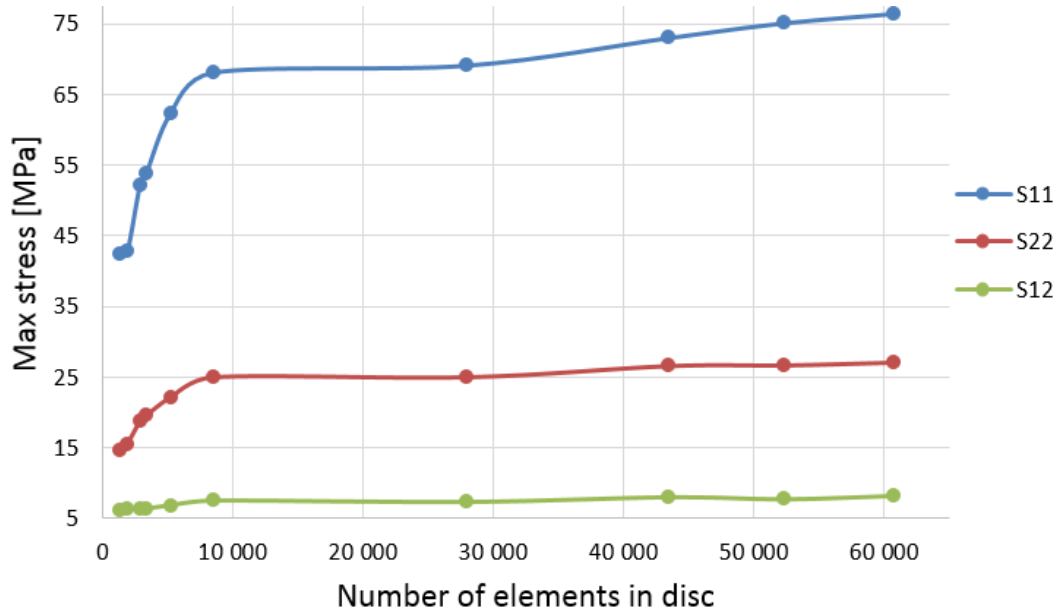


Figure 71: Element size convergence for the torque load case

A relatively sharp increase is seen up to around 10 000 elements, from where stress increases slowly. 22-tensile stresses stops its sharp increase at around 25MPa (Figure 71). This is at the material strength limit, and some local matrix cracking is therefore expected. The stresses in the discs will now be discussed in more detail, with a 28 000-element model, and emphasis on the 22-tensile direction. Figure 72 shows a detailed view of the 22-tensile stresses in a disc hole.

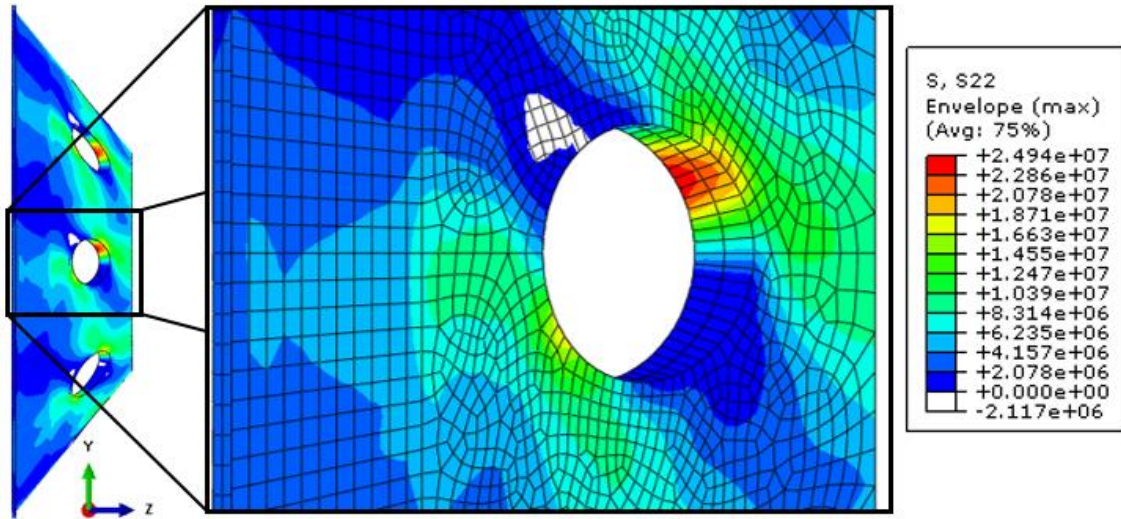


Figure 72: Detail view of the 22 tensile stress in a disc hole.

The extent of the area close to material strength is small, and the stresses drops quickly away from the holes. As described earlier in section 7.2.3, the stress levels are different in the two discs because of torsional flexibility in the shaft. The disc closest to the loaded end of the shaft experience higher stresses, as seen in Figure 73, which shows the 22-tensile stresses in both discs.

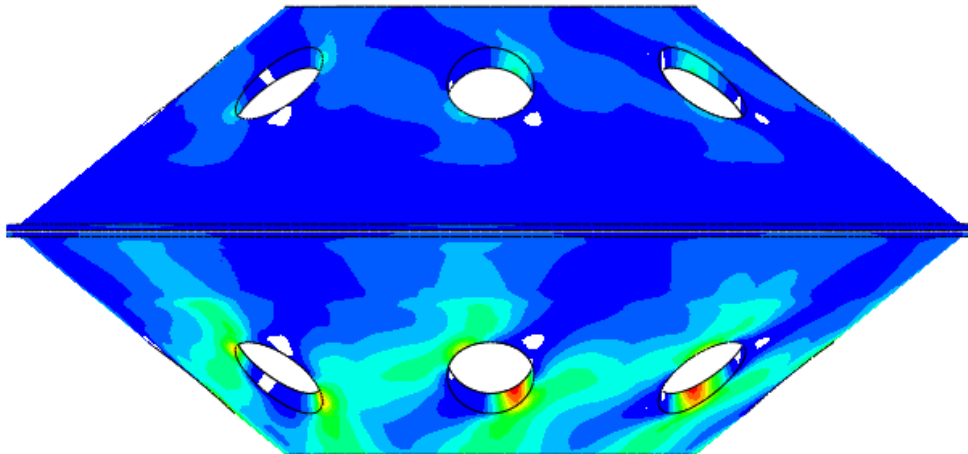


Figure 73: 22 tensile stresses in both discs. The bottom disc is in the loaded end of the shaft.

Max 22-tensile stresses are 25 MPa and 9 MPa for the bottom and top disc respectively. The approach in chapter 7, where a 75% - 25% distribution of loads were assumed seems therefore reasonable. A structure without these holes was analysed, and results are compared in Table 32.

Table 32: Comparison of stresses in structure with and without disc holes.

Direction	Disc with holes		Disc without holes	
	Max stress [MPa]	Utilisation	Max stress [MPa]	Utilisation
11-compression	69	12%	51	9%
22-tensile	25	100%	17	68%
12	7.3	16%	9	20%

Stress values reported here are max absolute values, as tensile and compressive were equal in magnitude for both structures. The material utilization shown in parenthesis is evaluated against the lowest of the tensile and compressive strength (from Table 10) in each direction. For the disc without holes, the point of maximum stress relocates to the corner between the bolted surface and the beginning of the coned part of the disc (Figure 74), where there is a corner giving stress concentrations. The figure shows the discs viewed from the inside. Maximum displacement of the discs with holes are 0.461 mm.

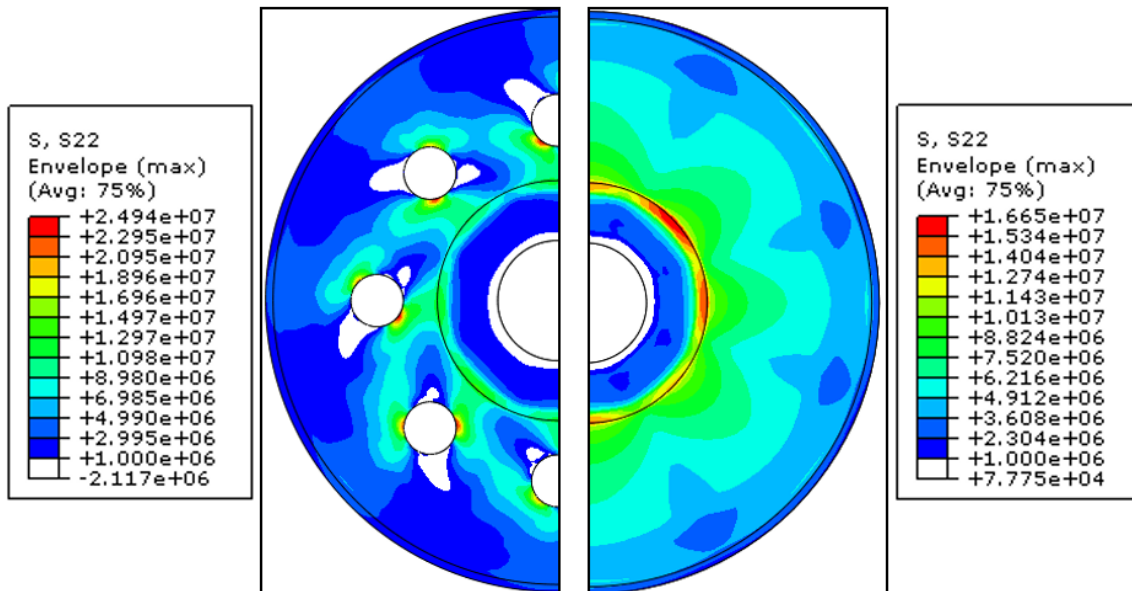


Figure 74: Comparison of stress fields for disc with (left) and without (right) holes.

The stresses in stiffener rings, yoke and shaft with hubs are all within their strength limits. Some comments are made below. Figure 75 shows the 22-tensile stress distribution in the highest stressed stiffener ring. Max stress is 5.4 MPa.

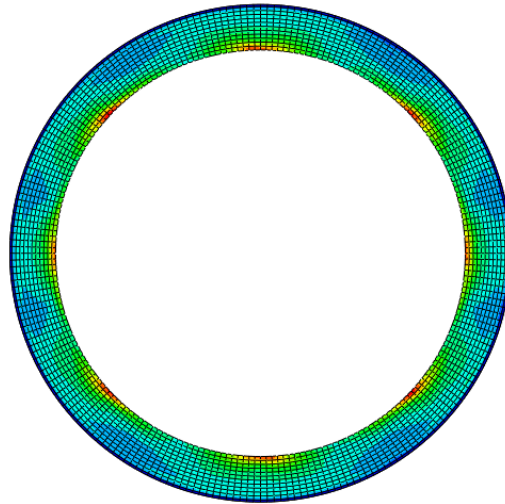


Figure 75: Tensile stress in 22 direction the stiffener rings.

In the yoke, the shear stresses near the main disc joints are the most significant. They are however much lower than the material strength; 1.6 MPa shear stress vs. 63 MPa material strength. Common for the composite disc and the stiffener ring is that the stress distribution is clearly higher in at the angles coinciding with the fibre directions. This is transferred to the yoke through the main joint causing the interesting shear distribution seen in Figure 76.

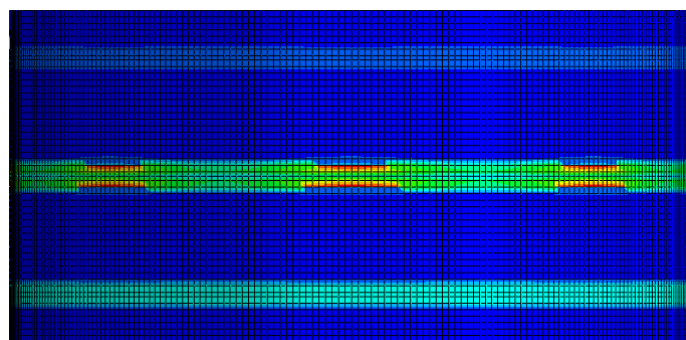


Figure 76: Max absolute shear stress (12) in the yoke.

The shaft/hubs part has a maximum von Mises stress of around 146MPa which is low compared to a yield strength of 355 (Figure 77). NB: fatigue is not considered here.

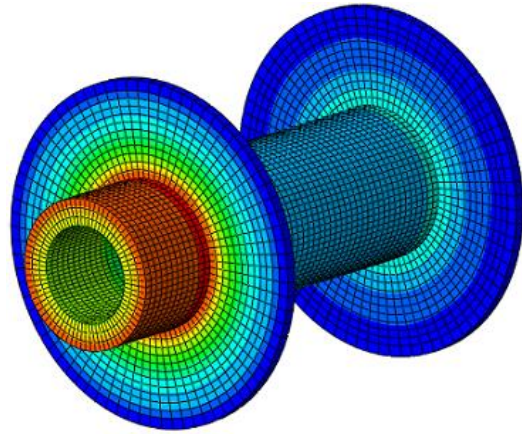


Figure 77: Von Mises stress shaft/hub part. Max is 146 MPa (red).



### **9.2.3 Linear elastic buckling eigenvalue analysis**

A linear elastic buckling eigenvalue analysis of the structure was performed to predict the theoretical buckling loads. The first eigenvalue (EV) is the most interesting because its corresponding mode is assumed to be the first to occur for the given loads and boundary conditions.

The buckling mode shapes are normalized vectors and do not represent actual magnitudes of deformation at critical load. These buckling mode shapes are often the most useful outcome of the EV analysis, because they predict the likely failure mode of the structure [37].

The magnitude of the loads in such an analysis is not important, as it will be scaled by load multipliers. Here the loads in the previously described load cases will be used, so that the resulting EV's will show what to multiply these loads with to get the critical buckling load. E.g. an EV of 10 means that the critical buckling load for this mode is 10 times the applied load.

Negative EV's usually indicates that the structure would buckle if the load were applied in the opposite direction [37]. There are some exceptions where negative EV's do not have a physical meaning, but this is not the case for these results. Most of the modes identified for this structure has both a positive and a negative EV's that are very close in absolute terms. Absolute values will therefore be presented in these results.

Element-size convergence studies were performed for all three buckling load cases until the lowest eigenvalues and corresponding eigenmodes are not significantly affected by further mesh refinement.

### 9.2.3.1 Torque buckling

Figure 78 shows the results for torque buckling mesh convergence studies. At the sharp increase in EV, the lowest eigenmode changed from a simpler local one (Figure 79 a)) to a symmetric disc global mode (Figure 79 b)). This coincided with an increase in through-the-thickness number of elements from one to two for the disc. EV's are at least 24 times the applied load, so torque buckling is disregarded as a failure mode candidate.

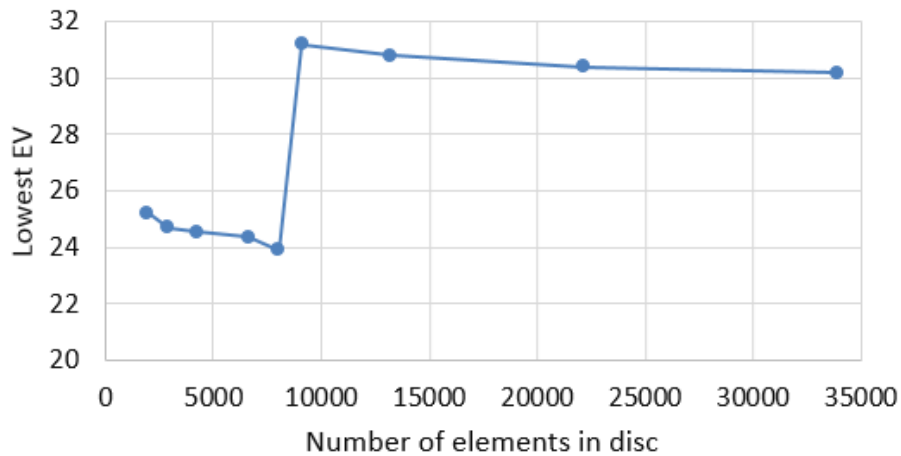
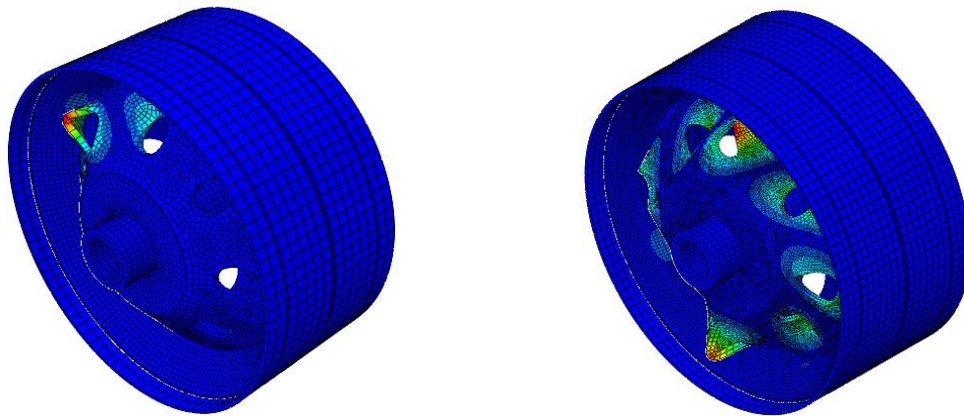


Figure 78: Mesh convergence for torque buckling load.



a) First eigenmode for 1 element in the thickness of the disc: local warping close to one of the holes. Approximate EV 24.

b) First eigenmode for 2 elements in the thickness of the disc: global warping of the disc. Approximate EV 30.

Figure 79: Mode shapes for torque buckling load.

### 9.2.3.2 Axial gravity buckling

Element size convergence studies (Figure 80) here also reveals a change in eigenmode. For coarser meshes the lowest mode is buckling of the hub (Figure 82 a)). However, when the number of through the thickness elements in the hub is increased from one to two, the mode with the lowest EV changes to warping of the disc (Figure 82 b).

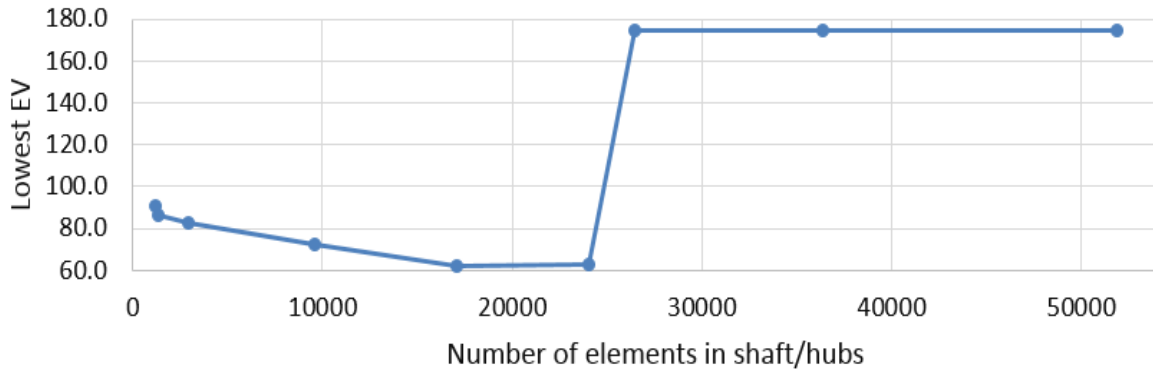


Figure 80: Element size convergence for axial gravity hub buckling.

A new convergence study was done to study this eigenmode. The results in Figure 81 shows that this mode has a sudden increase in EV when the number of elements through the thickness of the disc is increased from one to two. The first analysis with two through the thickness elements was done with less total number of elements than the last with one element through the thickness.

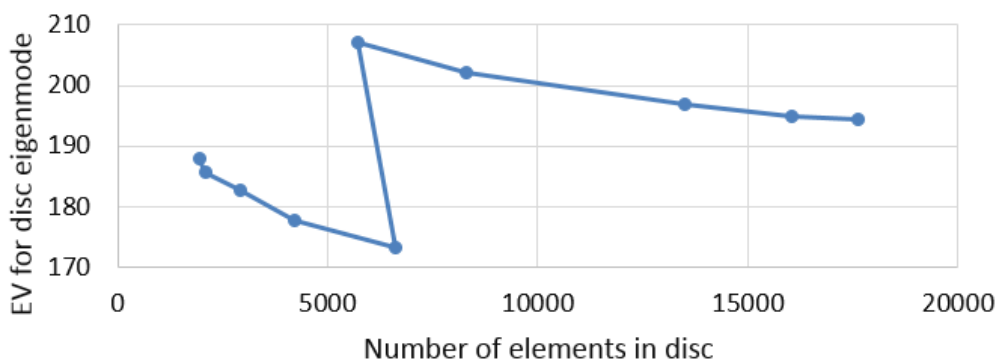
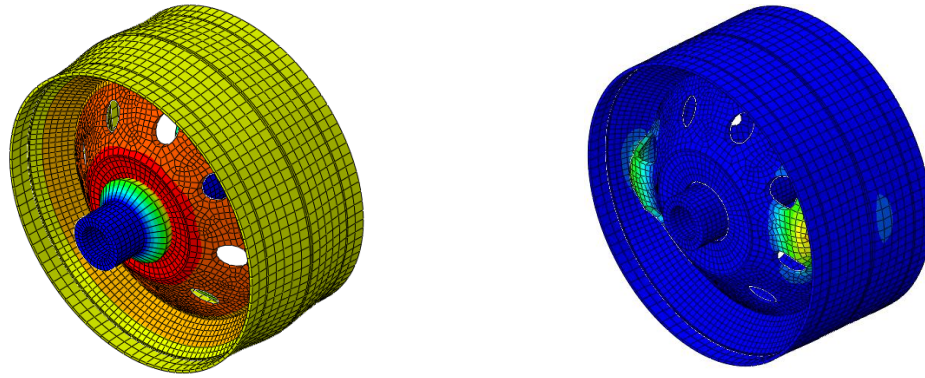


Figure 81: Element size convergence study for the disc-warping mode.



a) Hub buckling, EV 60

b) Disc warping, EV 174

Figure 82: Mode shapes for axial gravity buckling load.

### 9.2.3.3 Radial gravity buckling

Radial gravity buckling shows no change in eigenmode with increasing number of elements, or thought-thickness elements. No clear EV convergence is found. The lowest EV is above 174 for all meshes. The last data point in Figure 83 has two elements in the yoke thickness. The two first eigenmodes are shown in Figure 84 a).

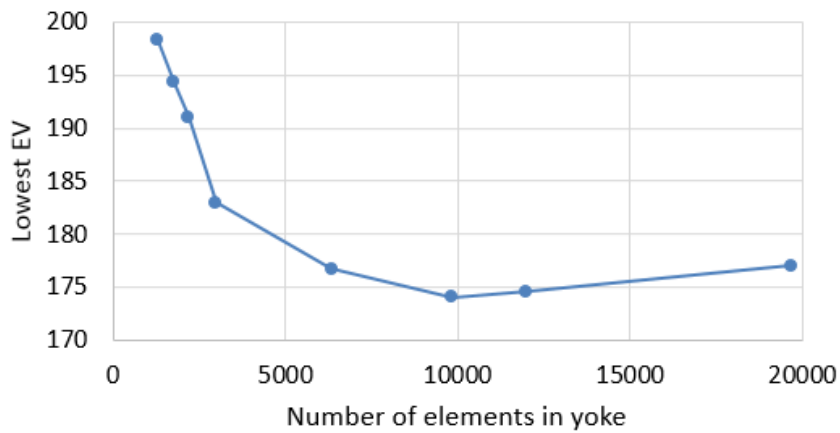


Figure 83: Element size convergence for radial gravity buckling.

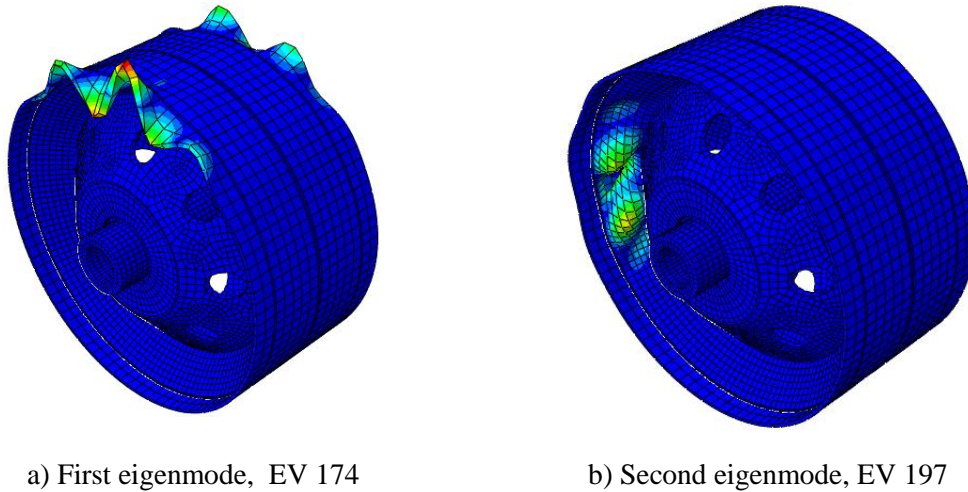


Figure 84: Eigenmodes for radial gravity buckling load.

Findings are summarized in Table 33. The lowest eigenvalue occurred for the torque load case, at 24 times the applied load. This is high enough to disregard buckling as a likely failure mode for this structure, even though only linear analyses were performed.

Table 33: Eigenvalues (EV) and mode shapes for the load cases.

Load case	EV	Mode level	Mode description
<b>Torque</b>	24	Local in structural member	Warping around one disc hole
	30	Global in structural member	Warping of disc
<b>Axial gravity</b>	60	Local in structural member	Axial warping of one hub
	174	Global in structural member	Deformation between disc holes
<b>Radial gravity</b>	174	Local in structural member	Flapping of yoke
	197	Local in structural member	Warping of stiffener ring

### **9.3 Summary**

For the radial and axial gravity load cases, the maximum displacements of the yoke is 0.25 mm and 1 mm respectively, which is acceptable compared to the chosen limit of 2 mm. Stress levels are insignificant. The structure stiffness is therefore considered acceptable for the given load cases.

Local stresses for the torque load case were higher. 22-tensile were slightly exceeding material strength near the disc holes, and some local matrix cracking is expected. 11-compression and 12-shear reached 12% and 16% material utilization respectively. Stress on other structural components are acceptable.

The linear buckling analyses indicated that the lowest EV occurs for the torque load case, at a value of 24. Buckling is therefore disregarded as a likely failure mode for this structure.

## 10 Manufacturing and Assembly

This chapter describes relevant manufacturing processes for the composite parts, and a possible manufacturing and assembly procedure for the preferred solution with short bolts. Figure 85 shows the completed rotor assembly on a mounting jig with a 1.90 m tall mannequin for scale.

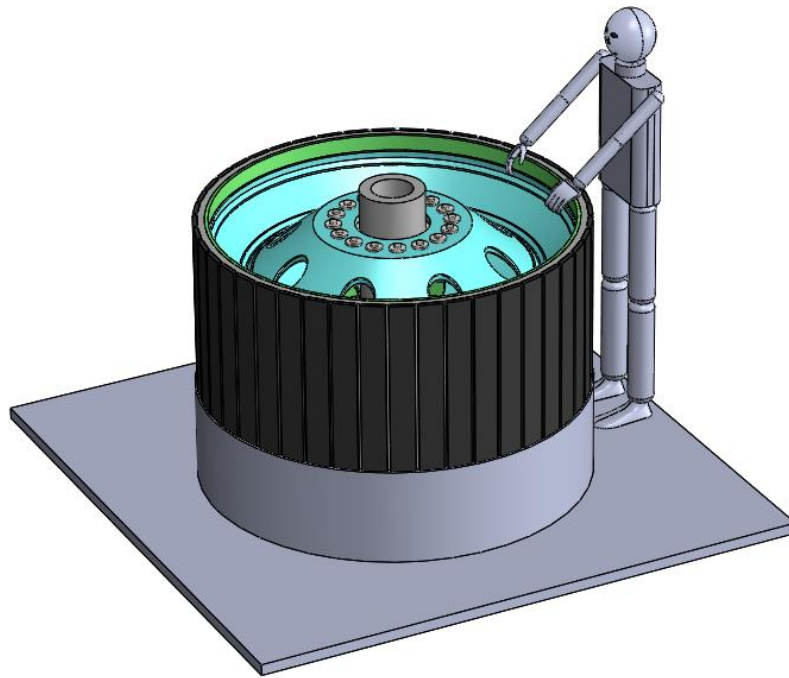


Figure 85: Complete rotor on jig with 1.90 m mannequin for scale.

### 10.1 Manufacturing processes

Spray-up is an open-moulding process, where continuous fibres are chopped, mixed with pressurised resin, and sprayed into the mould using a chopper gun (see Figure 86 [31]). The material is compacted with consolidation rollers and left for curing. Additional mats/fabrics can be added by hand for improved properties. Spray-up has been used for many years and is a cheap way of depositing fibre and resin. The resulting material is resin rich and has limited mechanical properties.

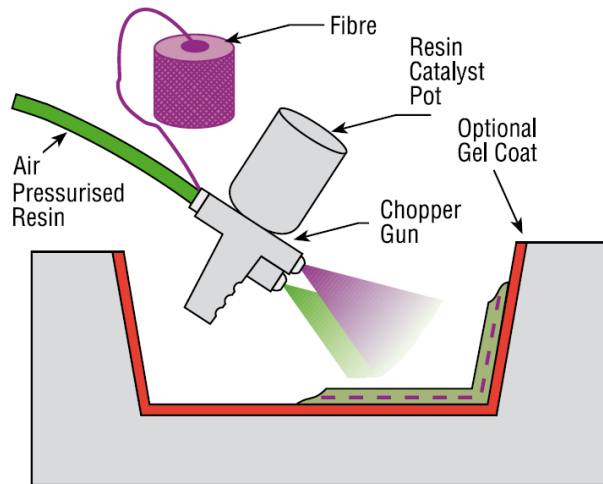


Figure 86: Illustration of the spray-up process.

The wet layup/hand layup process use dry reinforcement placed in an open mould and wetted out with resin by consolidation rollers (see Figure 87 [31]). This method is widely used for many years using simple low cost tools. The resulting properties are dependent on the skills of the workers. Higher volume fractions with longer fibres are possible compared to the spray-up process, but the method is still only applicable to low stressed components.

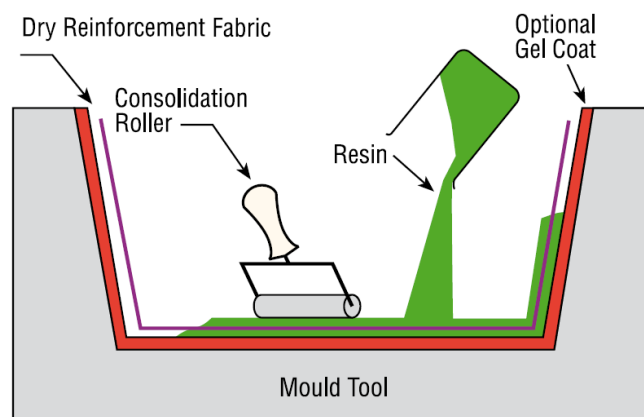


Figure 87: Illustration of the hand layup process.

Vacuum bagging can be viewed as an extension of wet layup in which the laid up laminate is covered with a vacuum bagging film (see Figure 88, adapted from [31]). Connecting a vacuum pump to the assembly creates a pressure difference between the atmosphere and inside the bag, which compress the laminate and removes air and excessive resin. This leads to increased fibre volume-fraction, lower void content and thus improved mechanical properties.



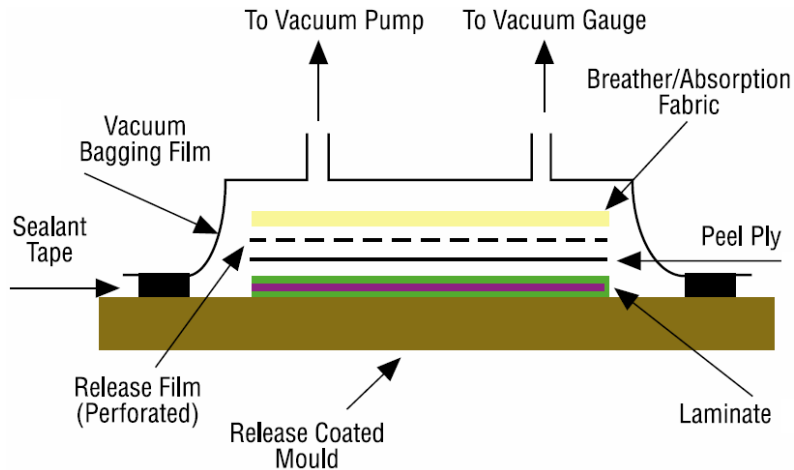


Figure 88: Illustration of vacuum bagging.

Resin infusion process covers a variety of processes. Reinforcement are laid up dry and covered with a vacuum bag. Resin is pulled through the fabric using vacuum (see Figure 89, adapted from [31]). This process gives high fibre-volume laminates with potentially lower labour time and better control over volatile emissions.

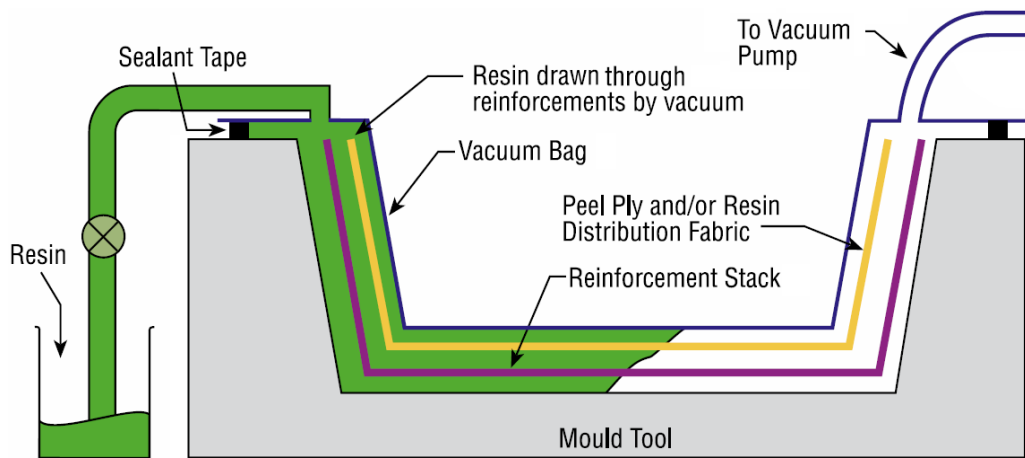


Figure 89: Illustration of the infusion process.

Traditional machining techniques such as drilling, sawing and routing/milling can be used for composite materials. There are however two serious difficulties with this; tool wear and normal forces leading to part damage and the need for appropriate fixturing. Laser machining and waterjet cutting have been used successfully with composite materials, but are limited by laminate thickness [28].

## 10.2 Manufacturing and assembly of inner structure

The shaft with hubs (Figure 90) can be manufactured in the same way as for the original design. Drilling/reaming of boltholes should preferably be done after welding. For the through bolt concept, the support pipes would be inserted and fastened with point welds or adhesive at this point.

The composite laminate discs and stiffener rings are made by vacuum bagging or resin infusion in a one-side mould with the layup described in section 6.3.5. Heated curing is recommended, especially for the disc, where good properties are necessary. Mould design should ensure that as many mating surfaces as possible will be tool surfaces. Both mating surfaces of the stiffener ring can be tool surfaces, and all surfaces on one side of the discs (critical dimensions illustrated in Figure 91). The discs requires some machining to ensure correct dimensions and create the holes. The position and diameter of the boltholes are especially important (explained in section 6.3.7). The dimensions of the stiffener ring are less critical and some post mould grinding may be sufficient. The bolts must have correct length to avoid bearing from threads in the laminate.

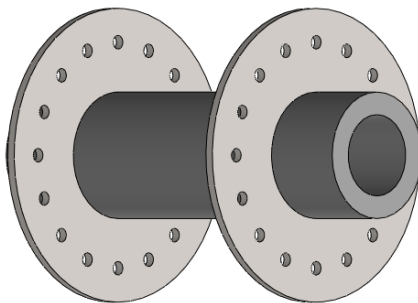


Figure 90: Shaft with welded onto hubs.

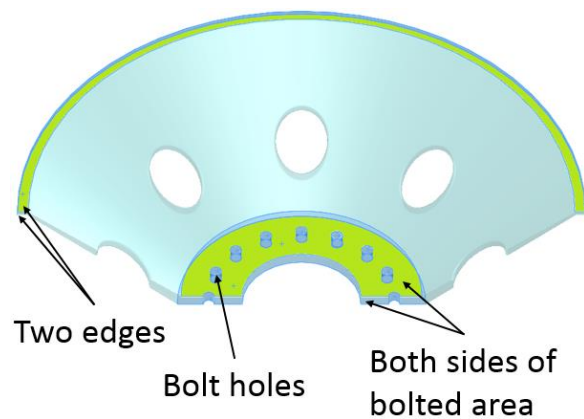


Figure 91: Areas with critical dimensions highlighted.

The inner structure (except stiffener rings) can be preassembled independently of the rest of the process. An adhesive would first be applied on the hub/disc interface if this joint type were chosen. Then the first disc is bolted on to one of the hubs (Figure 92). The figure shows that the bolts of the first disc are accessible from both sides. The assembly holes in this disc is therefore unnecessary for the short bolt solution. In addition to reduced machining, this is beneficial for the stress levels in the structure.

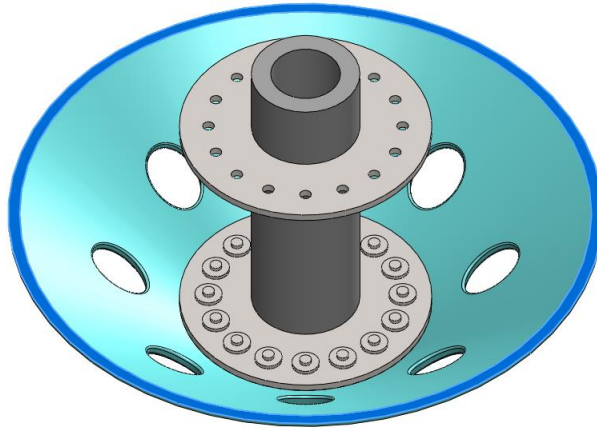
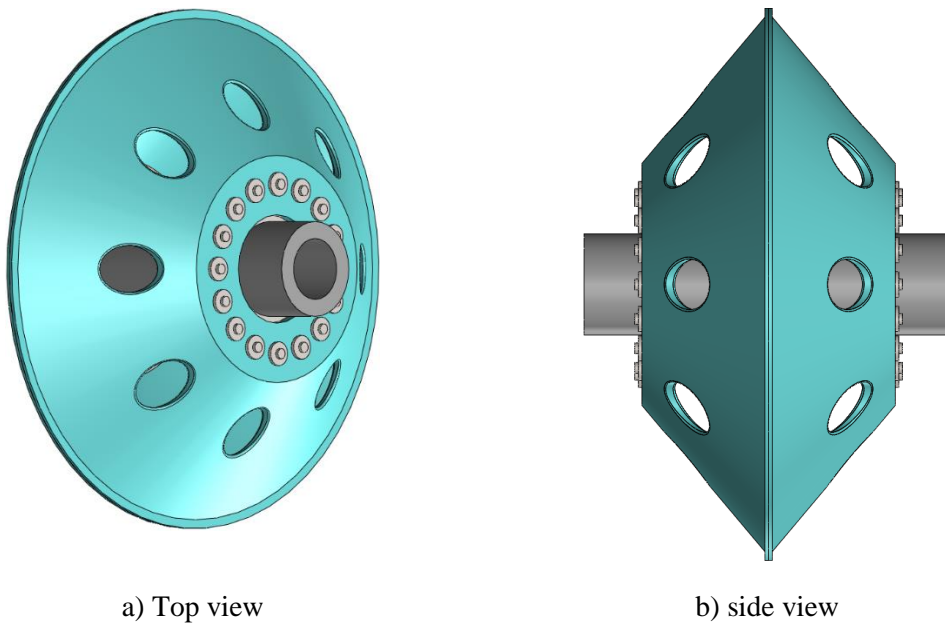


Figure 92: First disc bolted on to the shaft. Dark blue indicates applied adhesive.

The second disc is entered and bolted to the second hub. The bolting will hold the discs together for curing of the disc-disc adhesive (see Figure 92) and the optional hub-disc adhesive. The finished preassembly is shown in Figure 93.



a) Top view

b) side view

Figure 93: Second disc entered and bolted.

### 10.3 Manufacturing of magnetic core and yoke

The magnetic core is assembled, heat-treated and placed onto a jig for structure assembly. Some initial sketches of such a jig is shown in Figure 94, and an evaluation of a vertical vs. horizontal jig is attached in Appendix I. The pipe in the middle of the jig will be used to position the shaft, but can also be used to aid tooling (e.g. roller and spray-up gun guiding, measuring) during layup of the yoke.

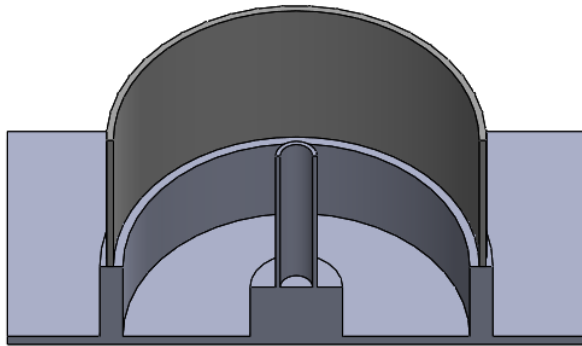


Figure 94: Section view of a simple assembly jig with the magnetic core.

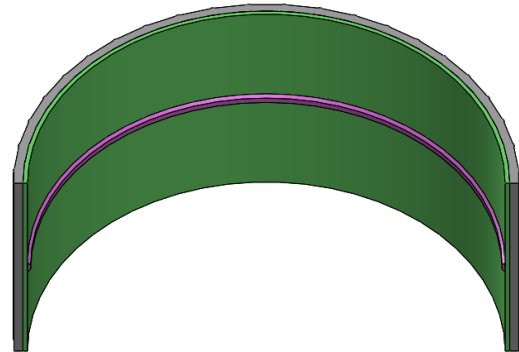


Figure 95: Sprayed up yoke (green) with joint backing in place (purple).

The magnetic core must be round, parallel and stable at this point, either with the help of a temporary support structure on the outside or by welding. It must also be concentric to the jig pipe, which determines the position of the shaft.

The yoke is laid up by hand layup or spray-up of chopped fibres, packed with consolidation roller and left for curing (Figure 95). A problem with the spray-up process is controlling the thickness of the deposited material. Measurements and, if necessary, redistribution of some material is critical at this point.

A pad/backing (see 5.1) for the main structure/yoke joint is placed inside the yoke (Figure 95). In addition to improving the joint, this will make for an easier entering of the structure, as its outer diameter can be smaller than the inner diameter of the yoke.

### 10.4 Final assembly

The jig pipe guides the preassembled inner structure into position (Figure 96). Small gaps and misalignments between the structure and the yoke can be taken up in the laminated joint. The important here is the alignment between shaft and the magnetic core.

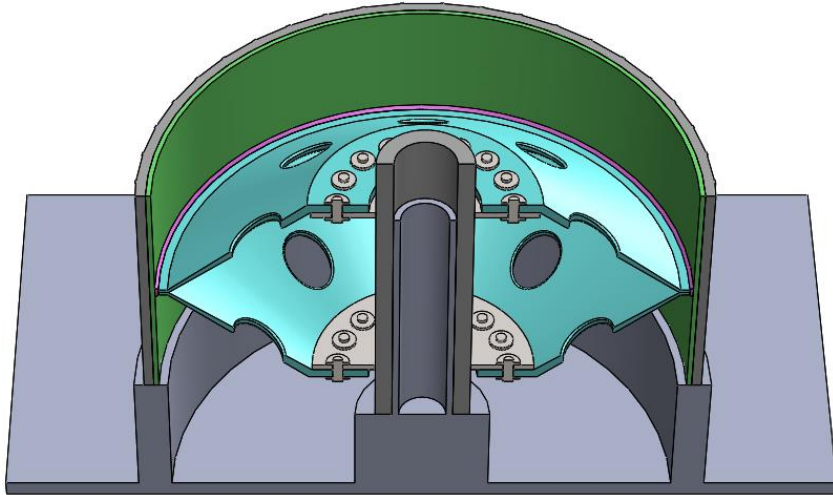


Figure 96: Shaft and structure in position inside the yoke.

One side of the main joint is then laid up, and the first stiffener ring entered and joined by lamination (Figure 97). The structure is then turned around and the same procedure is repeated for the other side. Dimensions and position of the stiffener ring is not of great importance.

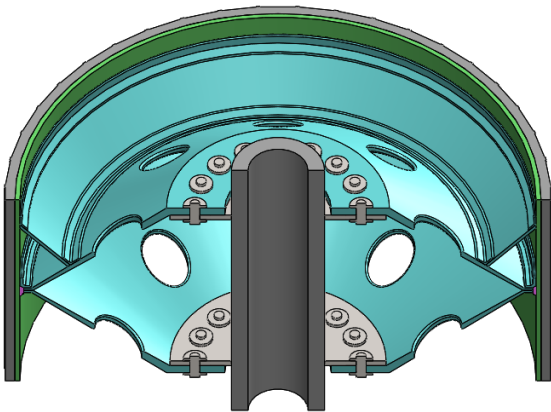


Figure 97: Stiffener ring entered and three laminated joints completed.

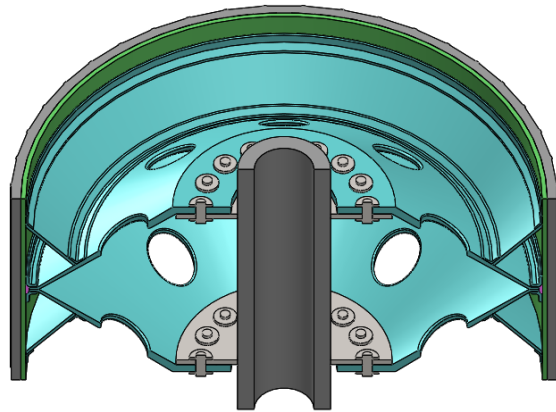


Figure 98: Structure turned around with all joints completed.

Figure 99 shows a detailed view of the main joint. Pad/backing is shown in purple, and the one tabbing on each side of the discs. Note that the mating surfaces of the discs are also adhered as described earlier. This is the joint responsible for torque load transfer, and its quality is of great importance. The magnets can now be mounted in the same manner as for the original rotor.

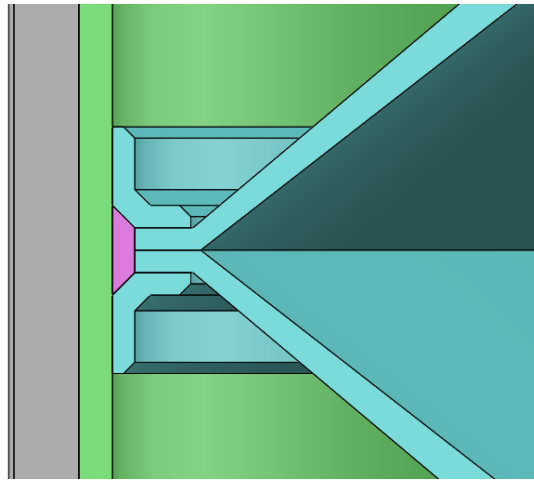


Figure 99: Detailed view of the main joint.

# 11 Discussion

The overall objective of this study was to enable reduced mass and inertia of the rotor through a redesign of its carrying structure utilizing non-magnetic composite materials and design for efficient manufacturing. A composite structure and manufacturing procedure have been proposed, and analyses have indicated acceptable local and global response to given load cases.

## 11.1 Design input

The robustness of the results obtained depends on the assumptions they were based on and the methods that were used. Chapter 4 formed the design philosophy, and several assumptions and simplifications were made. The author acknowledges that taking on the full use of C501 was a too demanding task. The structural analysis methods used does not follow the recommendations of section 9 in C501. The methods used here can at best be seen as a simplified version of the linear failure analysis with non-degraded properties (B400 in section 9 [25]). This method is able to predict fibre failure and first occurrence of matrix cracking, but not maximum deformation. The results need therefore be seen in the light of this knowledge.

The results are only valid for the provided load cases, which were assumed to be exactly known. Several failure mechanisms were omitted, the most important being stress rupture, fatigue and unacceptably large displacements.

The E-glass/epoxy properties were obtained from a reliable source, but the properties of the CSM/polyester might not be representative. E-glass/epoxy for discs and stiffener rings was chosen for its good mechanical properties. CSM/polyester for the yoke followed from the choice of manufacturing methods, and lower mechanical property requirements. Parts of the material degradation were omitted. A thorough assessment of residual strength and degradation from other possible fatigue cycles should be done. Only the yoke needs further consideration of temperature because of the machine operating at 60 °C.

The applied design criteria were simplified, and some even violated recommendations in the standard. Simplified partial factors were used to account for uncertainties in load effects and resistance, and these are considered appropriate based on the input. Precise determination of probabilistic load-distributions could allow for lower partial safety factors. A higher resistance-model factor could have been used for the chopped strand material because of the unreliable properties. A load model factor of 1.1 was used for the bolted joint contact analysis to account for uncertainties in the engineering model. For the global

model, 1.0 was used. It can be argued that the latter should be higher to account for the simplifications with the nonstructural mass, joints, and bearings and generator resistance being modelled as infinitely stiff.

C501 was not followed to the letter, but the results can be used to indicate the feasibility of the proposed composite structure. A foundation for further improvement and design using C501 have been established.

## 11.2 Joints

The bolted joint analysis concluded that local stresses from the static torque was acceptable. The resulting bolt load of 57 kN is comparable to the recommended 30 mm pin bearing strengths in 20 mm thick pultruded FRP profiles [50]. These are 32 kN and 69 kN for the longitudinal and transverse directions respectively. Even though they apply to a different material and laminate thickness, they show that the answer is not totally of the scale.

The bolted joint was assessed by visually inspecting the predicted extent of matrix cracking. This is not a robust way of designing, but gives a good indication its strength. According to [25], matrix cracking is assumed not to cause fracture in multi axial laminates, but it was considered unwanted here because of possible long-term fatigue problems. Higher utilization of fibre strength may be permitted by other assessment methods. Examples are using other failure criteria or to do analyses with material damage models. Final verification of the joint is likely to require testing, and this might a better approach than performing additional analyses.

Thermal expansion was assumed not to cause problems in the joints. A 60 °C operating temperature can cause debonding of the yoke/magnetic core interface, or induce high strains in the underlying structure. Heat treatment may be required after final assembly. These issues should be assessed in further work.

Washers were modelled as part of the bolts, and a bolt/bolthole snug fit was assumed, both contributing to a possible overestimation of the stiffness of the joint. Pretension of bolts will have a mitigating effect. Re-tightening of bolts after allowing time for initial creep should be possible during manufacturing. Testing can reveal if this is sufficient to ensure pretension between maintenance intervals. Another approach for the contact analysis would be to analyse the composite disc isolated by using analytical surfaces rather than steel parts. This would however not give a realistic representation of the behaviour of hub and bolts, whose stiffness is much lower than infinite.



Shear stress calculations for the main lamination and hybrid joints indicated max shear stresses of 1.5 MPa and 4.8 MPa respectively. The first can be compared to the shear strength of epoxy resin, and the latter to a 10 MPa lap shear strength of a typical structural adhesive (1152PA [64]). Simple elastic stress theory were used, and design based on mean allowable shear strengths is not recommended. Detailed analyses should include nonlinearities and the different stiffness of the adhesive, bolts and adherends. A better approach would be testing in a realistic environment, which is also required for adhesive joints [25].

The proposed structural joints seems to be fit for purpose, but testing is required.

### **11.3 Structure**

Maximum global displacement for the yoke were predicted to be 0.25 mm and 1 mm for the radial and axial gravity load respectively. This is acceptable compared to the chosen limit of 2 mm. Stress levels were low for these loads, but higher for the torque load case. 22-tensile were locally slightly exceeding material strength near the disc holes, and some local matrix cracking is expected. The lowest natural frequency of the preferred solution was predicted to be 21 Hz, giving a large margin to the highest identified excitation frequency of 5 Hz for the tidal turbine generator rotor. Several issues about these results will be discussed.

The high stresses near the disc holes did not converge. It can be expected that an analysis with progressive damage, allowing for stress-redistribution after cracking, would lead to convergence. The stress results are therefore considered reliable.

The necessity of the disc holes depends on the chosen bolted joint solution. Only one disc with holes is needed for the short bolt solution, and none for the through bolt solution. The size and position of the disc holes was not optimized, but based on an evaluation of what would be necessary during assembly.

No edge blends were used in the FE-models, and doing so would reduce the effect of local stress concentrations. This applies to the re-entrant corner in the disc used in global cases, and in the bolt/washer part used in the bolt contact analysis.

Modelling the magnetic core and magnets as a nonstructural mass is conservative w.r.g.t. stiffness, as any contribution from the magnetic core is excluded. With this assumption, a considerable amount of mass was moved closer to the shaft (in a radial distance about 49mm). The system will therefore have a quicker response in the modal analyses, which is

conservative. For the gravity load cases however, this will have caused a small underestimation of bending forces in the structure causing higher stresses and larger displacements. Based on the design criteria, the results are still acceptable.

Some excitation frequencies were identified. Damping in the structure can mitigate the effects of higher excitation frequencies that were not considered, depending on their excitation force.

Care was taken not to overestimate the stiffness of the joints by using small areas in the tie constraints. It is assumed that this gave a good enough representation, especially for the laminated joints.

The discs mesh was distorted in the area between the holes. This is thought to have had an on the buckling analysis results. Mesh refinement in the torque and the axial gravity load cases showed a sudden change in EV of the lowest eigenmode. This coincided with an increase in elements in the disc thickness from one to two. The mesh refinement may have decreased the influence of mesh distortions; hence suppressing local modes. Global modes natural for a symmetric structure could then take over. Another explanation could be a change in the through-thickness properties of the laminate from increased elements.

Stresses and displacements for the structure seems reasonable, but there are uncertainties about the validity of the displacement results from the method that were used. Buckling and modal analysis results are more difficult, but these had high margins to failure.

## **11.4 Manufacturing and feasibility**

The structure was developed to be feasible for manufacturing. It was assumed that the magnetic core could be stacked, heat treated separately and placed on an assembly jig. Here the outer dimensions of the magnetic core must be ensured, and it is not known whether this is possible economically or practically. An alternative to the composite carrying structure is to use the existing steel structure in combination with the new composite yoke. This might be sufficient to ensure the reduction in magnetic core thickness.

Mass and moment of inertia for the parts in the reference rotor (data from [4]) and the new proposed solution are compared in Table 34. A detailed breakdown is provided in Appendix J.

Table 34: Comparison of mass and inertia of reference structure and new proposed structure.

Property	Unit	Reference	New	Reduction	Reduction %
Mass	kg	3068	2212	856	28%
Moment of inertia	kg.m <sup>2</sup>	1682	1115	568	34%

The model used in the comparison is the “Model C” from chapter 8, with the short bolted solution. Total reduction in mass and inertia compared to the reference rotor is 28% (856 kg) and 34% (568 kg.m<sup>2</sup>). The majority of this comes from the thinner magnetic core. As pointed out in the report by Høyland [4] these reductions are on level with those achievable with structures made of stainless steel and aluminium (see Table 35).

Table 35: Compared to possible reductions with other non-magnetic materials

Reduction compared to steel reference	Stainless	Aluminium	Composite
Mass	28%	38%	28%
Inertia	30%	39%	34%

In the end, the feasibility of the composite structure boils down to costs, and estimations should be done as to whether changing to a non-magnetic structure will be economic. The composite structure should also be compared to alternative non-magnetic structures such as stainless steel and aluminium.



## **12 Conclusions and Further Work**

### **12.1 Conclusions**

A non-magnetic composite rotor structure, which is possible to manufacture, have been proposed and analysed implementing design philosophy from the DNV-OS-C501 standard. The standard was not followed in detail, but the results can be used to indicate the feasibility of the proposed composite structure. A foundation for further improvement and design using the standard have been established. This structure gives a reduction in weight (28%) and inertia (34%) compared to the original rotor with a steel structure, by enabling the use of a thinner magnetic core. Linear analyses indicated that global displacements and local stresses in the bolted joint and the structure are acceptable for the specified static load cases. A high margin of safety against buckling and resonance from identified excitation sources were predicted. The use of a composite structure seems therefore possible, but testing and analyses with more realistic load cases following the standard are required for verification. Before deciding to go further with a composite structure, a cost comparison of the existing- the new- and alternative non-magnetic structures should be performed.

### **12.2 Further work**

Obtain material properties by testing of materials made by chosen production methods and exposed to a realistic environment. Alternatively perform an improved degradation evaluation of material properties by taking into account temperature exposure, reduction in strength from permanent loads, and cyclic loads.

Analysis of more detailed load cases following C501, and assessment of fatigue, creep, stress relaxation, and stress rupture. Optimization of disc-hole size, position, areas with stress concentrations and tapering in the discs.

Experimental testing of joints. Analysis of the effects of thermal expansion, more realistic bolt/bolthole fit, and loose washers. Further development of the through bolt concept including a FE-bolt load analysis to study at the effects of laminate creep.

Estimate manufacturing and through-the-lifetime cost for the composite structure and alternative non-magnetic structures. Compare these to actual costs of the reference structure. Mock-up for verification of the manufacturing and assembly procedures.



# References

- [1] J. I. Koa, "Design of a super-light carrying structure for a floating tidal turbine," Specialization project 2013.
- [2] IEA, "World Energy Outlook 2013 - Executive summary," International Energy Agency 2013.
- [3] IPCC, "Climate Change 2007: Synthesis Report," Intergovernmental Panel on Climate Change 2007.
- [4] J. Høyland, "Non-magnetic support structure - evaluation of concepts," 0 First Draft, 2013.
- [5] SmartMotor AS, "SmartMotor AS acquired by Rolls-Royce Matine AS," ed, 2013.
- [6] SmartMotor AS. (October 10.). *Company*. Available: <http://www.smartmotor.no/company>
- [7] WEC, "World Energy Perspective - Cost of Energy Technologies," World Energy Council, 2013.
- [8] WEC, "World Energy Resources," World Energy Council, UK 2013.
- [9] Alstom, "Tidal power solutions," ed, 2013.
- [10] MCT. (2013, 22. november). *Tidal Energy*. Available: <http://www.marineturbines.com/Tidal-Energy>
- [11] B. Elghali, S. E. Benbouzid, and M. E. H. Charpentier, "Marine Tidal Current Electric Power Generation Technology: State of the Art and Current Status," *Electric Machines & Drives Conference, 2007. IEMDC '07. IEEE International*, vol. vol.2, pp. 1407-1412, 2007.
- [12] EMEC. (2013, October 9.). *Tidal Devices*. Available: <http://www.emec.org.uk/marine-energy/tidal-devices/>
- [13] CBC. (2013, October 10.). *Bay of Fundy tidal turbine deployment 2 years away*. Available: <http://www.cbc.ca/news/canada/nova-scotia/bay-of-fundy-tidal-turbine-deployment-2-years-away-1.1311977>
- [14] BBC. (2010, October 10.). *Blade fault on giant tide turbine AK1000 in Orkney*. Available: <http://www.bbc.co.uk/news/uk-scotland-highlands-islands-11492829>
- [15] Neptune. (2013, October 10.). *Neptune Renewable Energy goes into liquidation*. Available: <http://www.neptunerenewableenergy.com/>
- [16] BBC. (2013, October 1.). *Pentland Firth tidal turbine project given consent*. Available: <http://www.bbc.co.uk/news/uk-scotland-24100811>
- [17] MEYGEN. (October 10.). *Technology*. Available: <http://www.meygen.com/technology/>
- [18] BBC. (2013, Oktober 9.). *Alstom devices deal for Sound of Islay tidal array*. Available: <http://www.bbc.co.uk/news/uk-scotland-scotland-business-24114413>
- [19] J. Murphy. *Understanding AC induction, permanent magnet and servo motor technologies: OPERATION, CAPABILITIES AND CAVEATS*.
- [20] S. N. Vukosavic, *Electrical Machines*. New York: Springer, 2013.
- [21] J. Kirtley, in *MIT Open Courseware*, ed.
- [22] Ø. Krøvel, "Design of Large Permanent Magnetized Synchronous Electric Machines," PhD, NTNU, Trondheim, 2011.
- [23] M. Van der Giet, R. Rothe, and K. Hameyer, "Asymptotic Fourier decomposition of tooth forces in terms of convolved air gap field harmonics for noise diagnosis of electrical machines.," Institute of Electrical Machines, RWTH Aachen University.
- [24] J. F. Gieras, *Permanent Magnet Motor Technology, Design and Applications*, Third ed., 2009.
- [25] DNV, "DNV-OS-C501 Composite Components," ed: Det Norske Veritas, 2010.

- [26] P. László, G. Kollár, and S. Springer, *Mechanics of Composite Structures*. Cambridge, United Kingdom: Press syndicate of the University of Cambridge, 2003.
- [27] R. M. Mayer, *Design with reinforced plastics*. London: The Design Council, 1993.
- [28] P. K. Mallick, *Composites Engineering Handbook*: New York : Marcel Dekker, 1997.
- [29] S. Shchebetov, N. P. Vedvik, and A. Echtermeyer, "Typical Static Ply Properties For Composites," NTNU2012.
- [30] T. L. Anderson, *Fracture Mechanics: Fundamentals and Applications*, 3. ed., 2004.
- [31] Gurit, "Guide to composites (version 5)," Gurit Holding AG2013.
- [32] P. Davies and D. Choqueuse, *Fatigue in Composites*. Nio: Woodhead Publishing, 2003.
- [33] N. P. Vedvik, "Essential Mechanics of Composites," NTNU IPM, Trondheim2013.
- [34] G. Lubin, *Handbook of Composites*, 1982.
- [35] DNV, "DNV-OSS-312 Certification of Tidal and Wave Energy Converters ", ed, 2008.
- [36] F. Irgens, *Fasthetslære*. Trondheim: Tapir forlag, 1999.
- [37] 3DS, "Abaqus Analysis User's Manual 6.12," Dassault Systemes.
- [38] US Department of Defence, *MIL-HDBK-17-3F*, 2002.
- [39] Unknown. (2014, 05/05). *Capt'n Pauley's Virtual Boat Yard*. Available: <http://www.thevirtualboatyard.com/>
- [40] J. Schön and R. Starikov, "Fatigue of joints in composite structures," in *Fatigue in Composites*, B. Harris, Ed., ed Nio: Woodhead Publishing, 2003, pp. 621-643.
- [41] F. L. Matthews, P. F. Kilty, and E. W. Godwin, "A review of the strength of joints in fibre-reinforced plastics. Part 2. Adhesively bonded joints," *Composites*, 1982.
- [42] M. D. Banea and L. F. M. da Silva, "Adhesively bonded joints in composite materials: An overview," *Proceedings of the Institution of Mechanical Engineers, Part L: Journal of Materials Design and Applications*, vol. 223:1, 2009.
- [43] R. L. Ramkumar, E. S. Saether, and D. Cheng, "Design Guide for Bolted Joints in Composite Structures," Northrop Corporation, Aircraft Division1986.
- [44] E. I. Godwin and F. L. Matthews, "A review of the strength of joints in fibre-reinforced plastics Part 1. Mechanically fastened joints," *Composites*, 1980.
- [45] C. C. Chamis, "Simplified Composite Procedures for Designing Bolted Joints," presented at the 43rd Annual Conference of the Society of the Plastics Industry, Cincinnati, Ohio, February 1-5,, 1988.
- [46] D. Gay, S. V. Hoa, and S. W. Tsai, *Composite Materials*: CRC Press 2002, 2002.
- [47] A. S. Mosallam, *Design Guide for FRP Composite Connections*. Reston, Virginia: American Society of Civil Engineers, 2011.
- [48] G. Kretsis and F. L. Matthews, "The strength of bolted joints in glass fibre/epoxy laminates," *Composites*, vol. 16, pp. 92-102, 1985.
- [49] J. R. Doyle, "Behaviour of Bolt and Adhesive Connections in Glass Fiber-Reinforced Plastic Members," Master, Department of Civil Engineering, West Virginia University, Morgantown, WV, 1991.
- [50] Fiberline, "Fiberline design manual for structural profiles of composite materials," Fiberline Composites A/S, Kolding2003.
- [51] J. Ekh and J. Schön, "Load transfer in multirow, single shear, composite-to-aluminium lap joints," *Composites Science and Technology*, vol. 66, 2006.
- [52] CEN, "Eurocode 5: Design of Timber Structures " in *Part 1-1: General - common rules and rules for buildings.*, ed. Brussels: European Committee for Standardization, 2004.
- [53] J. L. Clarke, "Structural design of polymer composites: EUROCOMP design code and handbook," E & FN Spon, London1996.
- [54] P. A. Lynn, *Onshore and Offshore Wind Energy : An Introduction*. Hoboken, NJ, USA: Wiley, 2011.




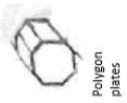


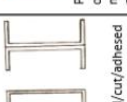
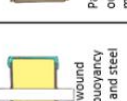

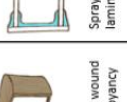
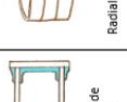



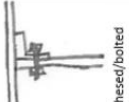
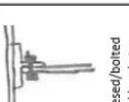
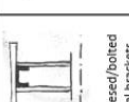
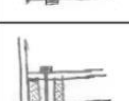
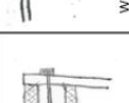





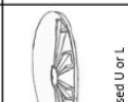

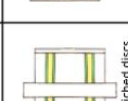
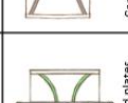


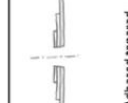


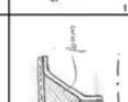
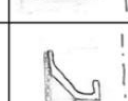
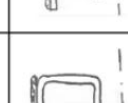

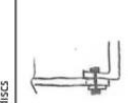





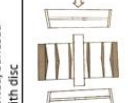
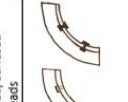

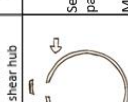
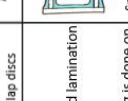

- [55] ISO, "ISO 898-1:2013," in *Mechanical properties of fasteners made of carbon steel and alloy steel -- Part 1: Bolts, screws and studs with specified property classes -- Coarse thread and fine pitch thread*, ed, 2013.
- [56] Norwegian Technology Centre, "NORSOK M-001," in *Materials Selection*, ed, 2002.
- [57] CEN, "Eurocode 3: Design of steel structures," in *Part 1-9: Fatigue*, ed. Brussel: European Committee for Standardization, 2005.
- [58] ISO, "ISO 261:1998," in *ISO general purpose metric screw threads -- General plan*, ed, 1998.
- [59] 3DS, "Abaqus/CAE User's Manual 6.12," Dassault Systemes.
- [60] Firehole Composites, "Abaqus Composite Tutorial - Bolted Joint Contact Definition."
- [61] Tingstad AS, "Teknisk Informasjon - Skruer," ed, 2014.
- [62] EMEC, "Guidelines for Design Basis of Marine Energy Conversion Systems," ed. London, 2009.
- [63] DNV, "DNV Ships / High Speed, Light Craft and Naval Surface Craft," in *Part 4, Chapter 8, Section 3: Equipment in general vibration, B. Environmental Requirements, B200 Vibrations and accelerations*, ed, 2013.
- [64] Scott Bader, "Crystic Crestomer Structural Adhesives Range and Application Guide," in *Crestomer UK 7/13 Issue 4*, ed.



# Appendix A Product Requirement Specification

Number	Description	Value and unit	Shall	Should
<b>1</b>	<b>Functional requirements</b>			
1.1	Magnet and shaft dimensions and properties as in the original design		x	
<b>2</b>	<b>Operation environment requirements</b>			
2.1	Operation in submerged marine environment (fouling, seawater)		x	
2.2	Operational temperatures	-2 °C to 30 °C	x	
2.3	Possibly filled with seawater			x
2.4	Transport and storage temperatures	-20 °C to 30 °C	x	
2.5	Transport and storage in aerated marine environment		x	
<b>3</b>	<b>Operational requirements</b>			
3.1	Nominal torque	140 kNm	x	
3.2	Nominal speed	75 rpm	x	
3.3	Cycles start/stop	10 000 cycles	x	
3.4	2G in radial direction during transport	1000 cycles	x	
3.5	2G in axial direction during transport	1000 cycles	x	
3.6	Break load, dead start load?		x	
3.7	Max composite surface temperature	60 °C	x	
<b>4</b>	<b>Reliability requirements</b>			
5.1	Lifetime	20 years	x	
<b>5</b>	<b>Maintainability requirements</b>			
<b>6</b>	<b>Safety requirements</b>			
<b>7</b>	<b>Cost requirements</b>			
7.1	Reduced manufacturing costs compared to existing system			x
7.2	Reduced manufacturing time			x
<b>8</b>	<b>Standards</b>			
8.1	DNV-OS-C501 Composite Components			
8.2	DNV-OSS-312 Certification of Tidal and Wave Energy Converters (WEC)			
8.3	Guidelines on design and operation of WEC (DNV/Carbon Trust)			
8.4	ISO Standards catalogue 83.120: Reinforced plastics			
<b>9</b>	<b>Environmental requirements</b>			
<b>10</b>	<b>Form requirements</b>			
10.1	Circular or close to circular shape for mounting lamination package		x	
10.2	Connect structure to steel shaft		x	
10.3	Holes in the sides of structure			x
10.4	Possibilities for filling the structure with buoyancy material			x
10.5	Shaft and steel laminations concentric and parallel in axial direction			
10.6	Outer diameter	1600mm	x	
10.7	Working length	770mm	x	
10.8	Shaft diameter	280mm	x	
10.9	Non-magnetic material last mm radially		x	
10.10	Composite materials			x
<b>11</b>	<b>Documentation requirements</b>			
<b>12</b>	<b>Production requirements</b>			
12.1	Possibilities of steel lamination package mounting			x

# Appendix B Morphology Matrix

Solutions / Sub-Functions	1	2	3	4	5	6	7	8	9	10
1. Yoke (and combined structures)	 Filament wound or centrifugal moulded	 Polygon plates	 Monocoque infused	 Z-part infused and adhered	 Wound/cut/adhered	 Partially wound outside buoyancy material and steel plates	 Partially wound outside buoyancy material	 Completely wound outside buoyancy material	 Spray-up inside laminations	 Radial sectioning
2. Yoke /structure interface	 Adhered axial brackets	 Adhered/bolted radial brackets	 Adhered/bolted radial brackets	 Adhered/bolted radial brackets	 Adhered/bolted radial brackets	 Wound into ring	 Adhered to wound-in support II	 Lay-up/laminated	 Circular struts	
3. Axial stiffness/support structure	 Infused disc	 Adhered rectangle	 Adhered T	 Adhered U or L	 Sandwiched H, U or I	 Sandwiched discs	 Conical plates	 Smaller diameter pipes		
4. Axial stiffness/support structure	 Simple infused disc	 Adhered tapered discs	 Tapered disc	 Array of pultruded profiles: I H U	 Bolted/adhered double shear disc	 Bolted/adhered double lap discs	 Adhered			
5. Support structure/hub/shaft interface	 Bolted/adhered simple	 Bolted/adhered with disc	 Bolted/adhered threads	 Compressed yoke	 Sectioned lamination package: Mounting is done on yoke surface.	 Spray-up inside laminations				
6. Yoke / lamination package interface	 Concentric adhered	 Keyway	 Interference, heat	 Welded	 Keyless frictional	 Hirth				
7. Hub/shaft interface	 Splines									

# Appendix C SN-Curves and Detail Category

From Eurocode 3, Part 1-9 [57].

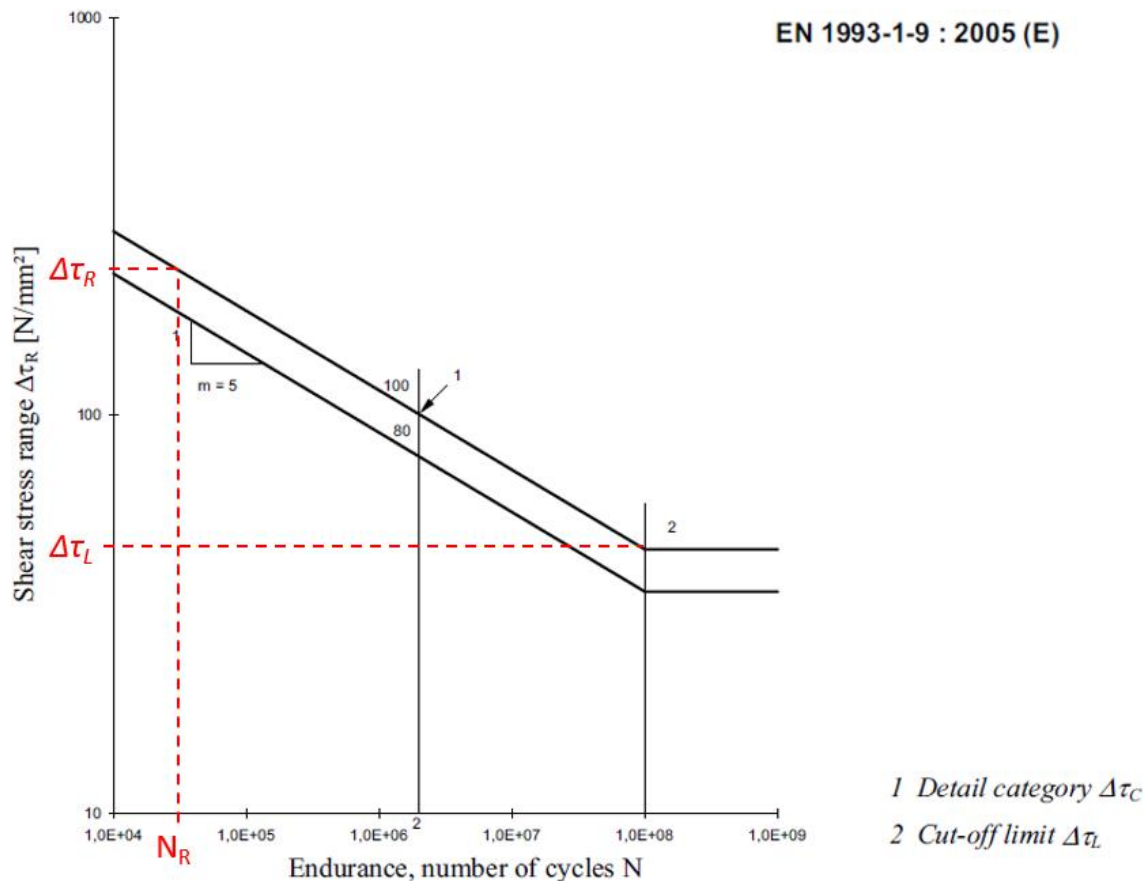


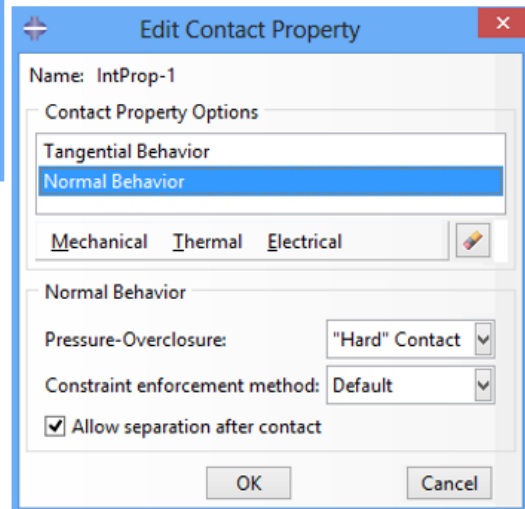
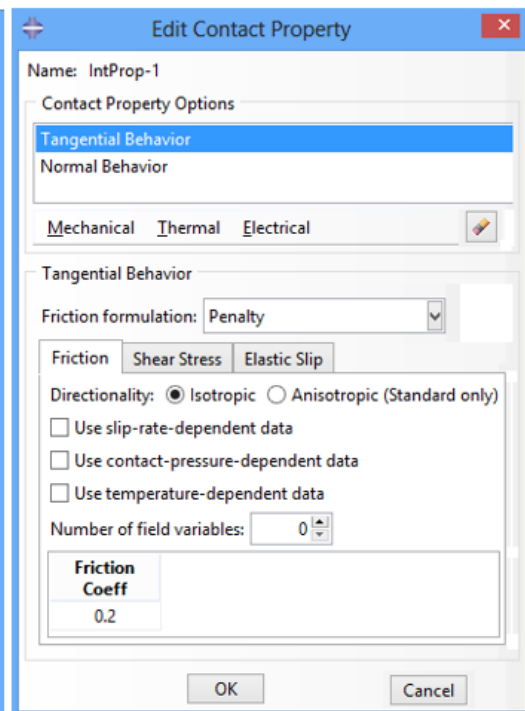
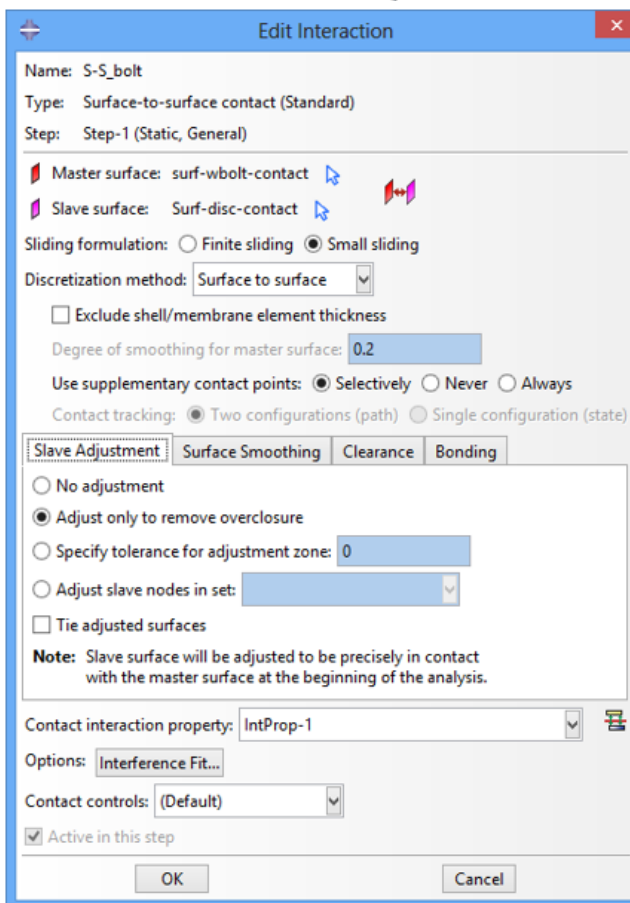
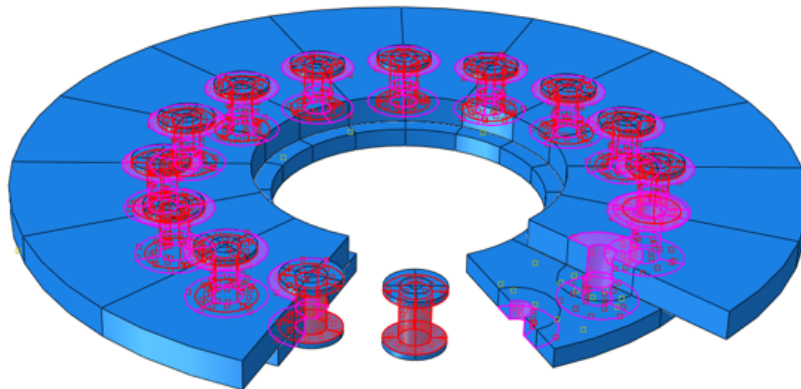
Figure 7.2: Fatigue strength curves for shear stress ranges

EN 1993-1-9 : 2005 (E)

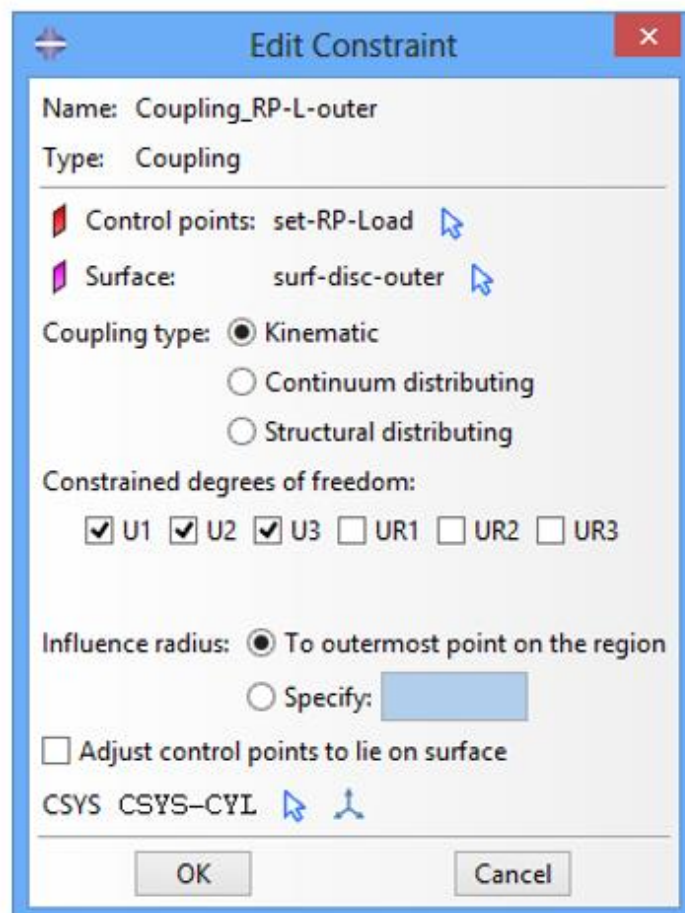
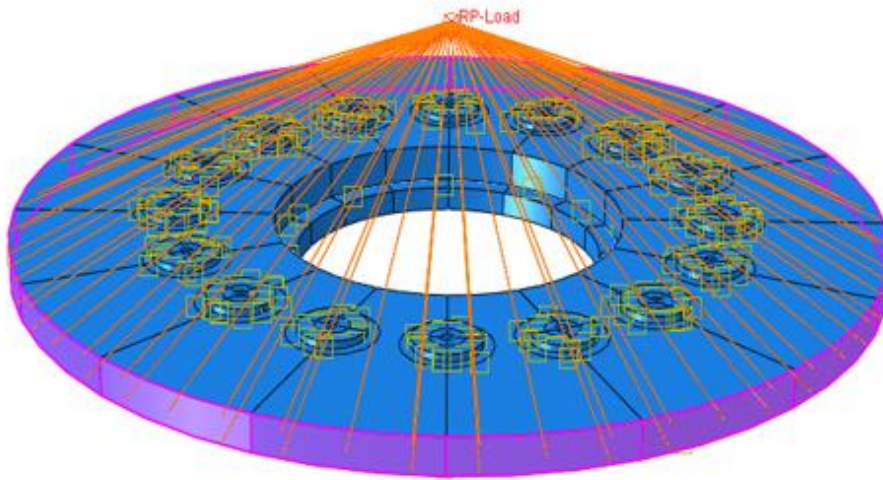
Table 8.1 (continued): Plain members and mechanically fastened joints

Detail category	Constructional detail	Description	Requirements
100 m=5		<u>Bolts in single or double shear</u> Thread not in the shear plane 15) - Fitted bolts - normal bolts without load reversal (bolts of grade 5.6, 8.8 or 10.9)	15) $\Delta\tau$ calculated on the shank area of the bolt.

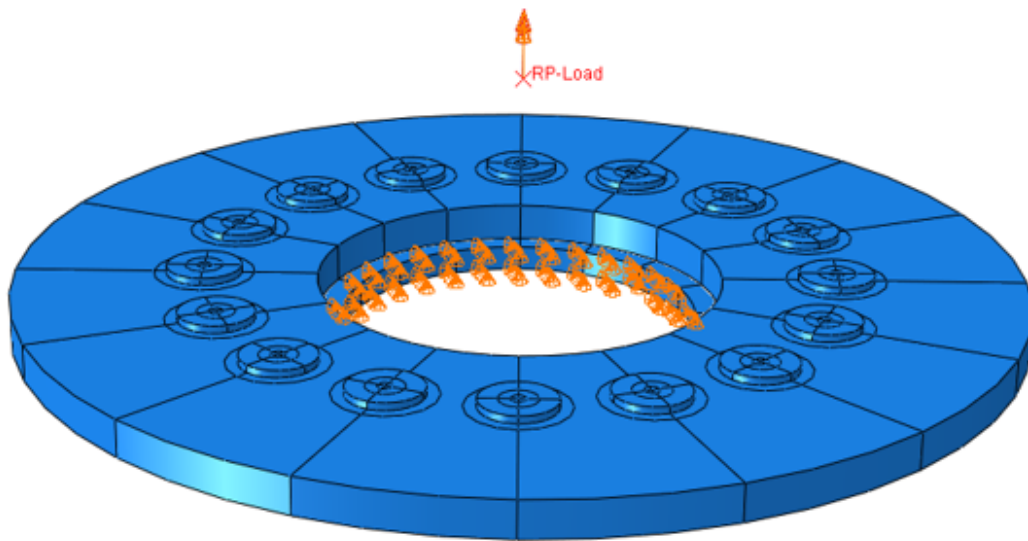
# Appendix D Surface-Surface Contact Definition



# Appendix E Constraint in Bolt Contact Analysis



# Appendix F Boundary Conditions



**Edit Boundary Condition**

Name: Fix-RP  
 Type: Displacement/Rotation  
 Step: Step-1 (Static, General)  
 Region: disc\_steel\_inner

CSYS: (Global)

Distribution: Uniform  $f(x)$

U1: 0  
 U2: 0  
 U3: 0  
 UR1: [ ] radians  
 UR2: [ ] radians  
 UR3: [ ] radians

Amplitude: (Ramp)  $f(x)$

**Note:** The displacement value will be maintained in subsequent steps.

OK Cancel

**Edit Load**

Name: Moment\_RP-L  
 Type: Moment  
 Step: Step-1 (Static, General)  
 Region: set-RP-Load

CSYS: CSYS-CYL

Distribution: Uniform  $f(x)$

CM1: 0  
 CM2: 0  
 CM3: 206000

Amplitude: (Ramp)  $f(x)$

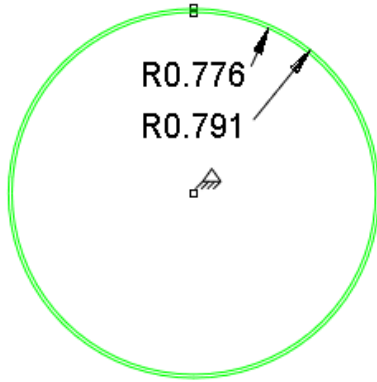
Follow nodal rotation

**Note:** Moment will be applied per node.

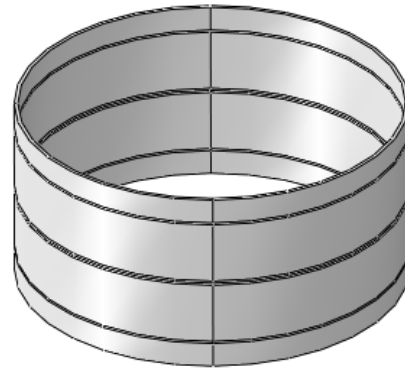
OK Cancel



# Appendix G Dimensions in Global FE Model

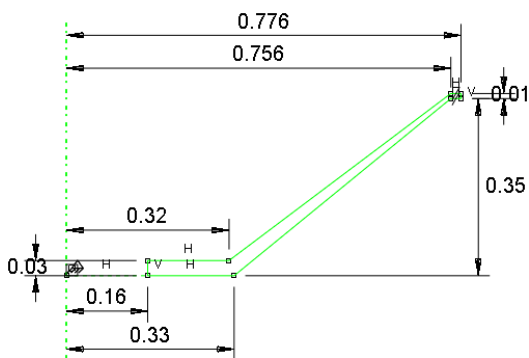


a) Yoke dimensions. Depth is 0.77m

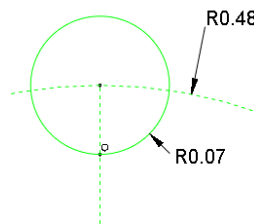


b) Revolved yoke

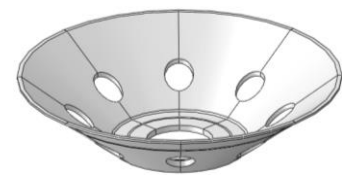
Yoke dimensions and partitions



a) Main dimensions

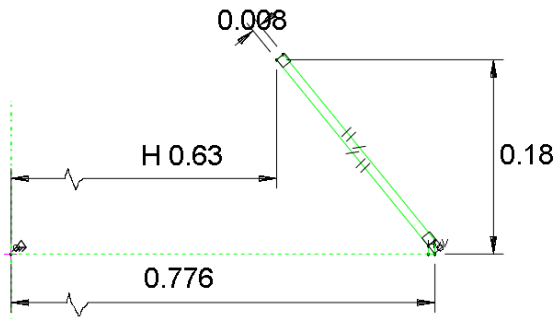


b) Hole details

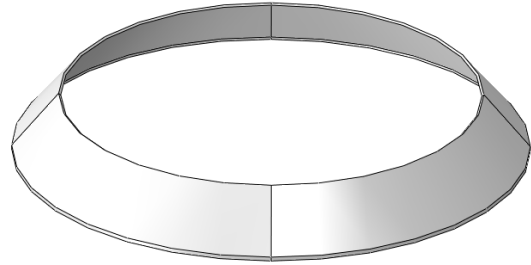


c) Disc with holes made with extruded cut.

Disc dimensions.

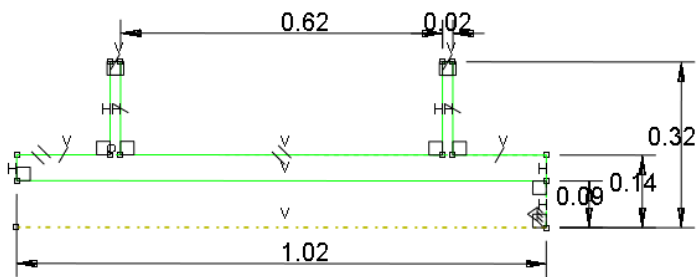


a) Dimensions for the stiffening discs

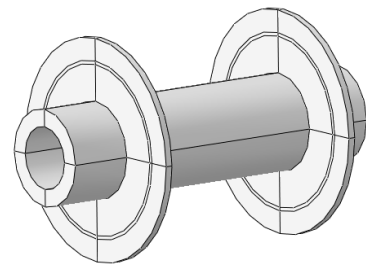


b) Revolved stiffening disc

Dimensions for the stiffening disc



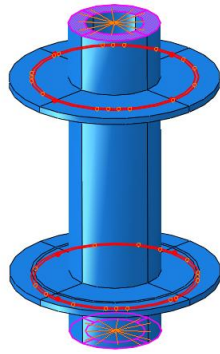
a) Dimensions of the shaft with hubs



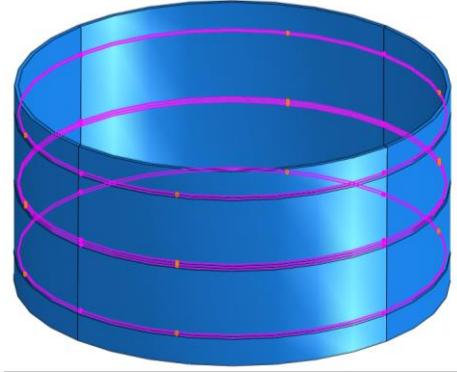
b) Revolved shaft with hubs

Dimensions of the shaft with hubs

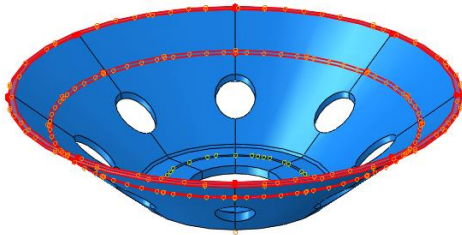
## Appendix H Constraints on Part Level



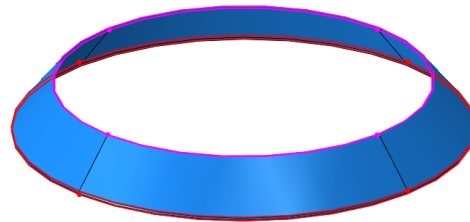
a) Shaft and hubs



b) Yoke



c) Disc

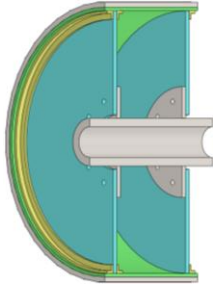


d) Stiffener ring

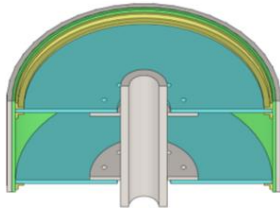
Constraint surfaces for all parts.

# Appendix I Horizontal vs. Vertical Jig Assembly

Comparison between laying (horizontal) and standing (vertical) assembly.



- Easier access to both sides
- Uniform yoke curing facilitated by rotation
- Difficult to maintain ovality of the magnetic core
- More advanced jig necessary





- Simpler jig
- Magnetic core supported by its own weight
- Underside less accessible; turning might be necessary
- Sticky resin system is necessary to avoid creep during curing of yoke.

## Appendix J Details of Mass and Moment of Inertia

The table below contains a comparison between the reference rotor and the proposed composite rotor's mass and inertia on a part level. Laminated-joints are not included. It is not known whether the data on the discs for the reference structure also includes axial stiffener plates.

Property	Unit	Ref.	New	Red.	% red.
<b>Outer diameter</b>	mm	1600	1600		
<b>Active length</b>	mm	700	700		
<b>Magnetic core thickness</b>	mm	60	30	30	50%
<b>Mass</b>	<b>kg</b>	<b>3068</b>	<b>2212</b>	<b>856</b>	<b>28%</b>
Magnets		527	527	0	0%
Steel laminations		1771	940	831	47%
Yoke		227	114	113	50%
Discs		255	163	93	36%
Stiffener plates/rings		?	32	?	?
Shaft		289	289	0	0%
Hubs		0	81	-81	-100%
32 bolts w nuts & washers		0	67	-67	-100%
<b>Moment of inertia</b>	<b>kg.m<sup>2</sup></b>	<b>1682</b>	<b>1115</b>	<b>568</b>	<b>34%</b>
Magnets		363	363	0	0%
Magnetic core		1111	610	501	45%
Yoke		130	70	60	46%
Discs		74	42	32	43%
Stiffener plates/rings		?	16	?	?
Shaft		4	4	0	0%
Hubs		0	5	-5	-100%
32 bolts w nuts & washers		0	4	-4	-100%

# Appendix K Risk Assessment

NTNU	Kartlegging av risikofylt aktivitet	Utarbeidet av	Nummer	Dato	
		HMS-avd.	HMSRV2601	22.03.2011	
HMS		Godkjent av	Side	Erstatter	
		Rektor	1 av 1	01.12.2006	

Enhet:



Dato: 2013-09-05

Deltakere ved kartleggingen (m/ funksjon): JIK (Stud. Techn.)

Kort beskrivelse av hovedaktivitet/hovedprosess: Kontorarbeid ifbm fordypningsprosjekt IPM høst 2013

ID nr.	Aktivitet/prosess	Ansvarlig	Eksisterende dokumentasjon	Eksisterende sikringstiltak	Lov, forskrift o.l.	Kommentar
1	Sykle til/fra arbeidssted	JIK		Refleks på sykkel	Veitrafikkloven	
2	Kontorjobb	JIK			Arbeidsmiljøloven	
3	Labarbeid viklemaskin		MAW 20 LS 4/1 Filament Winding Machine User Manual	PPE HMS kurs NTNU Spesifikt labkurs	Arbeidsmiljøloven	Vurderes i eget skjema dersom det bli aktuelt
4	Labarbeid Komposittlab			PPE HMS kurs NTNU Spesifikt labkurs	Arbeidsmiljøloven	Vurderes i eget skjema dersom det bli aktuelt
5	Labarbeid mekanisk verksted			PPE HMS kurs NTNU Fagbrev	Arbeidsmiljøloven	Vurderes i eget skjema dersom det bli aktuelt
6	Labarbeid mekanisk verksted SmartMotor			PPE Fagbrev	Arbeidsmiljøloven	Vurderes i eget skjema dersom det bli aktuelt

*De 2013-10-21  
Mils Rødt Kone*

NTNU	Risikovurdering	Utarbeidet av	Nummer	Dato	
		HMS-avd.	HMSRV2603	04.02.2011	
HMS/SKS		godkjent av	side	Erstatter	
		Rektor	1 av 3	9.2.2010	


Enhet:

Dato: 2013-09-05

Linjeleder:

Deltakere ved risikovurderingen (m/ funksjon): JIK (Stud. Techn.)

ID Nr.	Aktivitet fra kartleggings-skjemaet	Mulig uønsket hendelse/ belastning	Vurdering av sannsynlighet (1-5)	Vurdering av konsekvens:				Risiko-Verdi WC?	Kommentarer/status Forslag til tiltak
				Menneske (A-E)	Ytre miljø (A-E)	Øk/ materiell (A-E)	Om-dømme (A-E)		
2a	Kontorjobb	Skli/fall	3	B	-	-	-	B3	Rent, ryddig, belysning, rapporter skade på belysning/tepper ol.
2b	Kontorjobb	Elektrisk sjokk fra data/elanlegg	2	C	-	B	-	C2	Visuell inspeksjon av utstyr, rapporter skade på kabler etc.
2c	Kontorjobb	Belastningsskader p.g.a. sittestilling	2	B	-	-	-	B2	Ta pauser jevnlig. Ivareta god fysisk form. Sørg for god positur. Varier sittestilling, bytt stol
2d	Kontorjobb	Belastningsskader p.g.a. monotont arbeid med tastatur/mus	2	B	-	-	-	B2	Ta pauser jevnlig. Ivareta god fysisk form. Varier arbeidsstilling
2e	Kontorjobb	Brann i bygg	1	E	B	D	D	D1	
2f	Kontorjobb	Arbeid utenfor arbeidstid	5	A	-	-	-	A5	Kan tillates pga god helsetilstand og mobiltelefon. Gå hjem før man sovner.
2g	Kontorjobb	Manuell håndtering av tunge objekter	4	B	-	-	-	B4	Bruk tralle dersom mulig. Plasser tunge ting lavt Bruk god løfteteknikk
1a	Sykle til/fra arbeidssted	Bli påkjørt/syklet av medtrafikanter	2	C	-	A	B	C2	Refleksvest/klær med sterke farger. Lys på sykkel. Hjelm
1b	Sykle til/fra arbeidssted	Sykle på noe/noen/utfor veien	2	C	-	A	B	C2	Vær uthvil/konsertert Hjelm

NTNU	<b>Risikovurdering</b>	utarbeidet av	Nummer	Dato
		HMS-avd.	HMSRV2603	04.02.2011
HMS/KS		godkjent av	side	Erstatter
		Rektor	2 av 3	9.2.2010

**Sannsynlighet**

1. Svært liten
2. Liten
3. Middels
4. Stor
5. Svært stor

**Konsekvens**

- A. Svært liten
- B. Liten
- C. Moderat
- D. Alvorlig
- E. Svært alvorlig

**Risikoverdi (beregnes hver for seg):**

- Menneske = Sannsynlighet x Konsekvens Menneske**  
**Ytre miljø = Sannsynlighet x Konsekvens Ytre miljø**  
**Økonomi/materiell = Sannsynlighet x Konsekvens Øk/materiell**  
**Omdømme = Sannsynlighet x Konsekvens Omdømme**

**Sannsynlighet vurderes etter følgende kriterier:**


Svært liten 1	Liten 2	Middels 3	Stor 4	Svært stor 5
1 gang pr 50 år eller sjeldnere	1 gang pr 10 år eller sjeldnere	1 gang pr år eller sjeldnere	1 gang pr måned eller sjeldnere	Skjer ukentlig

**Konsekvens vurderes etter følgende kriterier:**

Gradering	Menneske	Ytre miljø Vann, jord og luft	Øk/materiell	Omdømme
<b>E</b> Svært Alvorlig	Død	Svært langvarig og ikke reversibel skade	Drifts- eller aktivitetsstans >1 år.	Troverdighet og respekt betydelig og varig svekket
<b>D</b> Alvorlig	Alvorlig personskade. Mulig uførhet.	Langvarig skade. Lang restitusjonstid	Driftsstans > ½ år Aktivitetsstans i opp til 1 år	Troverdighet og respekt betydelig svekket
<b>C</b> Moderat	Alvorlig personskade.	Mindre skade og lang restitusjonstid	Drifts- eller aktivitetsstans < 1 mnd	Troverdighet og respekt svekket
<b>B</b> Liten	Skade som krever medisinsk behandling	Mindre skade og kort restitusjonstid	Drifts- eller aktivitetsstans < 1 uke	Negativ påvirkning på troverdighet og respekt
<b>A</b> Svært liten	Skade som krever førstehjelp	Ubetydelig skade og kort restitusjonstid	Drifts- eller aktivitetsstans < 1 dag	Liten påvirkning på troverdighet og respekt

**Risikoverdi = Sannsynlighet x Konsekvens**

Beregn risikoverdi for Menneske. Enheten vurderer selv om de i tillegg vil beregne risikoverdi for Ytre miljø, Økonomi/materiell og Omdømme. I så fall beregnes disse hver for seg.

NTNU	<b>Risikovurdering</b>	utarbeidet av	Nummer	Dato
		HMS-avd.	HMSRV2603	04.02.2011
HMS/KS		godkjent av	side	Erstatter
		Rektor	3 av 3	9.2.2010

**Til kolonnen "Kommentarer/status, forslag til forebyggende og korrigerende tiltak":**

Tiltak kan påvirke både sannsynlighet og konsekvens. Prioriter tiltak som kan forhindre at hendelsen inntreffer, dvs. sannsynlighetsreducerende tiltak foran skjerpet beredskap, dvs. konsekvensreducerende tiltak.

*de 2013-10-21*  
*Atle Kvern*